Tracing the Sveconorwegian orogen into the W Norway Caledonides using U-Pb zircon geochronology and structural investigations

Master of Science Thesis

in Geodynamics

Thea Sætren Sørstrand

Department of Earth Science

University of Bergen

November 2019

Abstract

Western Norway is a key area to understand the relation between the Caledonian and Sveconorwegian orogens. This study provides U-Pb Zircon ages from basement rocks in the transition from undeformed into strongly "Caledonized" Baltic Shield. This study contributes to the understanding of the regional geology of a poorly studied region in western Norway. New U-Pb zircons data are revealed from Sotra, Hardanger and Gulen. The Sotra and the Gulen areas are part of the strongly deformed Caledonian basement, whereas the Hardanger area represents mostly undeformed basement. Detailed geological mapping was conducted in the westernmost parts of Sotra, which is part of the Øygarden Complex, to study lithological relationships and the tectonic reworking by Caledonian deformation. Only a limited number of U-Pb Zircon ages are published from these areas so far, which have limited a clear interpretation of the geological evolution of the respective areas. The new U-Pb Zircon ages reveal Sveconorwegian igneous crystallization ages, which fall in two age groups at c. 1050-1030 and c. 970-940 Ma that correspond to the Sirdal Magmatic Belt and to the hornblende-biotite suite of SW Norway, respectively. The Øygarden Complex and the Hardanger area represent Sirdal Magmatic Belt rocks. This correlation suggests a NW-SE trending Sirdal Magmatic Belt that gets less voluminous towards the NW. Hornblende-biotite granite ages are revealed from both the Hardanger area and the Gulen area. The investigated HBG ages show distinct compositional variations from the HBG suite, indicating that magmatism in this period was more variable than previously thought. The U-Pb datasets and field observations show no clear signs of Sveconorwegian metamorphism, which may conform to a long-lived accretionary orogenic setting with voluminous magmatism and absence of widespread penetrative deformation.

A low-temperature resetting of metamict zircons at c. 474 Ma is the only record of Caledonian orogenic events in the U-Pb datasets. While there is no record of Scandian metamorphism in the U-Pb data, all the deformation investigated from this study is interpreted to be Caledonian based on the region context. The gneisses in the Øygarden Complex were deformed to various degrees during Devonian extensional collapse of the Caledonides, showing amphibolite facies metamorphism followed by greenschists facies metamorphism. The area shows consistent stretching lineations plunging towards the ESE, indicating that the gneisses formed during one phase of deformation. The structures in the Øygarden Complex show similarities with metamorphic core complexes in the Western Gneiss Region and Mid Norway.

Acknowledgements

Firstly, I want to thank my supervisor Joachim Jacobs and co-supervisor Johannes Wiest for guidance during my master thesis and for giving me the opportunity to work on this interesting project. I am grateful for all the help, feedback, constructive comments and for always being available for my questions. Also, thanks for giving me a detailed introduction to geological fieldwork.

I am grateful for everyone who participated during my fieldwork. Especially, Cheng-Cheng Wang for helping me with new perspective and feedback that improved my work.
I would also give a special mention to Runar Televik Blaalid, Linda Sørstrand, Anne-Lise Sætren, Anna Elisabeth Mæland and Victoria Rung for assistance during my fieldwork. It was greatly appreciated.

I would also like to thank Irina Dimitri for preparing several thin sections and Martina Suppersberger for giving med an introduction to the different phases of the mineral separation. Thanks to Leif-Erik Pedersen for helping me with mineral separation, CL imaging and studying thin sections.

And finally, thanks to all my fellow students at the University of Bergen. Five years of studying would never have been the same without you. Thanks to my boyfriend, family and friends for support and encouragement during this challenging work.

Thea S. Sørstrand
Bergen, 17. november 2019

List of contents

Chapter 1: Introduction

This thesis is primarily a regional geologic study that contributes to the better understanding of the magmatic and metamorphic evolution of the Baltican crust in western Norway during two orogenic periods: the Sveconorwegian and the Caledonian orogenies. Structural geology, petrography and U-Pb Zircon geochronology form the basis of this study.

The southern parts of Norway consist of a Sveconorwegian province, where several recent studies have attempted to understand the evolution of the Sveconorwegian orogenic period (e.g. Bingen et al., 2008b; Coint et al., 2015; Slagstad et al., 2018). In western parts of Norway, dominated by a Caledonian province, a number of authors have studied the Caledonian reworking (e.g. Fossen and Hurich, 2005; Fossen, 2010a; Wiest et al., 2018). In order to understand both orogenies and how they interact in the geological record, this study investigates rocks in a transect from the undeformed Sveconorwegian province into the strongly deformed Caledonian province to determine similarities and differences in petrography and deformation. This new approach provides important insight to the geological evolution of a poorly understood region in western Norway.

1.1 Study area and aims of the study

The study area covers the transition from the undeformed Baltican basement into basement complexes that were strongly affected by the Caledonian orogeny. Three different areas have been targeted: Sotra, Hardanger and Gulen (Fig. 1). The main focus has been put on the western part of the island of Sotra, which is part of the Øygarden Complex. The area hosts a large gabbroic body and a large granitic body. Detailed field mapping was carried out to constrain lithological field relationships and to investigate Caledonian deformation. Samples were collected from here as well as the Gulen area, which is part of the Western Gneiss Region that experienced similarly strong Caledonian reworking (Wiest et al., 2019). These samples were compared to the Hardanger area, which represents the undeformed Baltic Shield (Fossen and Hurich, 2005). In total, seven samples were obtained for U-Pb zircon geochronology to determine magmatic and metamorphic ages targeting the Mesoproterozoic formation of the Baltican basement.

Regional correlations are necessary to understand and reconstruct the evolution of the Baltican Shield. Magmatic crystallization ages from Sotra, Gulen and Hardanger provide

information related to main magmatic events in the Sveconorwegian orogenic period, whereas field data from Sotra contribute to the understanding of the Caledonian reworking.

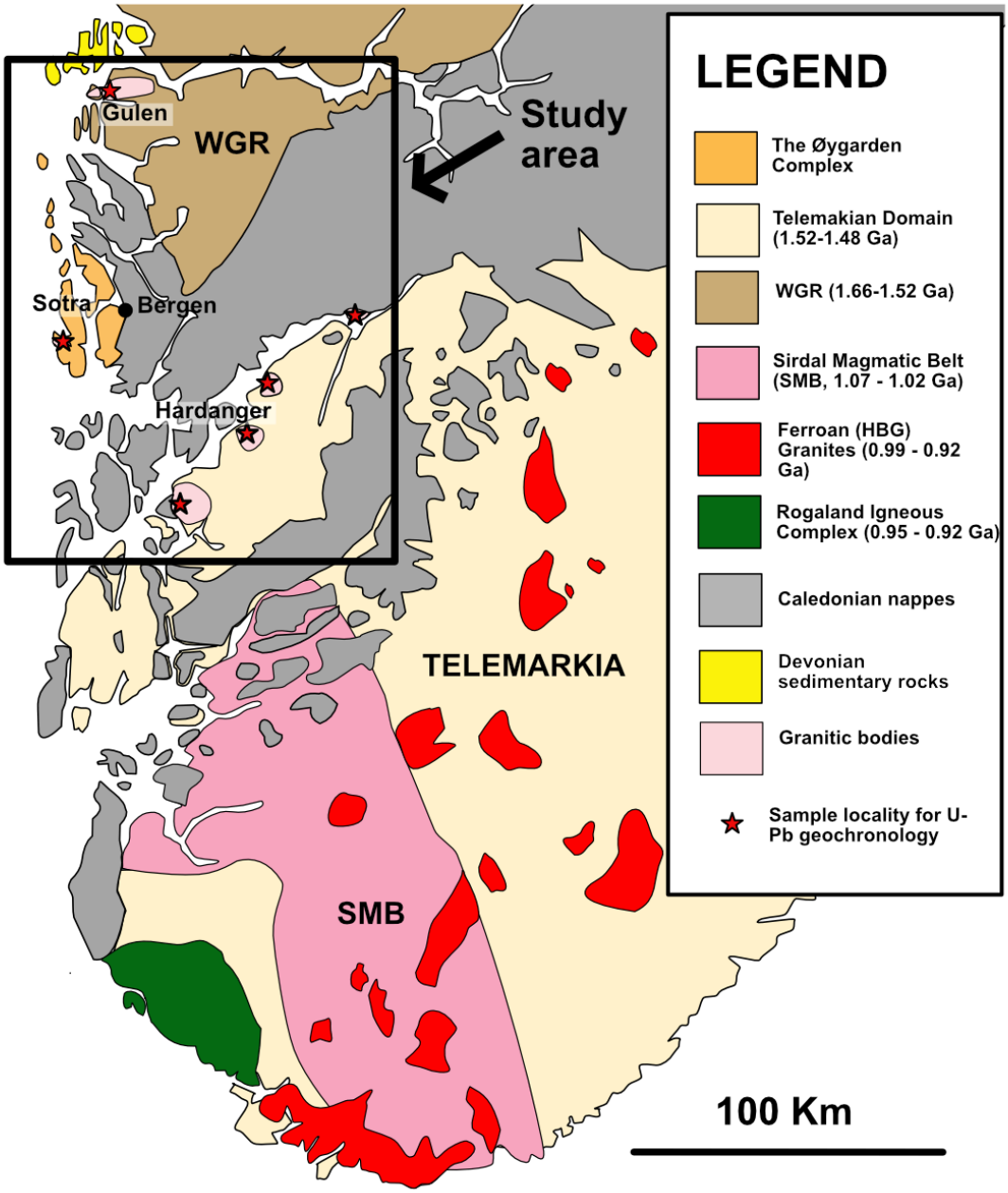

Fig. 1. Study areas and sample localities for U-Pb geochronology are marked on the simplified geological map. Detailed fieldwork was carried out on the western parts of Sotra. Modified from Fossen and Hurich (2005), Bingen et al. (2008a), Wiest et al. (2018), Wiest et al. (2019) and Slagstad et al. (2018).

Chapter 2: Geological background

2.1 Evolution of the pre-Cambrian basement

The geological evolution of Norway comprises several orogenic episodes of magmatism and metamorphism and involves the formation and break-up of different supercontinents.
Large parts of the Baltican basement evolved in the period between 1.9 – 0.9 Ga in several phases of continental growth in long-lived accretionary events along the active margin of the Fennoscandia (Roberts and Slagstad, 2015). The Fennoscandian Shield represents the NW part of Baltica and emerged as a continent during the amalgamation of the Columbia supercontinent at approximately 1.9 Ga (Roberts and Slagstad, 2015). Three main phases of continental growth can be distinguished, and are represented in distinct domains of the Baltican crust (Fig. 2): The Transscandinavian Igneous Belt (1.86-1.66 Ga) and the Gothian (1.66-152 Ga) and Telemarkian (1.52-1.48 Ga) domains. Formation ages of the different domains are predominately getting younger from E to W (Bingen et al., 2005).
As seen in fig. 2, the Baltican basement in SW Norway is of Gothian and Telemarkian age. The nature of the Gothian period has been debated but thought to involve switching tectonic events with accretionary and rifting processes as well as continental arc formation (Robert and Slagstad, 2015). Rocks in the Caledonian Western Gneiss Region (WGR) show mostly Gothian protolith ages. The Telemarkian period involves island and continental arc magmatism as well as continental rifting and defines the Telemarkia Domain and the Bamble-Kongsberg Terrane (Bingen et al., 2008b; Roberts and Slagstad, 2015).
At the end of Mesoproterozoic, the SW margin of Fennoscandia was reworked during the Sveconorwegian orogeny that represents the end of the accretionary events (Bingen et al., 2008b; Roberts and Slagstad, 2015).

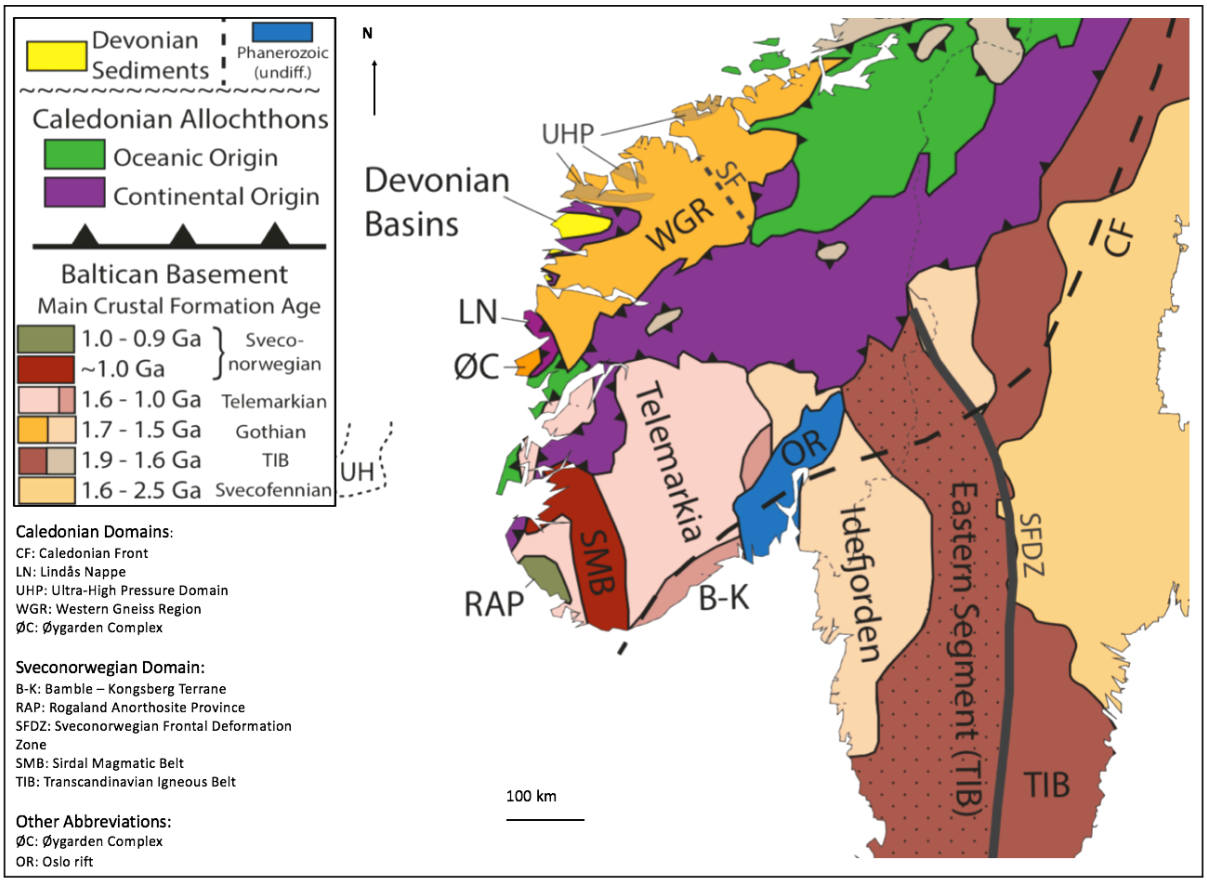

Fig. 2. Simplified geological map of southern Norway and Sweden, illustrating important Baltican domains. Crustal formation ages are getting younger from E to W. SW Norway are dominated by the Telemarkian and Gothian domains. Modified from Wiest (2016).

2.2. The Sveconorwegian orogeny

The assembly of the supercontinent Rodinia from the Mesoproterozoic to the early Neoproterozoic is characterised by intense orogenic activity (Rino et al., 2008). The Grenville orogenic belt is the orogeny with the greatest extent, and can be observed on all continents (Rino et al., 2008). The Sveconorwegian orogeny is interpreted as a part of the Grenville orogenic belt and involved magmatic, metamorphic and deformational processes between 1140 and 900 Ma in Norway and Sweden (Bingen et al., 2008b; Slagstad et al., 2018). Classically, the Sveconorwegian orogeny is interpreted to represent continental collision between Baltica, Laurentia and Amazonia (Bingen et al., 2008b). However, there is an ongoing debate about the direct correlation between the Grenvillian and the Sveconorwegian orogens evolving around the question whether the latter actually represents a continent collision or rather accretionary margin events (Bingen et al., 2008b; Slagstad et al., 2013). Several new findings from southern Norway point towards accretionary orogenic events and

the absence of continental collision in the Sveconorwegian orogeny (Fig. 3, Slagstad et al., 2013; Coint et al., 2015; Slagstad et al., 2018; Wiest et al., 2018).

SW Norway experienced three main phases of magmatic activity during the Sveconorwegian orogenic period, these are represented on fig. 4 by the Sirdal magmatic belt (SMB, c. 1070 - 1020 Ma), by Hornblende-biotite granites (HBG, c. 990 - 920 Ma) and by the Rogaland Igneous Complex (c. 950 -920 Ma, Auwera et al., 2008; Coint et al., 2015; Slagstad et al., 2018).

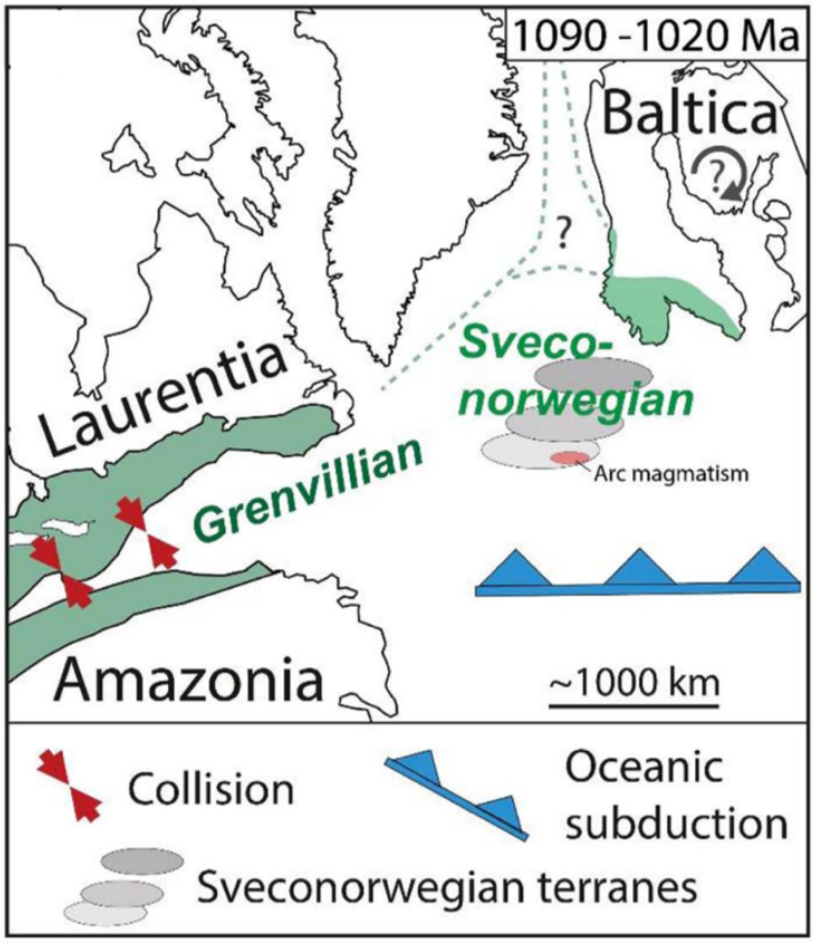

Fig. 3. Laurentia, Baltica and Amazonia from 1090-1020 Ma illustrating the Sveconorwegian orogeny as a part of the Grenvillian orogeny (Wiest et al., 2018).

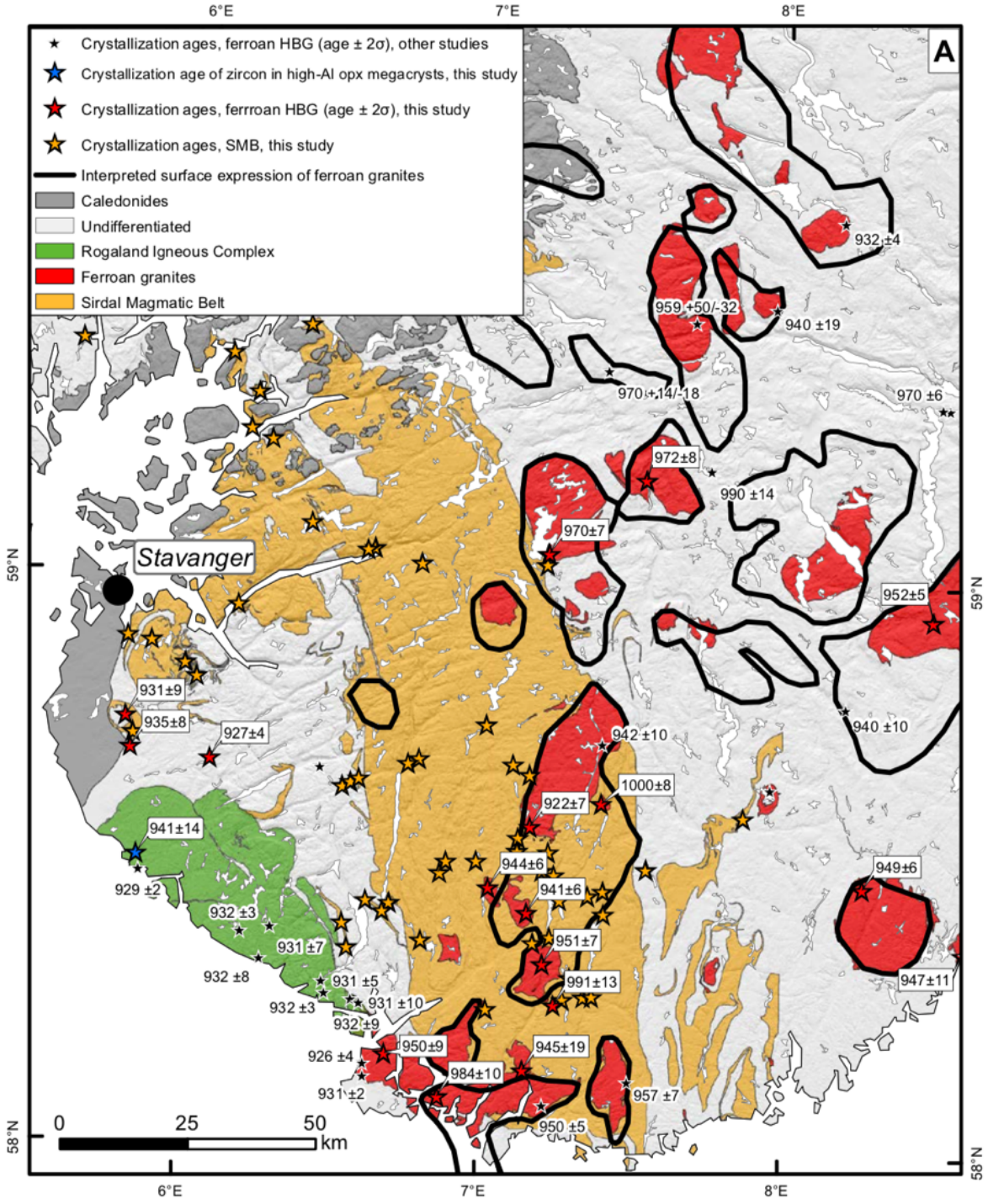

Fig. 4. Simplified geological map of SW Norway highlighting the Sveconorwegian magmatic rocks (Slagstad et al., 2018).

2.2.1 Continent-continent collision or long-lived accretionary margin?

Bingen et al. (2008b) describes the Sveconorwegian orogeny as a result of continent-continent collision and divided the Sveconorwegian orogenic belt into a Paleoproterozoic Eastern Segment and four Mesoproterozoic terranes. These are the Idefjorden, Kongsberg, Bamble and Telemarkia Terranes which are separated by major shear zones (Fig. 5). They further proposed a four-phase model to explain the geology of the four different units:

1) The Arendal phase (1140-1080 Ma) represents the collision between the Idefjorden and Telemarkia terranes and involved closure of an oceanic basin, accretion of a volcanic arc and high-grade metamorphism. The collision formed the Bamble and Kongsberg tectonic wedge.
2) The Agder phase (1050-980 Ma) represents the main Sveconorwegian oblique continent-continent collision, which involved crustal thickening of the Telemarkia terranes, voluminous syn-collisional granite magmatism from 1050 Ma to 1030 Ma, and high-grade metamorphism around 1035 Ma. In the Rogaland-Vest-Agder sector the metamorphism reached granulite facies conditions.
3) The Falkenberg phase (980-970 Ma) is seen as the final phase of convergence followed by beginning divergence. Eclogite conditions of the Eastern Segment at 970 Ma represent the last evidence for convergence in the Sveconorwegian belt.
4) The Dalane phase (970-900 Ma) reflects gravitational collapse of the orogen with post-collisional magmatism, exhumation of the Eastern Segment as a metamorphic core complex and emplacement of a gneiss dome in the Rogaland-Vest Agder sector. At 930-920 Ma the rocks in this gneiss dome underwent granulite-facies metamorphism during intrusion of a charnockite complex.

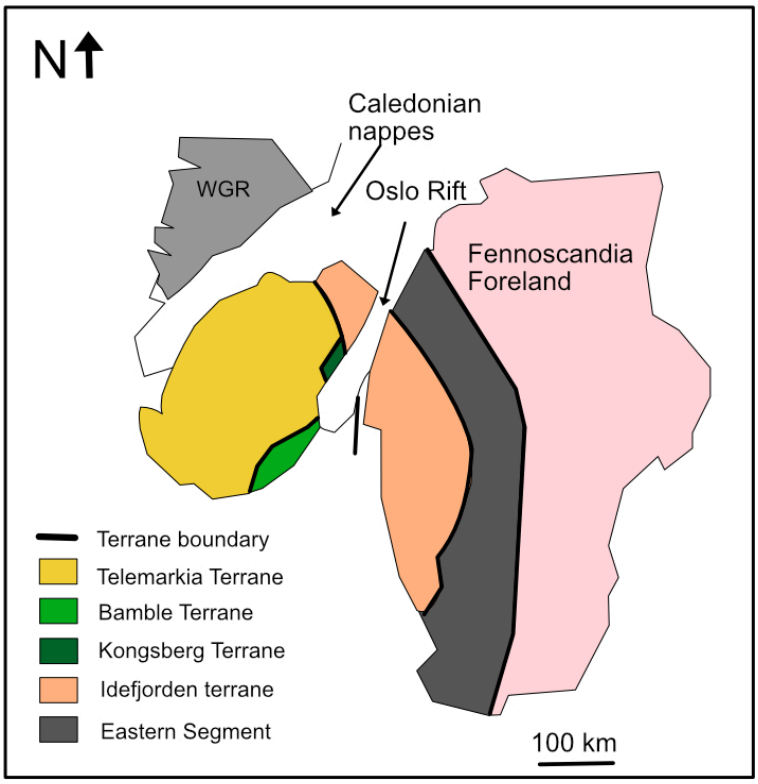

Fig. 5. Sveconorwegian orogenic belt divided into four terranes separated by shear zones. Modified from Bingen et al. (2008b).

Slagstad et al. (2013) challenged the classical interpretation of a continent-continent collision by demonstrating voluminous subduction related magmatism and restricted high-grade metamorphism. Slagstad et al. (2013) presented the SMB but it was studied in detail by Coint et al. (2015) and described as a 10 000 km^2 N-S trending magmatic belt consisting of unmetamorphosed calc-alkaline granitic batholiths that was much more voluminous than previously assumed (Fig. 4, Coint et al., 2015). Magmatism in the SMB was dated to start at 1070-1060 Ma and to end at approximately 1020 Ma, with peaks at 1050 and 1030 Ma. The main rocks in the SMB is porphyritic biotite granites, leucogranites and xenolith-rich zones, with coarse-grained to pegmatitic texture. The rocks are undeformed and unmetamorphosed, and only weakly foliated except from xenolith-rich zones (Coint et al., 2015). The new model proposed that the Sveconorwegian orogeny reflects a long-lived accretionary orogeny (Slagstad et al., 2013; Coint et al., 2015). Coint et al. (2015) described the undeformed voluminous magmatic body, and more localized metamorphism different from metamorphism related to continent-continent collision. Mafic underplating was mentioned as a potential heat source for the magmatism (Coint et al., 2015).

Magmatism in the SMB ceased at 1020 Ma and was followed by widespread and bimodal magmatism between 990 and 920 Ma with emplacement of the HBG and the Rogaland Igneous Complex (Fig. 4, Coint et al., 2015; Slagstad et al., 2018). HBG are abundant in the Sveconorwegian orogeny and represents relatively large isolated bodies throughout the orogeny (Auwera et al., 2008; Slagstad et al., 2018). HBG granites are dominated by intermediate to granitic composition with rare mafic enclaves. They are described as ferroan, metaluminous and typical A-type granites produced by partial melting of lower crustal sources (Auwera et al., 2008; Auwera et., 2011). According to Bingen et al. (2008b) the HBG granites are considered as a result of post-orogenic collapse, while Slagstad et al. (2013) and Slagstad et al. (2018) suppose extension in an active continental margin. HBG suite and the Rogaland Igneous Complex have corresponding ages from 950-950 Ma for both granitic and mafic magmatism. Slagstad et al. (2018) suggest that the corresponding ages for bimodal magmatism are a result of underplating. Anyhow, Slagstad et al. (2018) signify that there is no significant evidence for crustal thickening.

2.3 The evolution of Baltica from the Neoproterozoic to the Cambrian

The supercontinent Rodinia lasted for about 150 Ma years before it started to break up. In the period from c. 825 Ma and 740 Ma widespread continental rifting occurred with episodic magmatic events at c. 825 Ma, c. 780 Ma and c. 750 Ma (Li et al., 2008).

From approximately 615 to 570 Ma rifting and continental break-up resulted in the formation of the Iapetus Ocean. The opening started with the separation of Laurentia and Baltica and proceeded with opening between Laurentia and Amazonia (Li et al., 2008). At approximately the same time as the rifting started (c. 615 Ma), the NE margin of Baltica was a part of the Timanian orogeny and the margin remained active until late Cambrian times. The western and southern margins of Baltica became passive at c. 550 Ma (Slama and Pedersen, 2015).

Around 540-530 Ma Gondwanaland was completely formed and covered more than 90° of latitude (Li et al., 2008; Torsvik and Cocks, 2005). A long period of peneplanation and glacial erosion of Baltica in the Neoproterozoic formed a barren land with limited vegetation and flat topography (Slama and Pedersen, 2015).

2.4 The Scandinavian Caledonides

The Iapetus ocean reached its largest width at c. 480 Ma and by this time Baltica was located in southerly latitudes separated from Gondwana and Laurentia. During Ordovician to early Silurian times Baltica had a complex travel path including northward drifting and anticlockwise rotation towards equatorial position (Corfu et al., 2014; Torsvik and Cocks, 2005). This period involved several phases of ophiolite emplacement, arc magmatism and accretionary events. Gradually the Iapetus ocean closed and resulted in the major Scandian oblique continent-continent collision between Laurentia and Baltica in Silurian to early Devonian times, which formed the Caledonian orogeny (Fig. 6, Torsvik and Cocks, 2005; Corfu et al., 2014). The Baltican margin was subducted beneath Laurentia down to eclogite facies depths. Metamorphic conditions in the Western Gneiss Region reached more than 28 kbars/750° in the NW parts (Hacker et al., 2010). Ultra-high-pressure minerals like micro diamonds and coesite inclusions in garnets indicate burial to 100 km (Hacker et al., 2010). The continent collision emplaced parts of the previously formed passive margin as well as oceanic and island arc terranes from the Iapetus ocean onto the Baltican margin. The nappes rest on a basal décollement zone that acted as the sole thrust when the nappes were transported hundreds of kilometres from the collision zone towards the foreland (Fossen, 2010a). The E- to SE-vergent nappes were involved to varying degrees in the collision as reflected by varying metamorphic grades. The Caledonian nappes are traditionally grouped as Lower, Middle, Upper and Uppermost Allochthones (Roberts, 2003). Lower and Middle allochthones originate from Laurentia and upper and uppermost allochthones originate from the Iapetus ocean. The nappe stratigraphy is not straight forward and in several places the allochthones are found in a more complex order. They consist of both metasedimentary and metaigneous rocks bounded by major thrusts, extensional faults and strike-slip faults (Corfu et al.,2014).

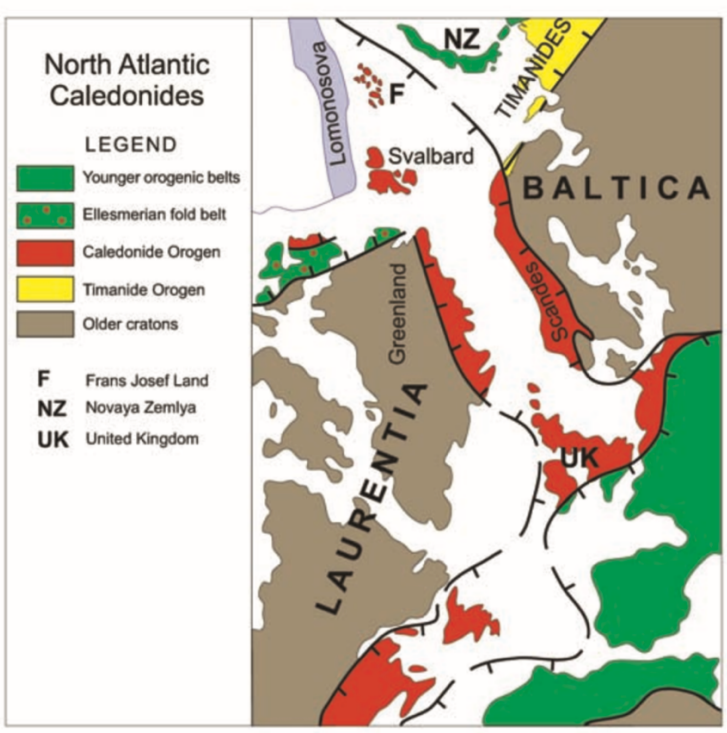

Fig. 6. The north Atlantic Caledonides (Gee et al., 2008).

2.4.1 Post-collisional extension

In the Devonian, extension resulted in the thinning of the orogenic crust, as well as large Devonian sedimentary basins and rapid exhumation of the eclogite facies rocks in the WGR (Corfu et al., 2014; Fossen, 2010a). Extensional structures are well preserved in the North Atlantic Caledonides and most of them are dated to 403-380 Ma (Fossen, 2010a). $^{40}Ar/^{39}Ar$ data shows that the change from contraction to extension was quick and happened between 408 to 402 Ma (Fossen and Dunlap, 1989). The extension was concentrated in the central and southern parts of the orogeny, with a main transport direction towards the hinterland (Fossen, 2010). Fossen (1992, 2000, 2010a) separated the extensional structures into three main stages: Mode I, Mode II and Mode III (Fig. 7).

- Mode I involved NW movement of the orogenic wedge and reactivation of the basal décollement zone. Top-to-NW fabrics, such as S-C structures, shear bands, asymmetric boudins, cleavage and asymmetric folds, along the basal décollement zone overprint the contractional top-to-SE structures (Fossen, 2000).
- Mode II deformation involved crustal collapse by formation of hinterland-dipping large-scale, low-angle extensional shear zones. The shear zones are cutting through the basal décollement zone and into the Baltican crust. An example of this is the

Nordfjord-Sogn Detachment Zone and the Hardangerfjord Shear Zone. The Nordfjord-Sogn Detachment Zone is the largest of these extensional shear zones and a 100 km displacement has been suggested (Fossen, 2000).

- Formation of hinterland-dipping shear zones proceeded with brittle faulting in the late Devonian and is termed mode III extension. These are high-angle structures formed as the crust cooled through the brittle-ductile transition zone. Semi-ductile elements in addition to cohesive fault rocks are important indicators for brittle-ductile deformation. West of Bergen, the fractures reached the brittle-ductile transition at 395 Ma based on U-Pb ages of sphene (Fossen, 2000; Larsen et al., 2003)

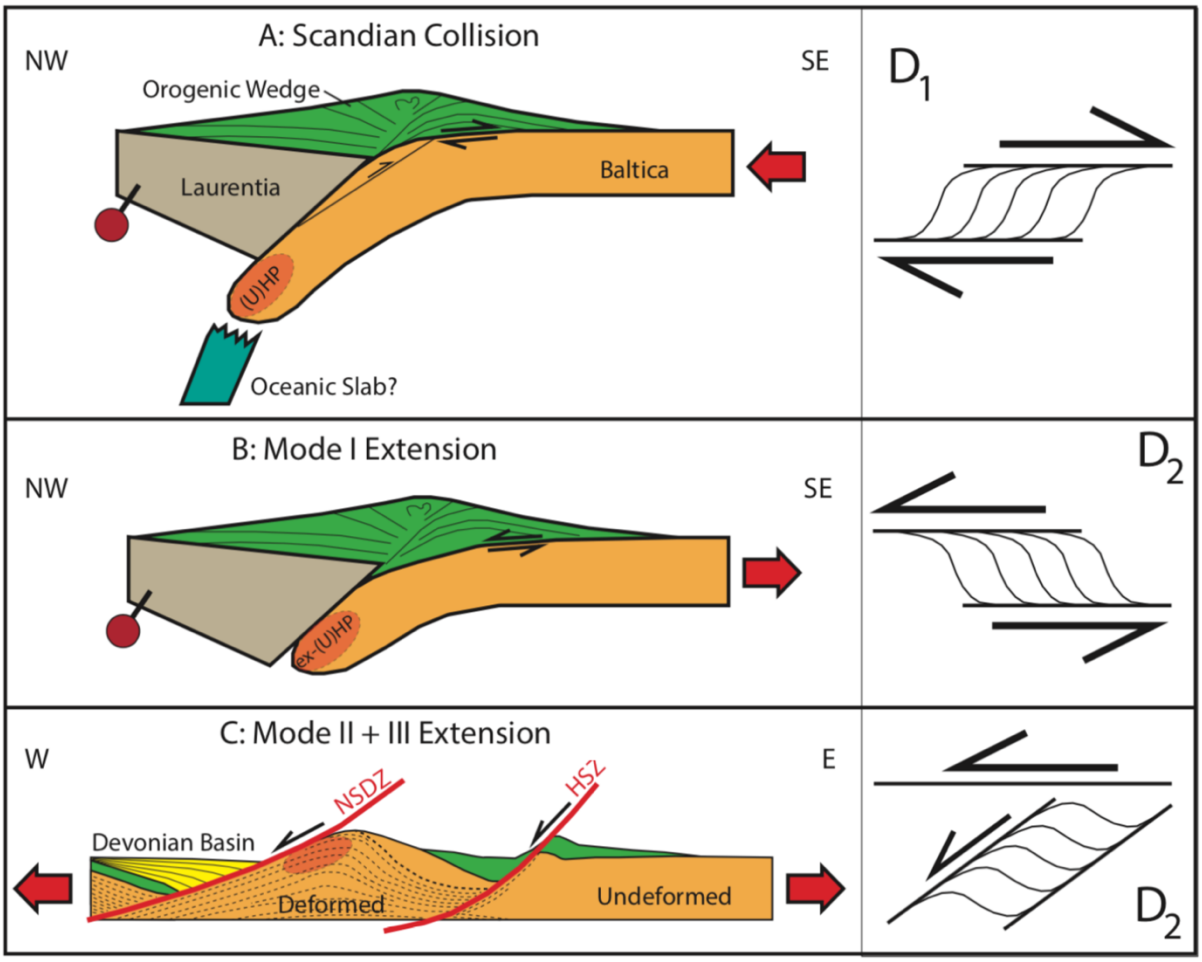

Fig. 7. Structural and kinematic situation in the Scandinavian Caledonides during Mode I, II and III extension. a) Continent-continent collision. b) Mode I, backsliding and NW movement of the orogenic wedge. c) Mode II and III, Crustal collapse with formation of NW dipping shear zones. Modified from Wiest (2016).

2.5 Geology of the study areas

2.5.1 The Øygarden Complex

The Øygarden Complex is located west of Bergen and is a well-exposed tectonic basement window, positioned in the central part of the Bergen Arc System. The Øygarden Complex has mylonitic contact to the Bergen Arc System which comprises of strongly folded units of Caledonian nappes (Fig. 8, Fossen and Rykkelid, 1990; Fossen and Dunlap, 1998; Wiest et al., 2018).

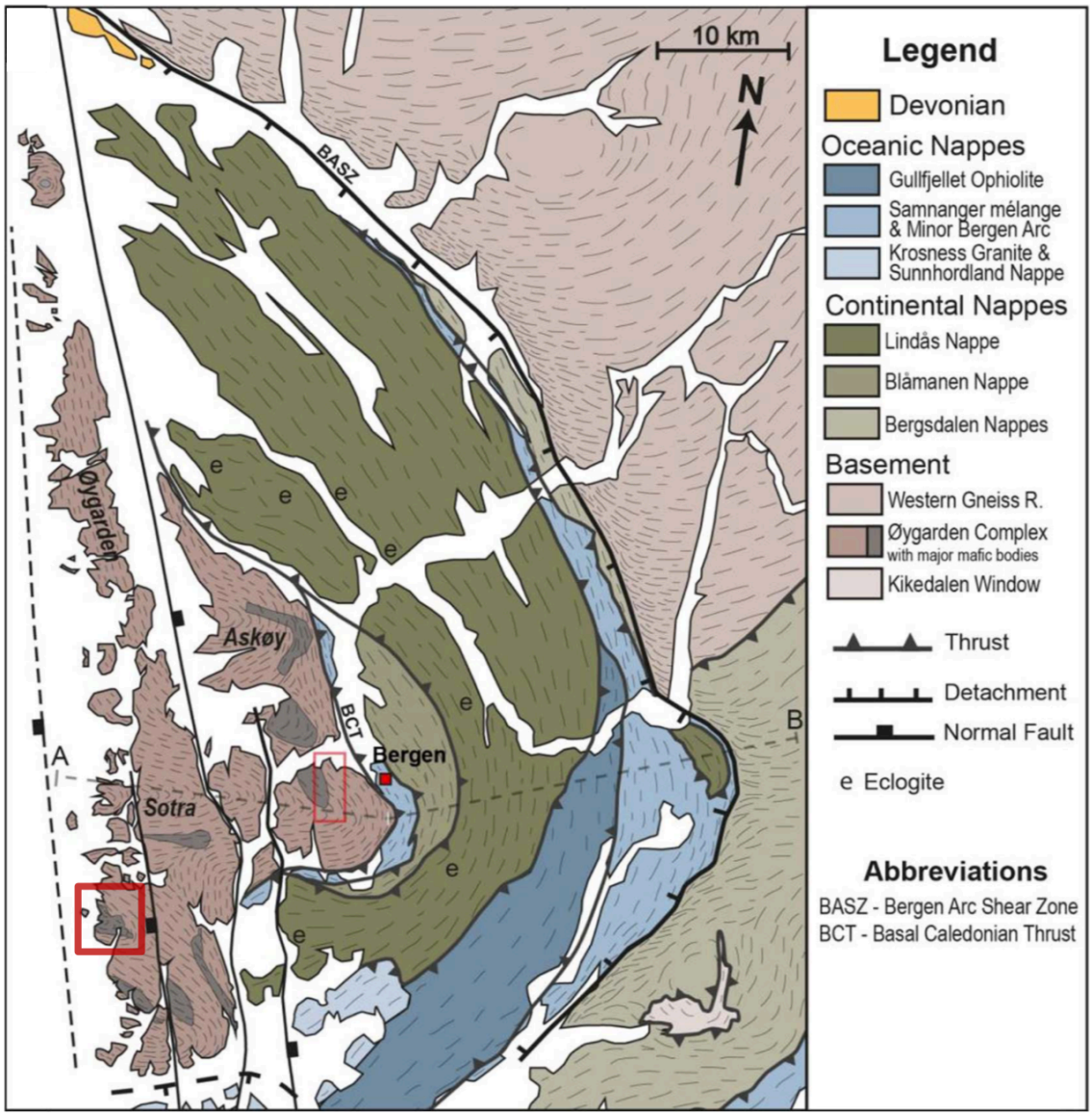

Fig. 8. The Øygarden Complex and the Bergen arc system (Wiest et al., 2018). The study area of this thesis is located in the westernmost part of the Øygarden Complex, marked with a red box.

The primary rocks of the Øygarden Complex are granitic, granodioritic and tonalitic gneisses and bodies of amphibolite and metagabbro (Bering, 1984; Larsen et al., 2003; Wiest et al., 2018). New geochronological U-Pb data from the eastern Øygarden Complex show mainly Sveconorwegian metaigneous rocks that intruded Telemarkian granitic basement (Wiest et al.,2018). Telemarkian granitic basement was dated to 1506 ± 5 Ma. Sveconorwegian magmatism can be separated into two phases, correlating with ages to the SMB. Hornblende biotite granite and gabbro intrusions have crystallization ages 1042 ± Ma and 1041 ± 3 Ma, while younger leucrogranitic intrusions were dated at 1027 ± 4 Ma and 1024 ± 6 Ma and at ca. 1022 Ma (Wiest et al., 2018). In the western part of the Øygarden Complex no U-Pb data are published so far. Rb-Sr dating from Sturt et al. (1975) shows ages ranging from 1750 Ma to 470 Ma.

The gneisses of the Øygarden Complex are dominated by pervasive S-L tectonites, and foliation is commonly anastomosing (Fossen, 1998). The foliation is generally E- dipping with constant E to SE plunging stretching lineation's (Larsen et al., 2003; Fossen, 1998). Major large-scale folds characterize the area such as the E-W trending Sotra and Sund antiforms that disturb the generally N-S parallel gneiss fabric (Larsen et al., 2003). Parallel to the streching lineations in areas with high strain, non-coaxial deformation with a top-to-W sense of shear is recognized (Fossen and Rykkelid, 1990). In the eastern part of the Øygarden Complex top-to-E sense of shear is investigated by Wiest et al. (2018) and propose the Øygarden Complex as a Devonian extensional core complex.

The Øygarden Complex is dominated by amphibolite-facies metamorphism overprinted by greenschist-facies metamorphism where brittle and ductile structures coexist (Larsen et al., 2003). The basement cooled rapidly from around 500°C at c. 404 Ma to around 350°C shortly after during top-to-NW transport of the allochthonous units (Fossen and Dunlap, 1998).

2.5.2 The Hardanger area

The geology of the Hardanger area is dominated by autochthonous Baltican basement partly overlain by Cambro-Silurian metasedimentary rocks and Caledonian nappes (Solli et al., 1978; Johannessen et al., 2013). The autochthonous basement is of Proterozoic age and consists of 1500 Ma gneisses and older migmatites which are intruded by a number of Sveconorwegian magmatic rocks (Bingen et al., 2005; Bingen et al., 2008b; Fossen and Hurich, 2005). Metarhyolites and granites are dated to around 1500 Ma in the Hardanger area and correlate the area to the Telemarkian domain and to the Sauda- Suldal region in SW Norway (Bingen et al., 2005; Roberts et al., 2013). Large parts of the basement are occupied by granitic gneisses with granitic to granodioritic composition (Sigmond, 1975; Solli et al., 1978; Sigmond, 1998). There are no published geochronological data of the granitic bodies. The Hardangerfjord shear zone is the largest tectonic structure in the Hardangerfjord region and is a 600 km-long low-angle NE-SW trending extensional structure located along the Hardangerfjord in SW Norway (Fig. 9, Fossen and Hurich, 2005). The area north of the Hardangerfjord shear zone is dominated by Caledonian allochthonous units (Lower and Middle allochthones) and the area SE of the Hardangerfjord shear zone the basement is generally autochthonous (Fig. 9). The autochthonous basement is primarily not affected by Caledonian deformation except for the uppermost part. In the NW part of the Hardangerfjord shear zone the Caledonian deformation is strong and widespread (Fossen and Hurich, 2005).

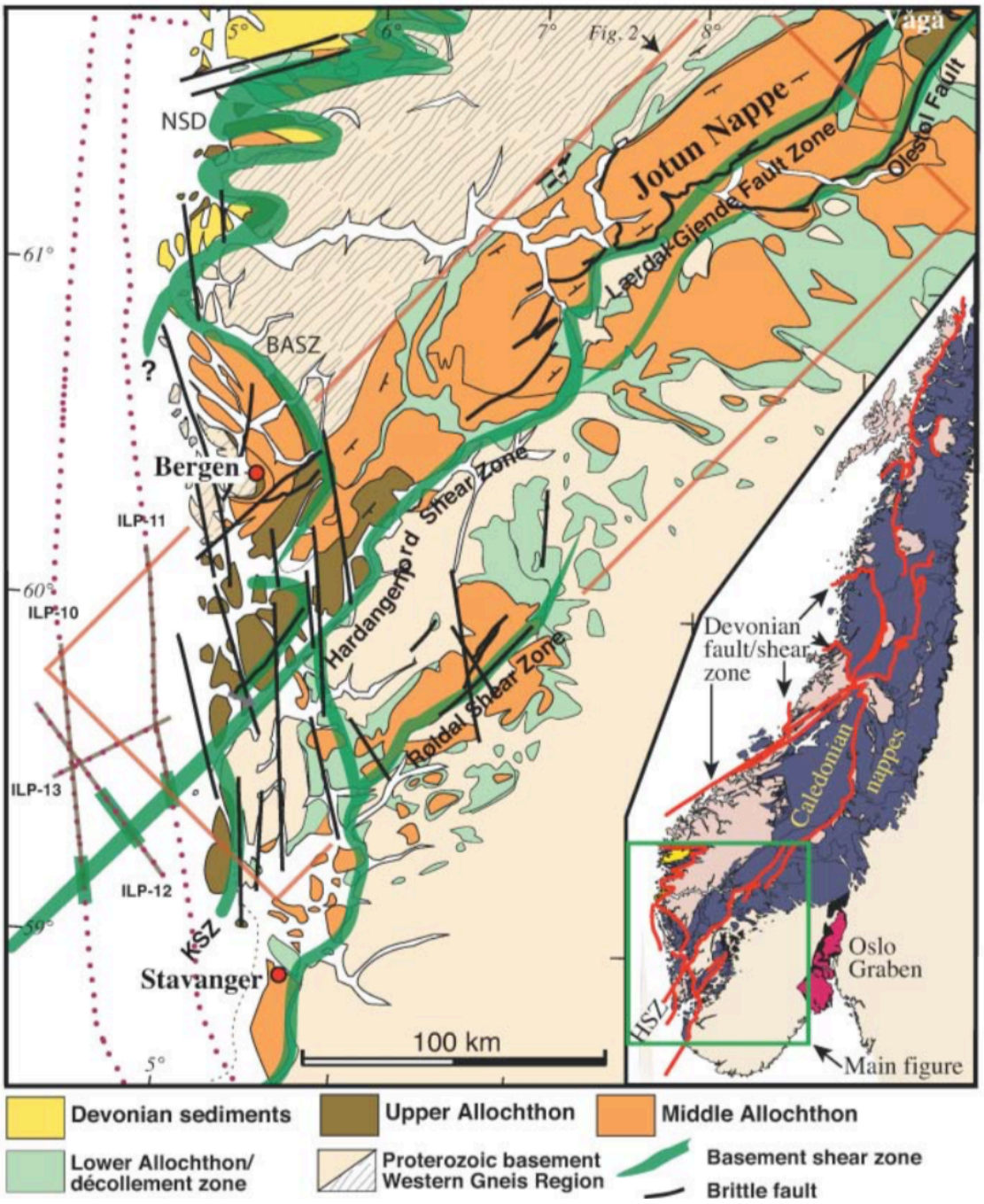

Fig. 9. Geological map of SW Norway and the Hardanger fjord area. Allochthonous units dominate north of the Hardangerfjord shear zone and Proterozoic basement dominates south of the Hardangerfjord shear zone (Fossen and Hurich, 2005).

2.5.3 The Gulen area

The Gulen area is located in the southern parts of the WGR. The WGR consists of rocks mainly formed during the Gothian orogenic period (1.52-1.66 Ga), and migmatitic orthogneisses with dioritic to granitic composition are the most prominent rock types (Skår and Pedersen, 2003). The southern part of WGR was intruded by plutons and dykes during the late stage of the Sveconorwegian orogeny (Skår and Pedersen, 2003). The WGR was strongly deformed and metamorphosed during the Caledonian orogeny (Hacker et al., 2010). A U-Pb zircon date from Hisarøya, yielded a discordia line with lower intercept at 987 ± 10 Ma, which is interpreted to date a Sveconorwegian granulite facies event (Røhr et al., 2004). The Gulen area is described as a metamorphic core complex in the footwall of NSDZ formed during post-collision extension of the Caledonian orogeny (Wiest et al., 2019).

Chapter 3: Principles of U-Pb zircon geochronology

U-Pb isotope dating of zircons is a valuable method because of zircons high U and Th contents, high mineral stability and its presence as an accessory mineral in both magmatic, metamorphic as well as sedimentary rocks (Corfu et al.,2003; Yuanbao and Yongfei, 2003). Zircon ($ZrSiO_{4)}$ is a tetragonal orthosilicate mineral in which SiO_4 tetrahedra sharing their edges with ZrO_8 (Harley and Kelly, 2007), and has a density of 4.66 g/cm^3 and a hardness of 7.5. The U-Pb system is mainly applied to date magmatic and high-grade metamorphic rocks because of zircons high closure temperature (900°C, Yuanbao and Yongfei, 2003). Additionally, zircon is extremely variable in morphology and texture reflecting the geological history of the mineral (Corfu et al., 2003). Magmatic zircons are commonly euhedral with oscillatory zoning with Th/U ratios around 1, while metamorphic zircons have more complex structures, often rounded, unzoned or sector zoned with Th/U ratios below 0.1 (Corfu et al., 2003). Analyses of zircons texture are essential for the best interpretation of U-Pb zircon ages.

The U-Th-Pb system consists of three radiogenic isotopes that decay into their stable daughter isotopes: ^{232}Th decays to ^{208}Pb with a half-life of 14 Ga, ^{238}U decays to ^{206}Pb with a half-life of 4.5 Ga and ^{235}U decays to ^{207}Pb with a half-life of 0.7 Ga (Davis et al., 2003; Allegre, 2008). The decay chain involves several intermediate products and short lived isotopes (Harley and Kelly, 2007). By measuring isotopic ratios one can calculate two radiogenic ages (Eq. 1 and 2, Harley and Kelly, 2007; Schoene, 2014). In a closed system all three ages will agree within the errors of measurements (Harley and Kelly, 2007). Also, a third equitation can be constructed by dividing eq. 2 on eq. 1 by using the modern-day ratio ($^{235}U/^{238}U$=137.88), then the measured $^{207}Pb/^{206}Pb$ can be used to directly calculate a date (Schoene, 2014). Non-radiogenic Pb (common lead) is essential to correct for, as this would lead to incorrectly old age estimates (Harley and Kelly, 2007). Common lead problems are generally related to contamination during laboratory work or by sampling (Schoene, 2014).

$$^{206}Pb = {}^{238}U\,(e^{\lambda 238}-1) \qquad (1)$$

$$^{207}Pb = {}^{235}U\,(e^{\lambda 235}-1) \qquad (2)$$

The most establish concordia diagrams are the conventional concordia diagram (Wetherill, 1956) and Tera-Wasserburg diagram (Tera and Wasserburg, 1972). The Conventional concordia diagram plots $^{207}Pb/^{235}U$ versus $^{206}Pb/^{238}U$. $^{207}Pb/^{235}U$ and $^{206}Pb/^{238}U$ are

proportional to time and is formed as a curve by the difference between the half-lives of ^{235}U and ^{238}U. Concordant ages will plot along the concordia curve if the system has remained closed since the time of crystallization. Then the $^{206}Pb/^{238}U$, $^{207}Pb/^{235}U$ and $^{208}Pb/^{235}U$ ages will agree. Ages that experienced some form of open-system behaviour, do not plot along the concordia curve and are called discordant (Schoene, 2014). Discordant ages that underwent diffusion of Pb are used to construct a discordia line that intersect the concordia line twice and gives information about primary rock forming events and secondary metamorphic events (Mezger and Krogstad, 1997; Harley and Kelly, 2007).

The "Tera-Wasserburg" diagram plots $^{238}U/^{206}Pb$ against $^{207}Pb/^{206}Pb$ (Fig. 10). The intersect with the concordia curve gives the time and the y-intercept gives the initial $^{207}Pb/^{206}Pb$. The two different concordia diagrams are mathematically equivalent (Ludwig, 2012), but the Tera-Wasserburg diagram has some visual advantages over the normal concordia. Errors are much less correlated, so that the relative scatter is more visually in the Tera-Wasserburg diagram compared to the Conventional concordia diagrams (Ludwig, 2012.

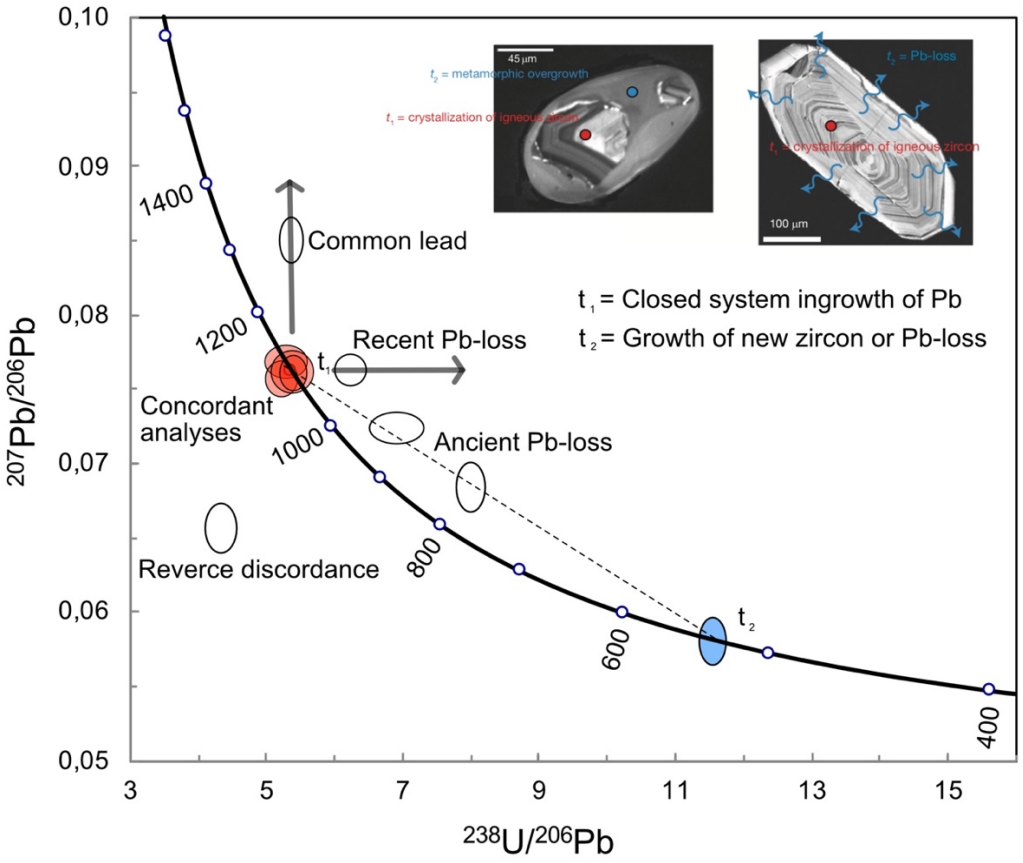

Fig. 10. Tera-Wasserburg diagram with concordant and discordant analyses. The cluster with concordant analyses and upper intercept represents the age of the photolith rock, while the lower intercept represents growth of new zircon or Pb-loss. Also, zircons with oscillatory zoning and metamorphic rim are shown on the figure. Modified from Schoene (2014).

SIMS analysis

Secondary ion mass spectrometry (SIMS) are used to measure the chemical and isotopic composition in zircons (Ireland and Williams, 2003). SIMS analysis are measurements relative to a standard. In SIMS a highly focused ion beam, typically O^- and O_2^-, is focused onto a polished sample surface, with targeted areas of 10 to 40 µm diameter and less than 4 µm deep (Fig. 11, Schoene, 2014). When the beam hits the sample, the atoms and molecules get liberated and a portion gets ionized. These secondary ions are then analysed by a mass spectrometer (Ireland and Williams, 2003). In the mass spectrometer the secondary ions run through the electrostatic analyser, and the magmatic sector and ends up in the detector based on their mass and charge. The combination of large radius magmatic sector and electrostatic analyser results in high mass resolution. High mass resolution is important to resolve isobaric interferences (Schoene, 2014).

SIMS analysis allowing numerous analyses to be performed within one single zircon grain. This is an advantage that make is possible to analyse different domains in the zircons. On the other hand, this method has lower analytical precision than ID-TIMS, but much better spatial resolution (Harley and Kelly, 2007).

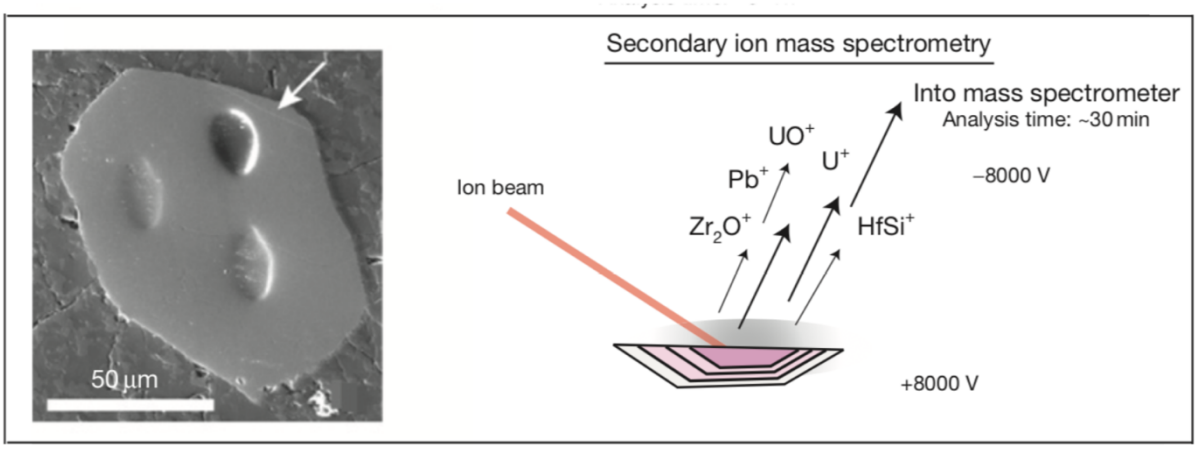

Fig. 11. Cartoon depicting secondary ion mass spectrometry analysis (Schoene, 2014).

Chapter 4: Methods

4.1 Fieldwork and sampling

Geological fieldwork was carried out in Telavåg, located on Sotra, west of Bergen (Fig. 14). The Telavåg area was mapped in detail during autumn 2018 and spring 2019. Standard mapping techniques were used: black and white topographic map, colour pencils, geological hammer and compass (Fieldmove clino). 131 outcrops where studied, and structural measurements were taken of linear and planar fabrics. In addition, outcrops were studied in Hardanger, from Kvandal to Valen south of Husnes. Sampling and outcrop observations was completed in the Hardanger area in the period from 25.06.18 to 29.06.18. In total, seven samples were selected for SIMS U-Pb zircon geochronology: four from the Hardanger area, two from Telavåg and one from the Gulen area. Thin sections were made of the seven samples to study mineral content and texture. Thin sections were prepared at the University of Bergen.

4.2 Sample preparation

Mineral separation

The seven samples were prepared at the University of Bergen. Rock samples were crushed to small slices using a hammer before the Fritsch Pulverisette 13 discmil pulverized the material to a grainsize finer then 315 μm (Fig. 12a). The crushed material was separated by Holman-Wilfley shaking table into heavy and light fractions (Fig. 12b). When the material was dried, a hand magnet was used on the heavy fraction to remove strong ferromagnetic minerals before the samples were put in the Frantz Magnetic Separator. The Frantz Magnetic separator was applied to separate magmatic heavy minerals (e.g. zircons and apatite) from weak ferromagnetic minerals, first with 0,6 V and then with 1.2 V with a constant 15° dip. Furthermore, two different types of heavy liquids were used to separate minerals with different density. Firstly, LST (Low toxicity Sodium heteropolytungstates) with a density of 2.9 g/ mL was used to remove quartz and feldspar (Fig. 12c). Then, DIM (Dilodomethane) with a density of 3.3 g/mL was applied to separate zircons from titanite and apatite. The separated minerals were afterwards cleaned with acetone and dried.

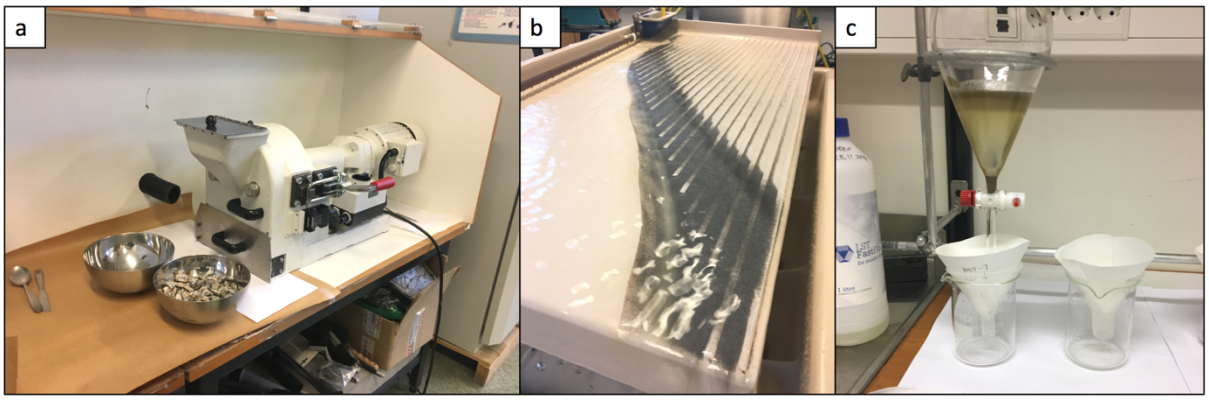

Fig. 12. a) The Fritsch Pulverisette 13 discmill and sample material before it became pulverized. b) Sample material on Holman-Wilfley shaking table, separating between heavy and light fraction. c) LST separating quartz and k-feldspar from heavy minerals.

Mount preparation

All zircons were handpicked under a Zeiss microscope from their mineral separates and systematic added onto a mount, approximately 80 zircons for each sample. Sample TSS-1 had poor zircons, and the picking was demanding. Further mount preparations were completed at the Nordsim laboratory in Stockholm.

Zircon imaging

Cathodoluminescence, transmitted light and reflected light images were taken at the University of Bergen on a Zeiss microscope. The three different images were used to compare and study the zircons, and to determine spot localities. Transmitted ligth and reflected images were used to exclude areas with inclusions, metamictization and fractures, while cathodoluminescence images were used for textural interpretations. Around 20-30 spots were selected for analyses for each sample. Only three spots were chosen for sample TSS-1.

4.3 SIMS analysis

U-Th-Pb analyses of zircons were preformed using a Cameca IMS 1280 instrument at the Nordsim laboratory in Stockholm. Geochronological analyses follow routine protocols described by Whitehouse et al. (1999) and Whitehouse and Kamber (2005). Sims data are reported in appendix 1.

Data processing

Isoplot was used for data processing, and the SIMS data were plotted in Tera-Wasserburg concordia diagram. Concordia ages were calculated for all analyses, plotted with 1σ error ellipse, whereas the presented ages have 2σ error. For some ages lower and upper intercept ages were calculated. The mean square of weighted deviated (MSWD) and probability values are of both equivalence and concordance. Both corrected and uncorrected ages are used for the datasets. Uncorrected data were reported when common lead concentrations are low, otherwise corrected ages were used. Mean ages were calculated for all Concordia ages.

Chapter 5: Results

The first part of this chapter describes field results from Sotra. Part two presents geochronological data and petrology of samples from Sotra, Hardanger and Gulen.

5.1 Field observations from the Telavåg area

The lithologies observed in the Telavåg area include granitic gneisses, metagabbros and amphibolites, pegmatites and banded gneisses. The area is dominated by one major granitic gneiss body located in the northern part of the study area and one major body of gabbroic rocks in the center of the study area. Banded gneisses are found in a wide shear zone in the southern part of the study area. Pegmatites are observed in all of the units. A geological map and cross section are shown in Fig. 13 and 14 as a result of detailed field mapping. List of outcrop and map of localities are shown in appendix 2 and appendix 3. Appendix 4 and 5 shows measurements of planar and linear fabric.

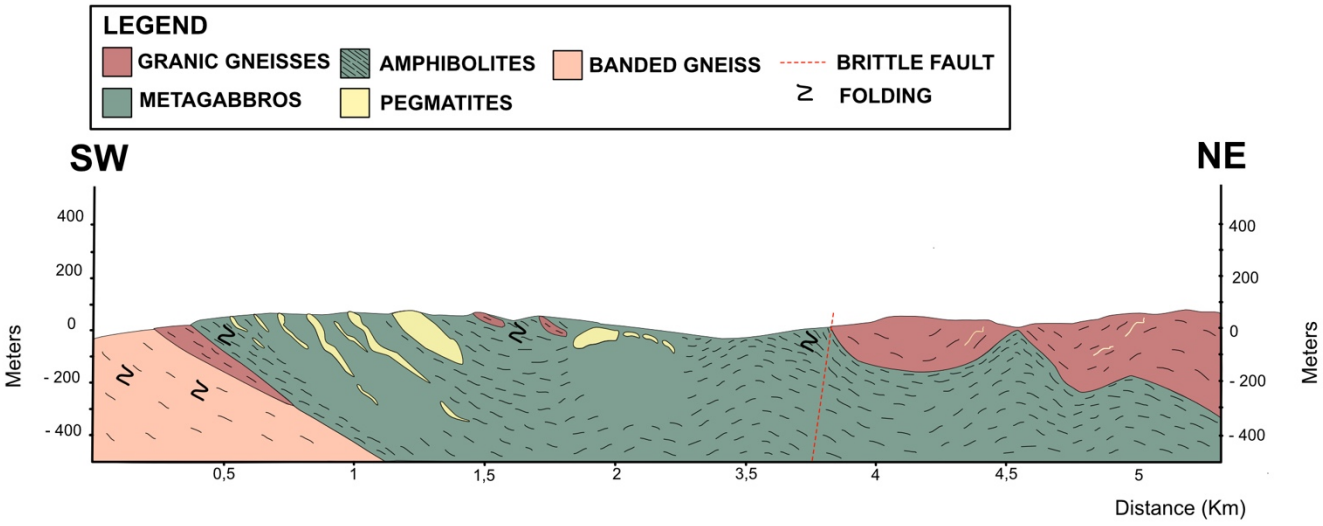

Fig. 13. Simplified cross-section from SW to NW.

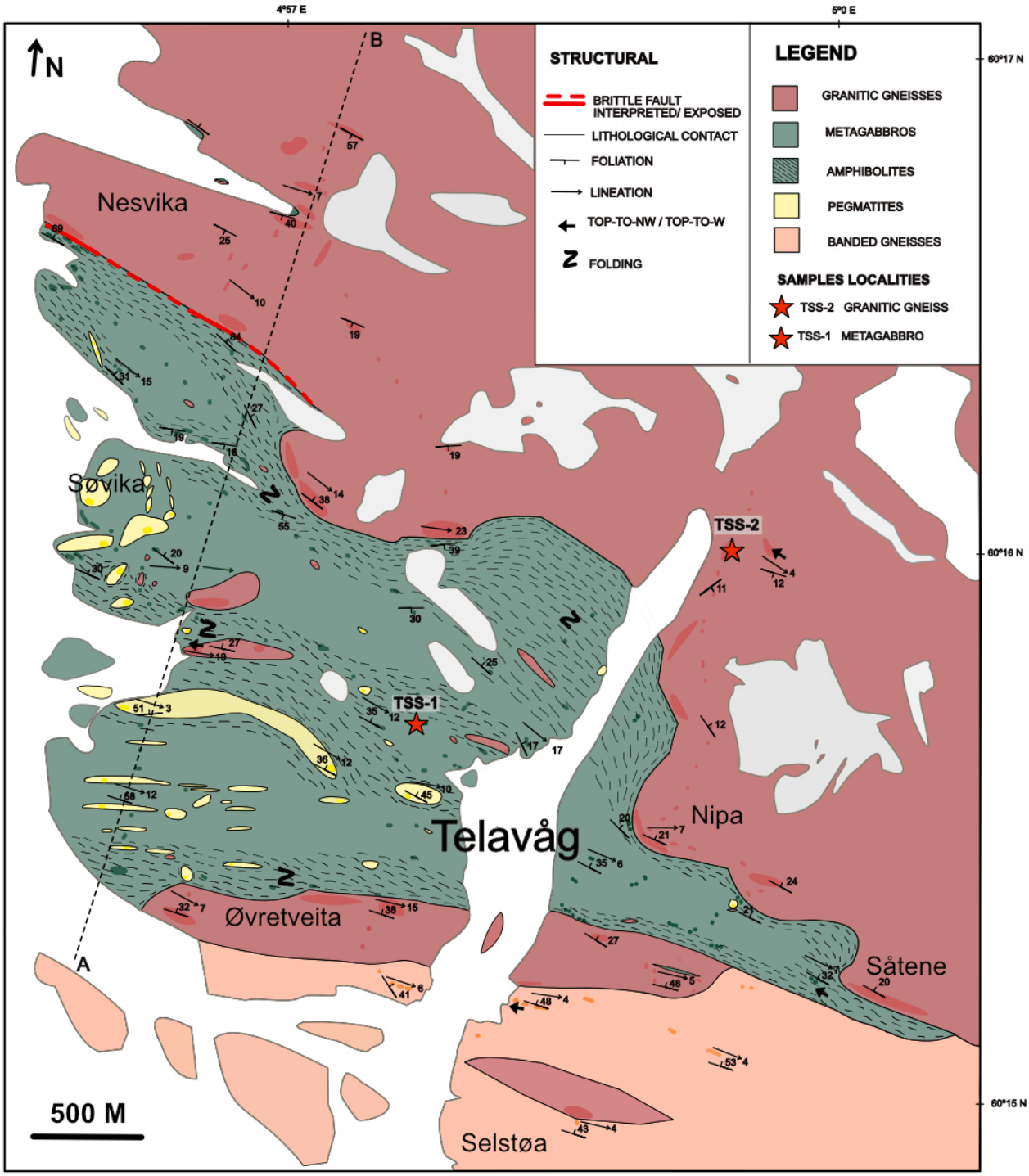

Fig. 14. Geological map of the Telavåg area. Outcrops are highlighted with colours. A number of representative foliation and lineations measurements are added on the map.

5.1.1 Petrology

Granitic gneiss

Granitic gneisses cover a large area in Telavåg. One main body is observed, and a number of minor bodies and dikes (Fig. 15a). The granitic gneiss is well exposed occupying topographic highs and forms a characteristic landscape with limited vegetation. The unit can generally be described as homogenous, except from local shear zones and outcrops with pegmatite intrusions (Fig. 15b). Texture is inequigranular consisting of medium to coarse grained k-feldspar and medium grained plagioclase, quartz and biotite. In some places the content of biotite is low (<5 %). The composition is generally monzogranitic, but syenograntic and granodioritic composition can be observed with diffuse transitions. The unit is dominated by a strong and characteristic L-fabric and is commonly weakly foliated (Fig. 16a). Shear zones have strong S = L fabrics. At Selstøa, in the southern part of the mapping area, the granite is strongly mylonitized (Fig. 16b). At Øvretveita and north of Selstøa the granitic gneiss has strong S = L fabrics. In area affected by high strain, anastomosing foliation can be observed (Fig. 16c). In several places, discontinuous shear zones of cataclastic phyllonites are observed in the major granitic body, consisting of fine-grained biotite and quartz. Ultracataclasite is also observed in the granitic gneiss (Fig. 16d).

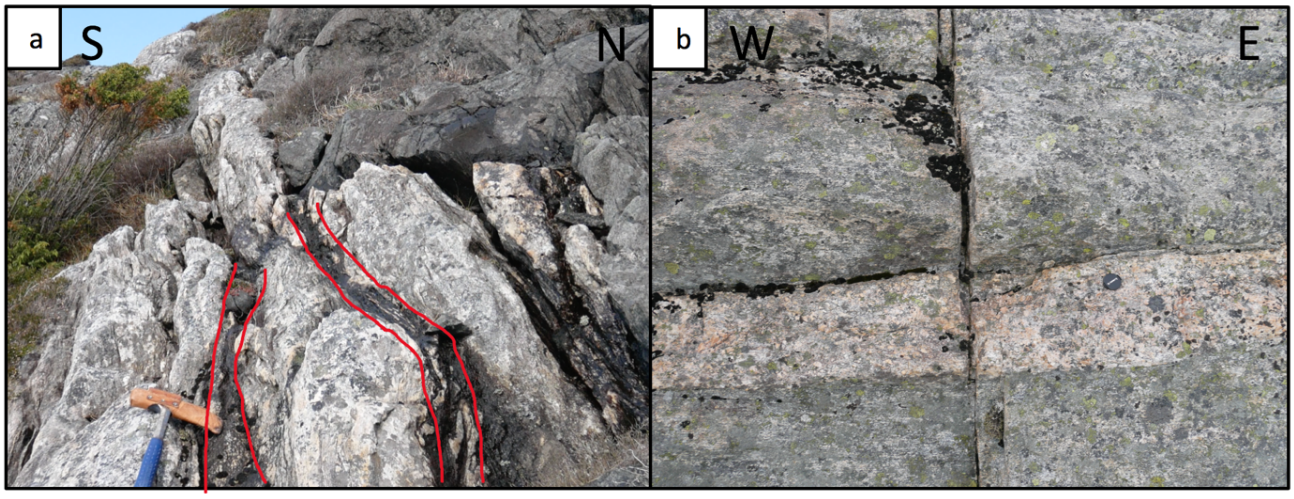

Fig. 15. a) 0.5-1 m wide intrusion of granitic gneiss in the gabbroic body. Two small layers of amphibolite in the intrusion (Loc. 94). b) Pegmatite dike in the granitic gneiss (Nesvika).

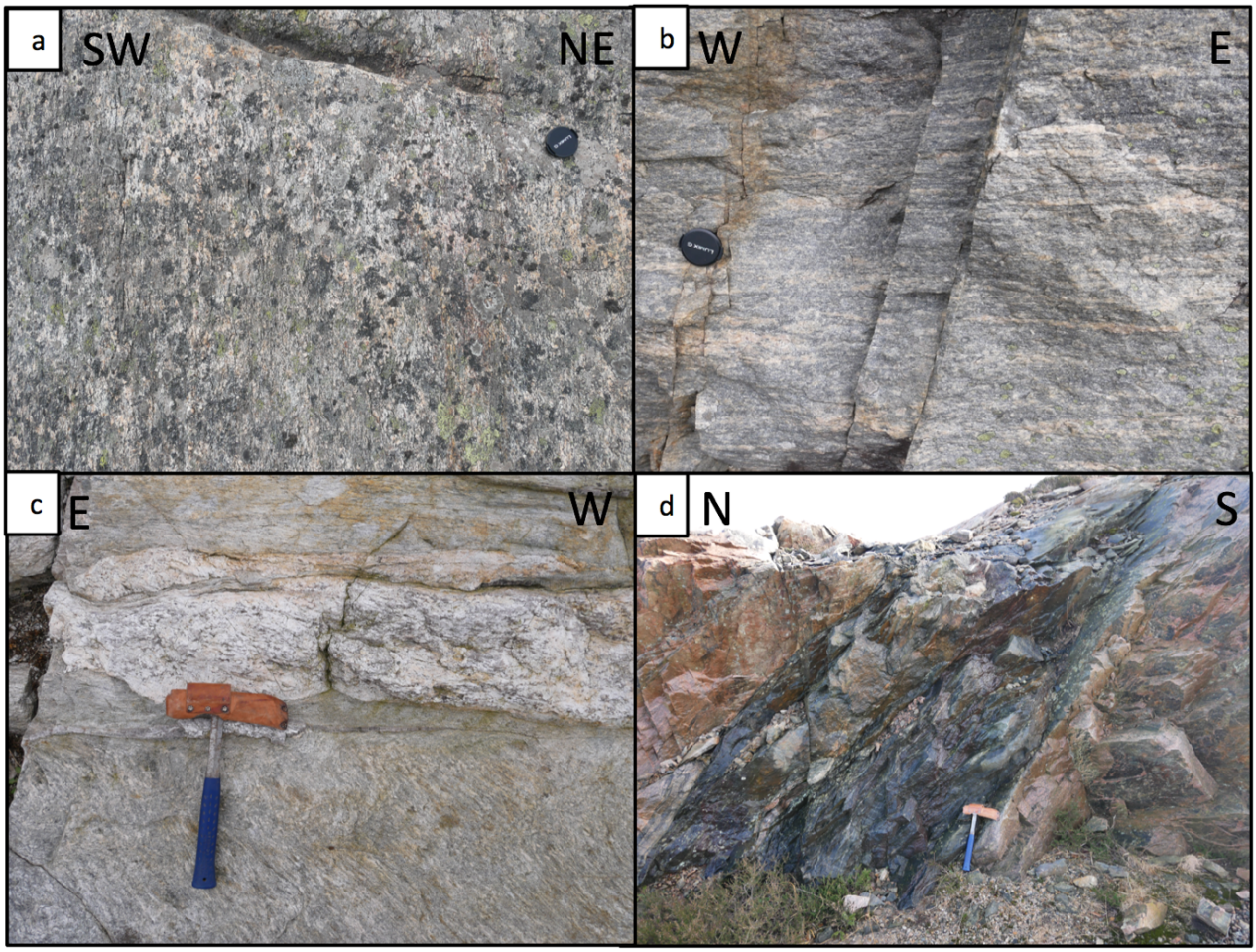

Fig. 16. a) Granitic gneiss with L>S fabric (Loc. 122). b) Mylonitic granitic gneiss (Loc. 128).
c) Tonalitic pegmatite in the granitic gneiss. The granitic gneiss has anastomosing foliation. (Loc. 70).
d) Granitic gneiss with 1-meter zone of ultracataclasite, parallel to the foliation (Loc. 54).

Amphibolites and metagabbros

A large heterogenous body of gabbroic rocks are located in the central part of the study area. The gabbroic rock has been transformed into metagabbros or amphibolites. The unit is generally covered by dense vegetation and poorly exposed, but well exposed outcrops can be studied close to the sea and in roadcuts. Metagabbros are found in the inner part of the gabbroic body and have diffuse transitions to the amphibolites. Metagabbros are also found near pegmatites in Søvika and north of Øvretveita. Metagabbros are equigranular, medium grained and consist mainly of plagioclase and hornblende (Fig. 17a). At some localities, layers with varied composition and grain size can be observed and may indicate primary layering (South of Nesvika and NW of Øvretveita, Fig. 17b). The layers are parallel to the foliation. At several localities secondary minerals such as chlorites occur.

In areas affected by high strain, close to the granitic gneiss boundaries and in local shear zones within the gabbroic rock body, amphibolites are present. The amphibolites are commonly dark with a similar mineralogy as metagabbros recrystallized into fine-grained minerals (Fig. 17c). Plagioclase veins are present in the amphibolites, ranging in size from 1 to 5 cm. The amphibolites are characterized by a marked S=L fabric with anastomosing foliation. In Søvika, I observed agmatites with intermingling layers of granitic veins and metagabbros (Fig. 17d).

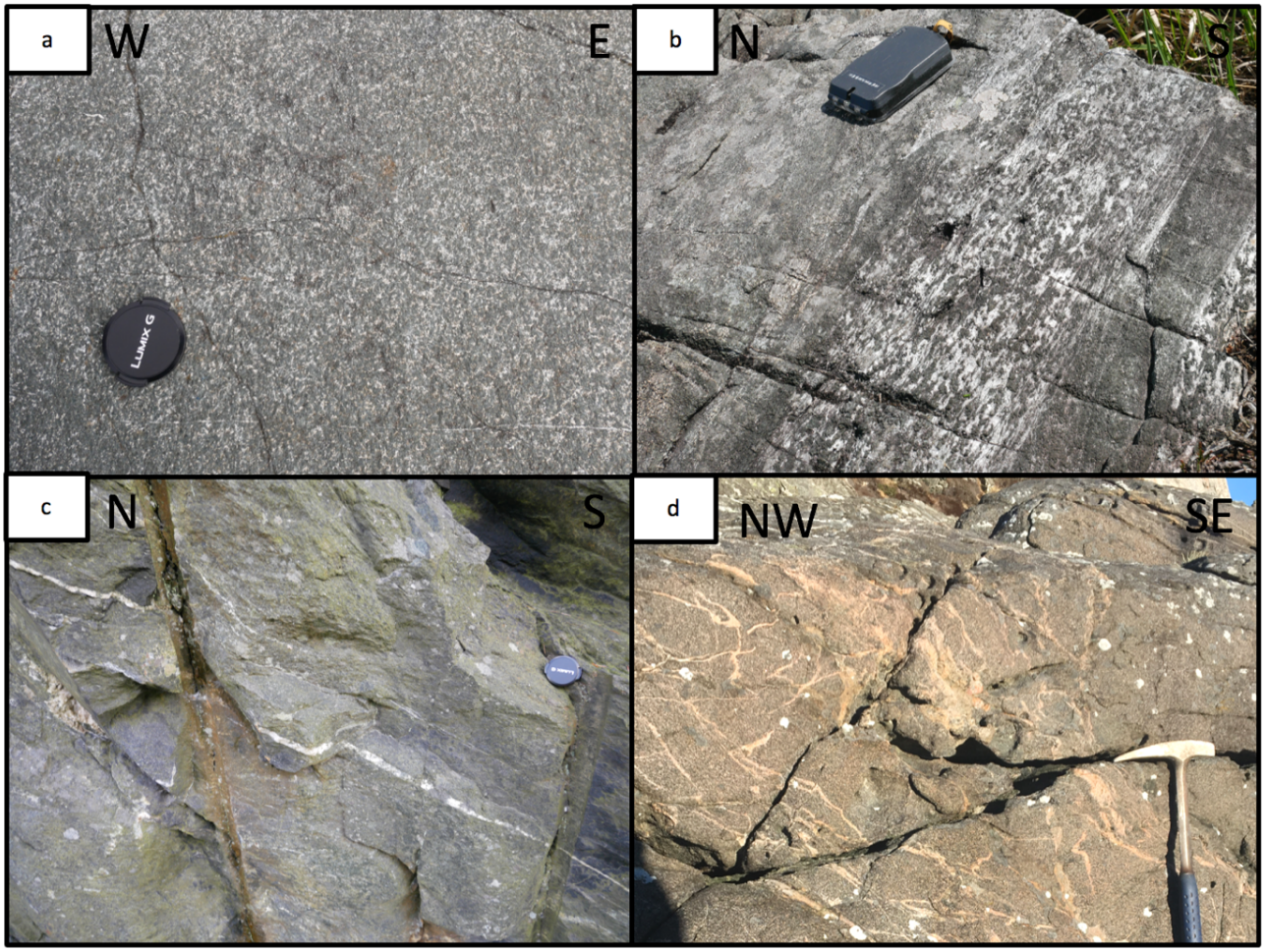

Fig. 17. a) Outcrop of metagabbro (loc. 121). b) Layer of coarse grained metagabbro surrounded by medium grained metagabbro. Layer has the same orientation as the foliation (loc. 96). c) Amphibolite with plagioclase veins (loc. 8). d) Agmatite with intermingling layers of granitic veins and metagabbros (loc. 66).

Pegmatites

Pegmatites are observed, intruding all lithologies in Telavåg. The pegmatites bodies are heterogenous and the size of the bodies can vary greatly from small dikes to voluminous bodies (10 of meters). The pegmatitesve mostly granitic composition but can range from alkali k-feldspar rich to tonalitic composition (Fig. 18a). The unit has mostly minor content of biotite, but a number of localities with high content of biotites have strong S-L fabrics. The grainsize is in general pegmatitic but grades locally into medium grained. Major pegmatites are observed in the gabbroic rocks making a characteristic landscape as small peaks (Fig. 18b). At Søvika the major pegmatites are folded and show boudinage structures. North of Øvretveita the pegmatites are W-E elongated (parallel to foliation, Fig. 18c). In the granitic gneiss the pegmatites are generally smaller and predominantly appear as dikes. The dikes can range in size from a few centimetres to a few meters and are parallel to the foliation. The area around Nesvika has a high occurrence of pegmatite intrusions. Xenoliths of amphibolites are observed in the pegmatites at several localities (Fig. 18d).

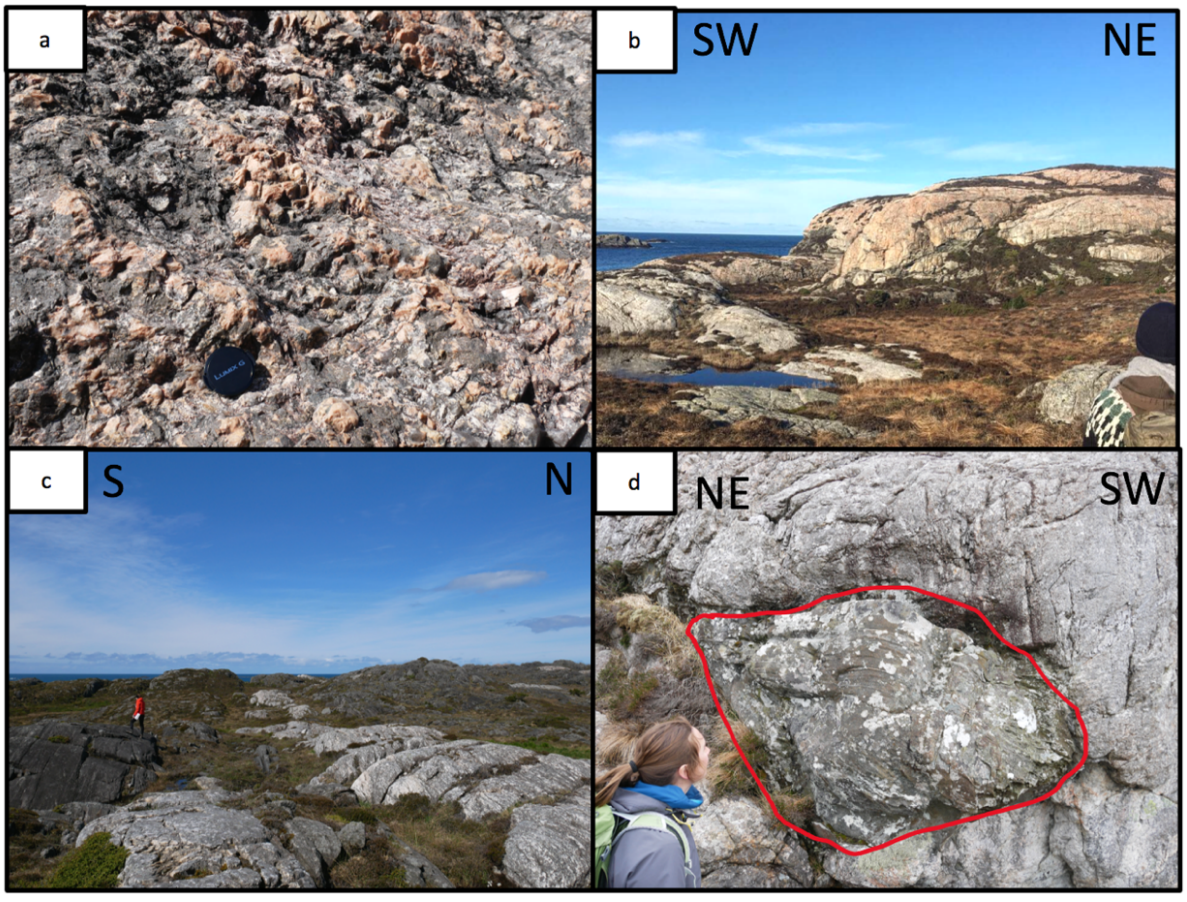

Fig. 18. a) Granitic pegmatite with grey weathering surface and high content of K-feldspars (Loc. 93). b) Picture from Søvika showing major pegmatites in the gabbroic body. c) E – W elongated pegmatite and a small body of granitic gneiss. (Loc. 95). d). Amphibolite xeonolith in the pegmatite (Loc. 73).

Banded gneisses

Banded gneisses are mapped in the southern parts of Telavågen and is a common rock on most of southern Sotra (Bering, 1984). The unit is very heterogenous and with compositional variations. The texture is inequigranular with coarse grained clasts of k-feldspar surrounded with fine grained material (Fig. 19a and b). The unit is dominated by S=L fabrics. The unit is extremely folded and refolded, and sheet folds have been observed north of Selstøa (Fig. 14). In the area around Såtene amphibolites grades gradually into banded gneisses with a mixture of previous described lithologies. Bering (1984) describes that is it difficult to separate between Telavåg gabbroic rocks and older gabbroic rocks which is a part of the banded gneiss in this area.

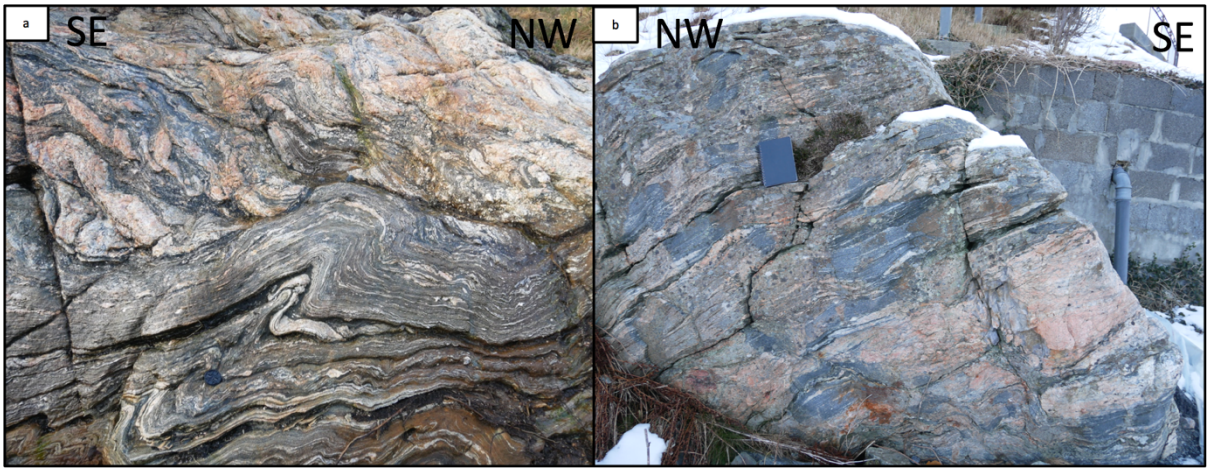

Fig. 19. a) Folded banded gneiss (Loc. 53). b) Banded gneiss with large K-feldspar and fine-grained groundmass and pegmatite (Loc. 37).

Lithological contacts and relationship

All observable lithological contacts are parallel to the foliation, and units are generally more deformed close to lithological contacts. The boundary between gabbroic rocks and granitic gneiss is generally very sharp and strongly sheared (Fig. 20a and b). This may indicate a primary contact that has developed into a shear zone. The granitic gneiss is in general overlaying the gabbroic body and some localities show intrusion of granitic gneiss into the amphibolite at the boundary, at Nesvika and Nipa (Fig. 20c). North of Selstøa and south at Såtene amphibolites gradually grades into banded gneisses (Fig. 14). South of Nesvika the amphibolite and granitic gneiss is separated by a vertical fault (Fig. 20d). Based on lithological relationships from all of the described units, my interpretation from oldest to youngest is: banded gneisses, amphibolite and metagabbros, granitic gneisses and pegmatites.

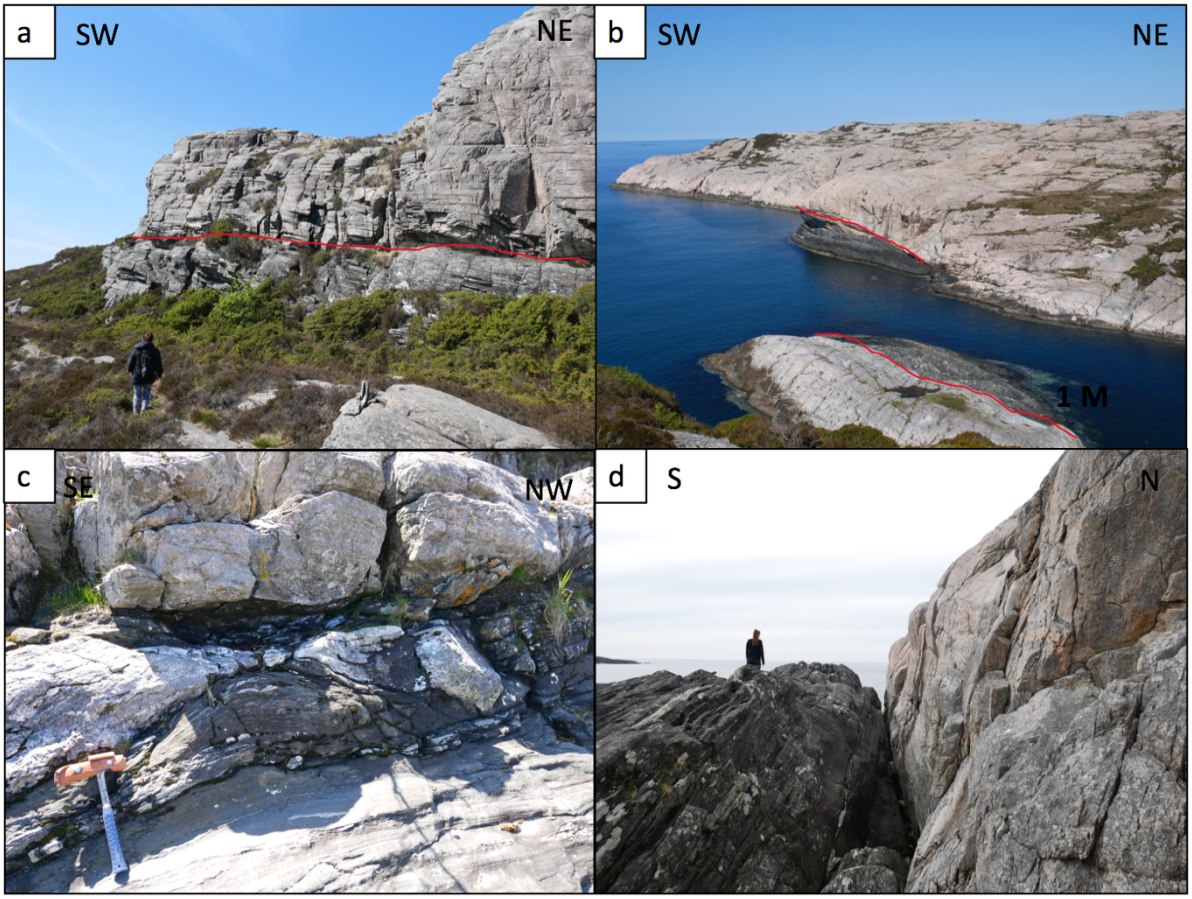

Fig. 20. a) Sharp boundary between granitic gneiss and amphibolite. Granitic gneiss on the top. The contact has the same orientation as the foliation (Loc. 87). b) Boundary between granitic gneiss and amphibolite. Contact follow foliation towards NE and SW (Nesvika). c) The granitic gneiss is intruding the amphibolite and show boudinage structure. Contact follows the foliation (Nesvika, Loc. 80). d) Vertical fault between the granitic gneiss and the amphibolite (Loc. 48).

5.1.2 Structural results

Ductile deformation

All the described units are metamorphosed and developed linear and planar fabrics. The granitic gneiss is dominated by strong L and L>S fabric, formed by recrystallization and stretching of quartz, k-feldspar and biotite. All other units have strong S-L fabrics. The granitic gneiss exhibits strong S-L fabrics in areas transformed into mylonites or phyllonites. Lineations have almost a constant plunge towards E and SE in all lithologies, with a calculated mean plunge of 118°. The foliation dips both towards the NNE and the SSW, but NE dipping foliation dominates (Fig. 21). Dip angles vary greatly in the area but are mostly between 20-40°. South of Nesvika the foliation dips around 60° and at Nipa it dips around 15°. Foliations are anastomosing, in high strain areas of both the gabbroic rocks body and in

the granitic gneisses. In the gabbroic rock body, shear zones consist of amphibolite, indicating at least amphibolite-facies conditions. Recrystallized k-feldspar in the mylonitic granitic gneiss also indicate amphibolite facies metamorphism. Epidote and chlorite minerals in the gabbroic rocks body indicates greenschists facies metamorphism.

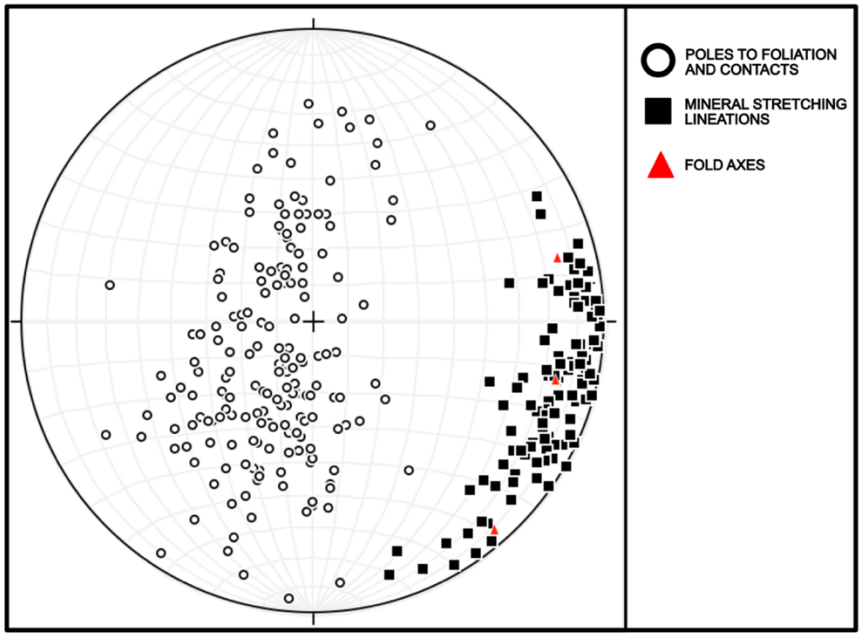

Fig. 21. Stereonet of poles to foliation, mineral stretching lineation and fold axis.

Folding

Folding is observed in all units on different scales. Planar fabric in Telavåg are defined by large-scales upright antiformal and synformal structures. Folds on the macroscale are mostly observed as tight, recumbent, similar folds (Fig. 22a, b, c and d). Measured fold axes show ESE-plunging folds that are parallel to mineral stretching lineations. A number of localities exhibit vertically plunging fold axes (Fig. 22e). The gabbroic rocks are more strongly folded and refolded than the homogenous granitic gneiss body. In the homogenous granitic gneiss, pegmatite dikes are observed as folded (Fig. 23a and b). Major pegmatites in Søvika shows large-scale antiformal structures and boudinage structures (Fig.14). The banded gneiss unit can be described as the most folded unit, which also includes sheath folding.

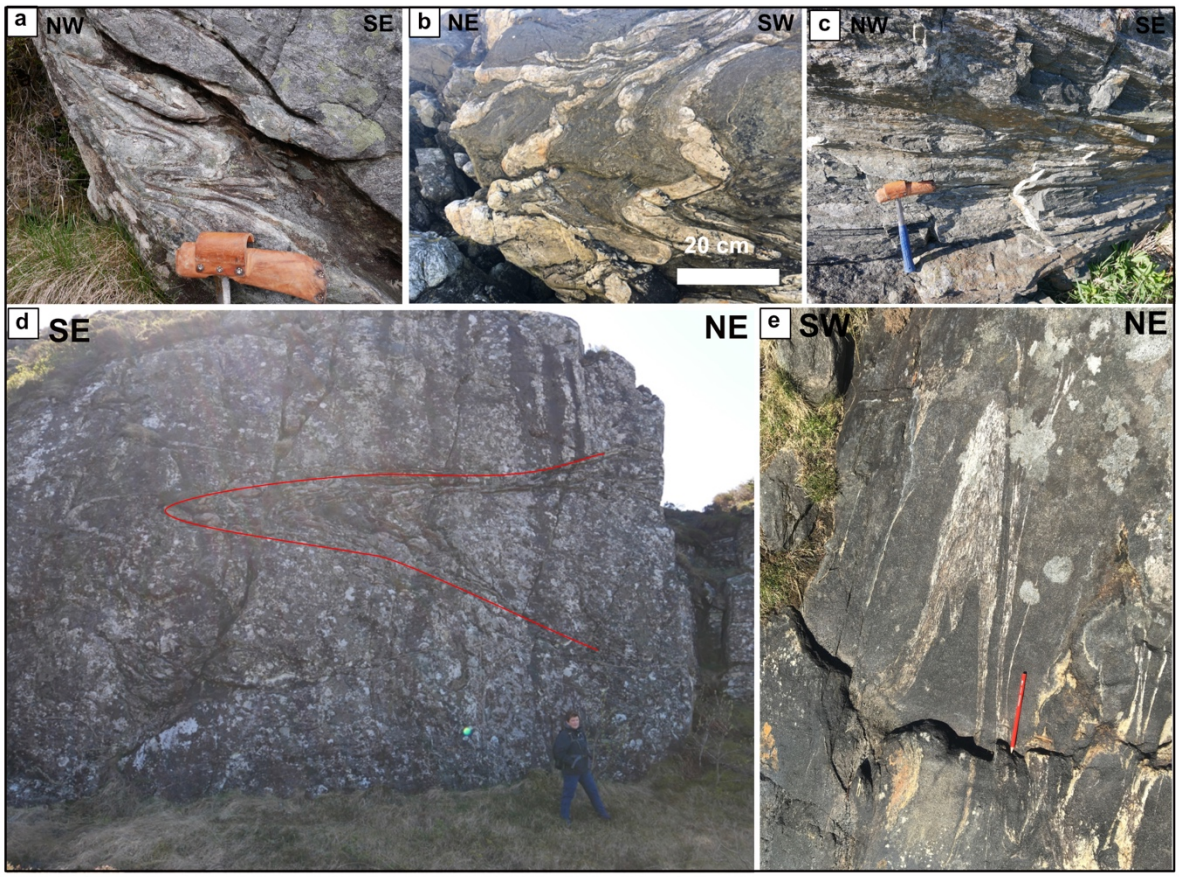

Fig. 22. a) Recumbent and tight fold in a shear zone in a minor granitic gneiss body (Loc. 28). b) Folded pegmatites in the gabbroic body (Loc.66). c) Planar fabric is recumbent and tight folded. Fold axis is SE plunging (Loc. 77). d) Recumbent and tight mesoscale fold of planar fabrics in the amphibolite. Shallowly NE dipping (Loc. 24). e) vertical, tight and similar fold (Loc. 25).

Fig. 23. a) Folding of pegmatites in the granitic gneiss (Loc. 89). b) Folding of pegmatites in a shear zone in a minor granitic gneiss body (Loc. 91).

Shear zones

A great number of shear zones are observed in Telavåg. Shear zones are dipping towards the NNE and the SSW. NNE-dipping shear zones dominate in the gabbroic rock body, and shallowly SE dipping shear zones dominates in the granitic gneiss. In the granitic gneiss the shear zones are in several places observed as discontinuous consisting of phyllonites while continuous shear zones of amphibolites are observed in the gabbroic rock body. The granitic gneiss also exhibits mylonitic shear zone which are NNE dipping. S-C and S-C´ structures, sigma and delta clasts in shear zones show top-to-NW and top-to-W sense of shear (Fig. 24a, b and c).

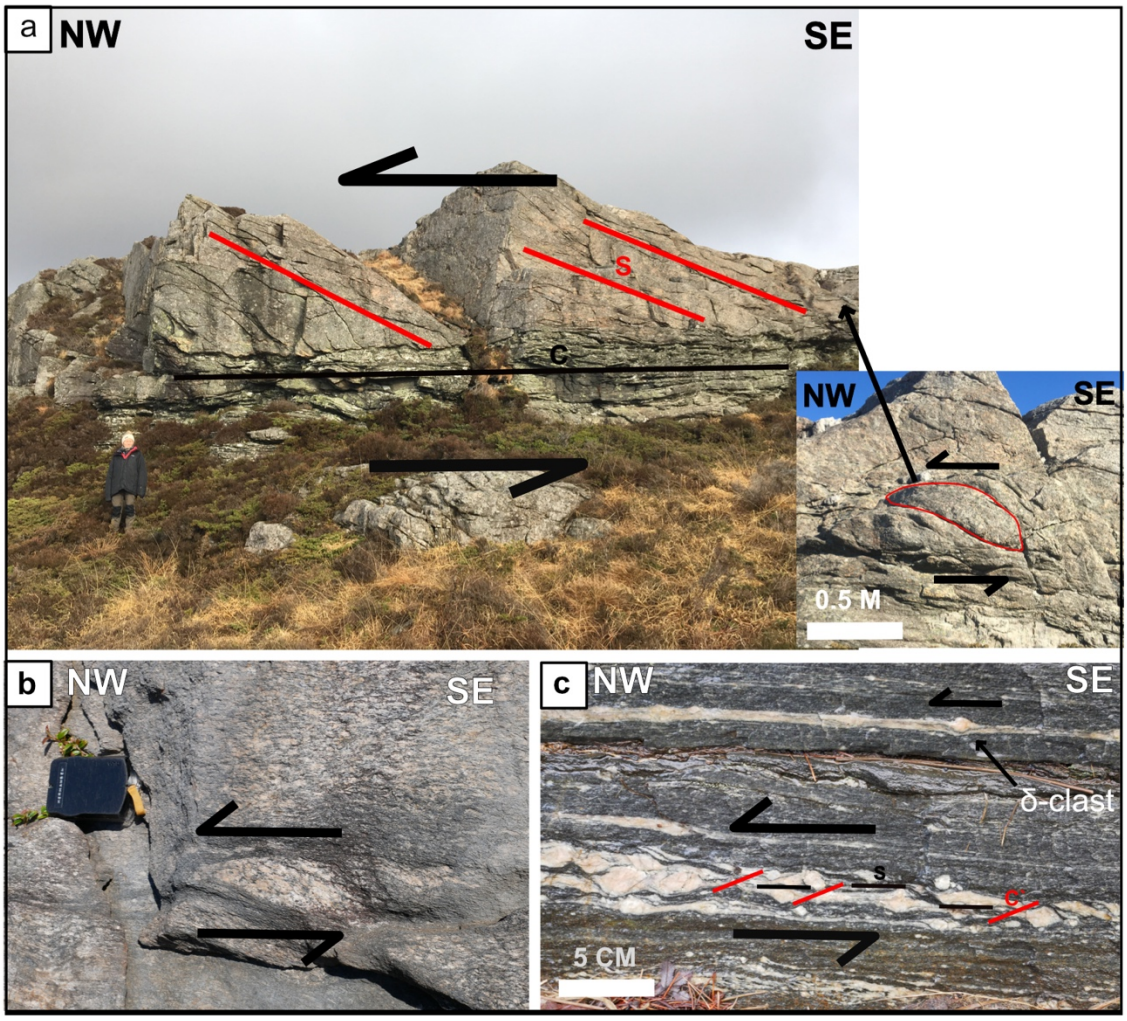

Fig. 24. All pictures are parallel to lineations. a) Shear zone consisting of phyllonites in the granitic gneiss with largescale S-C structure showing top to NW-movement, in addition to a sigma clast (Loc. 68). b) Sigma clast with top-to-NW movement in a shear zone in the granitic gneiss (Loc. 91). c) C`-S structures in banded gneiss and also delta clast, both show top-to-NW kinematics (Loc. 37).

Summary

The protolith of the banded gneisses are interpreted as the oldest unit, intruded by gabbroic, granitic gneiss and pegmatites. Lineations plunge towards the ESE in all the investigated lithologies, indicating that the rocks formed in one single deformation event. Measured fold axes are parallel to the stretching lineations. Foliations dip mostly towards NE and SW and are dominated by major upright folds and recumbent mesoscale folds. The folding patterns show similarities with christmas-tree folding. The area exhibits numerous shear zones with Top-to-NW and top-to-W sense of shear. Amphibolites and mylonitic shear zones in the granitic gneisses indicates that the rocks have been overprinted by amphibolite-facies metamorphism. Also, low-grade cataclastic shear zones are investigated in Telavåg. The field observations indicate that the area has been affected by retrograde metamorphism from amphibolite facies down to brittle-plastic transition.

5. 2 U – Pb Zircon Geochronology

Seven samples were analysed by SIMS U- Pb geochronology and the results are presented in table 1 and fig. 25. Description of samples localities, petrological characteristics, zircon internal textures and geochronological results are presented in this chapter. Fig. 26 illustrates different symbols used to present the analyses.

Table 1. List of sample localities and geochronological results.

Samples	Lithology	Coordinates	Outcrop description	Ages (Ma)
Hardanger				
HCT – 5	Augen gneiss	60°14'15.1"N 006°12'20.2"E	Roadcut, Jondal.	1048 ± 5 Ma
HCT – 12	Gneissic granite	59°50'11.6"N 005°49'16.8"E	Roadcut, Valen.	950 ± 4 Ma
HCT – 14	Granite	59°59'57"N 006°02'50"E	Outcrop along hiking trail, Melderskin.	948 ± 5 Ma
HCT - 1	Biotite granite	60° 27'18.7"N 006° 33'31"E	Roadcut, Lussand.	943 ± 11 Ma
Sotra				
TSS - 1	Metagabbro	60°15'37.3"N 004°58'46.1"E	Roadcut, Telavåg.	Unreliable age
TSS - 2	Granitic gneiss	60°16'00.7"N 004°59'44.6"E	Outcrop along hiking trail, Telavåg.	1028 ± 6
Gulen				
TSG – 3	Augen gneiss	60°59'11.4"N 005°02'11.3"E	Roadcut, Eivindvik.	969 ± 5 Ma

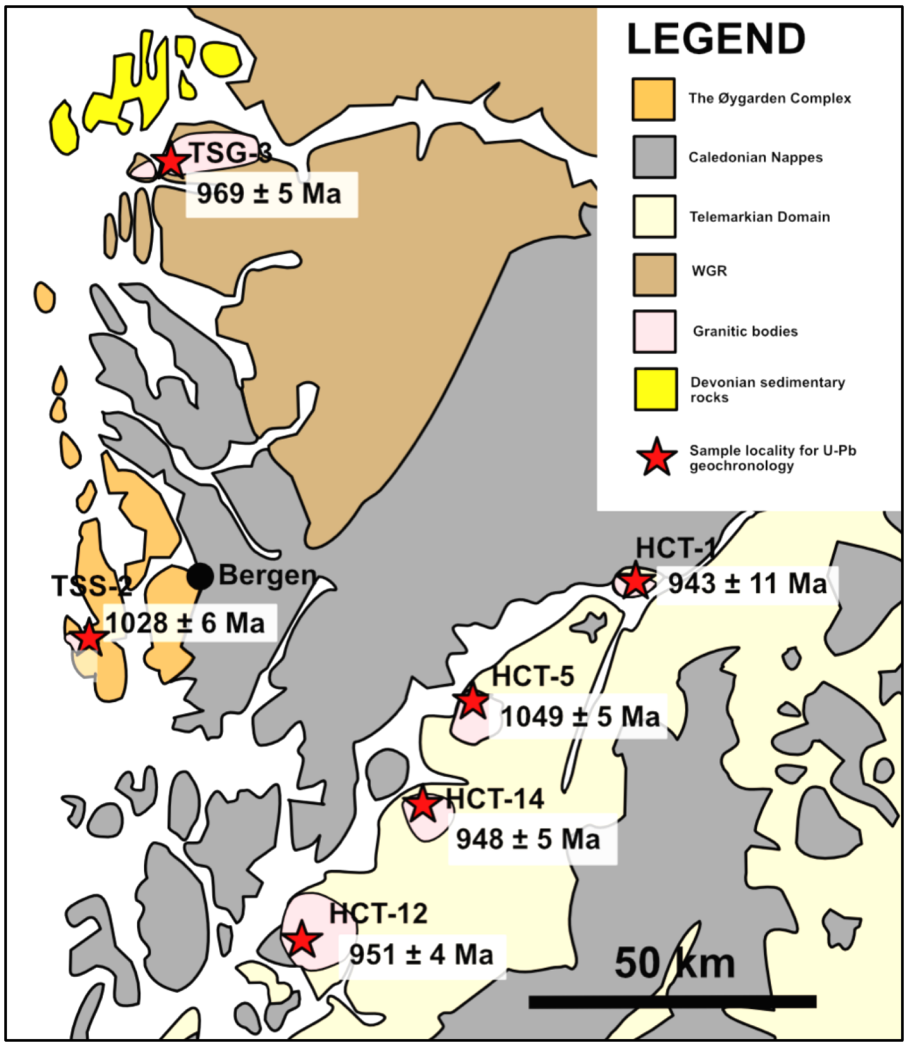

Fig. 25. Simplified geological map showing sample localities and igneous crystallization ages. Map modified map from Fossen and Hurich (2005), Bingen et al. (2008a), Wiest et al. (2017), Slagstad et al. (2018) and Wiest et al. (2019).

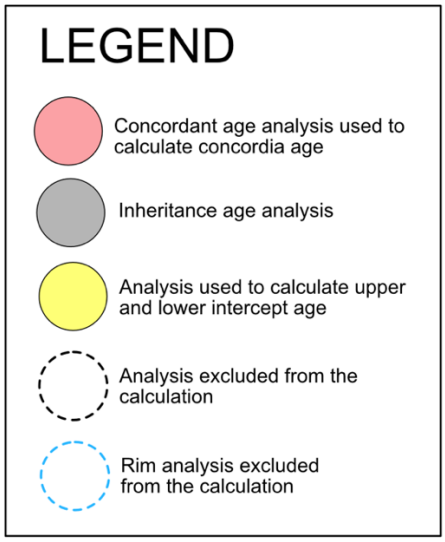

Fig. 26. Legend illustrating different symbols used to present the geochronological data.

Hardanger

The granitic bodies in the Hardanger area have earlier been mapped by Sigmond (1975) and Sigmond (1998) and all the four investigated granitic bodies are described as granite or granodiorite.

Augen gneiss (HCT-5)

Augen gneiss was collected from a roadcut in Jondal. The outcrop is well exposed and consists of three different lithologies: augen gneiss, granitic gneiss and granitic pegmatite. Pegmatite and granitic gneiss intrude the augen gneiss. The augen gneiss is moderately deformed and shows an inequigranular medium- to coarse-grained texture (Fig. 27a). The essential minerals are K-feldspar, quartz, biotite, plagioclase and hornblende, whereas titanite, epidote, zircon, apatite and opaque minerals are present as accessory phases (Fig. 27b). In addition, microcline with crosshatched twinning and orthoclase with perthite unmixing can be observed (Fig. 27c). Recrystallized quartz shows undulose extinction and lobate boundaries. K-feldspars show strong alteration by saussurititization.

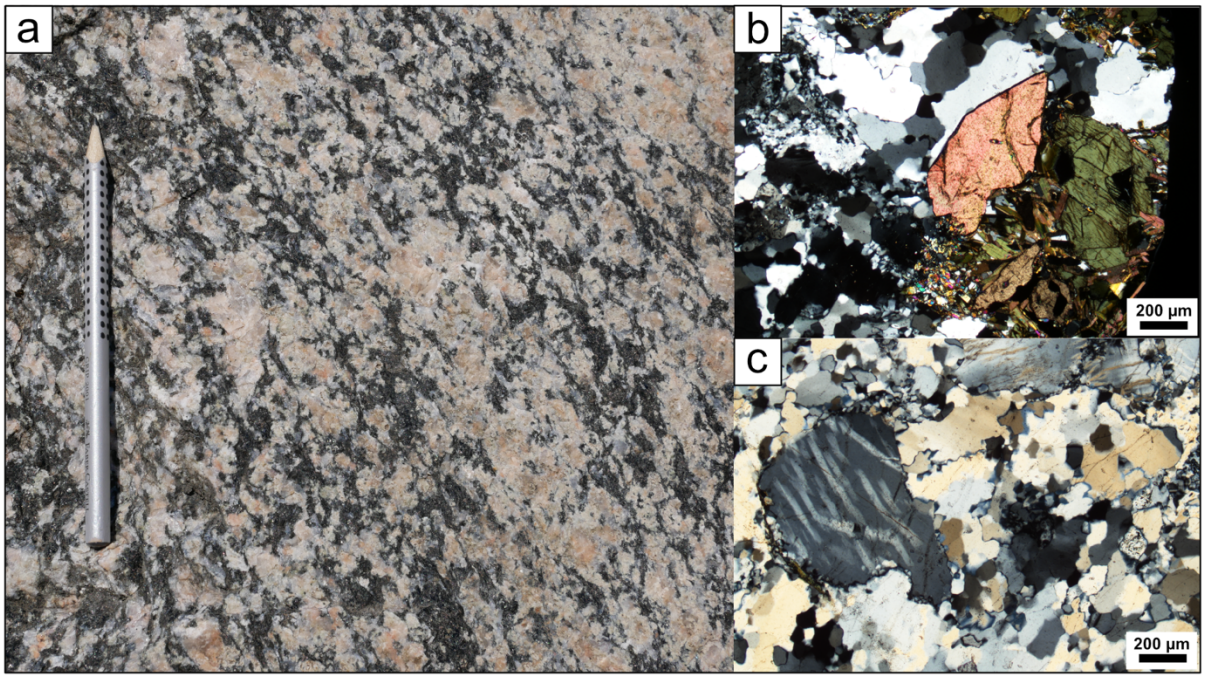

Fig. 27. a) Field photograph of the sampled augen gneiss (HCT-5). b) Microphotograph showing titanite, hornblende, epidote and quartz. c) K-feldspar with perthitic exsolution texture.

Zircons from this sample are typically subhedral to euhedral and elongated with length along c-axes around 200-250 µm and aspect ratios mostly around 4. They are colourless and

transparent, and sometimes pinkish and have in general few inclusions and fractures. In CL images, zircons have mostly medium bright cores surrounded by oscillatory zoned domains and thin dark, structureless rims (Fig. 28c).

Twenty-two spots were analysed on 18 zircons, placed in 15 oscillatory-zoned domains, 4 cores and 3 rims. There is no significant age difference between either of the different zircon domains. U concentrations in the zircons range from 31 – 317 ppm and Th/U ratio from 0.11-0.57. All analyses plot in a narrow cluster around Concordia. Nine analyses are excluded from the calculation of a Concordia age because of recent Pb loss, reversely discordance or high common lead. Thirteen analyses of uncorrected data give a Concordia age of 1048 ± 5 Ma (MSWD = 0.79, Fig. 28a). Concordant $^{238}U/^{206}Pb$ ages have a weighted mean age of 1051 ± 6 Ma (MSWD = 0.61, Fig. 28b). Based on zircon texture and Th/U ratios I interpreted the Concordia age as the crystallization age of the granitic protolith.

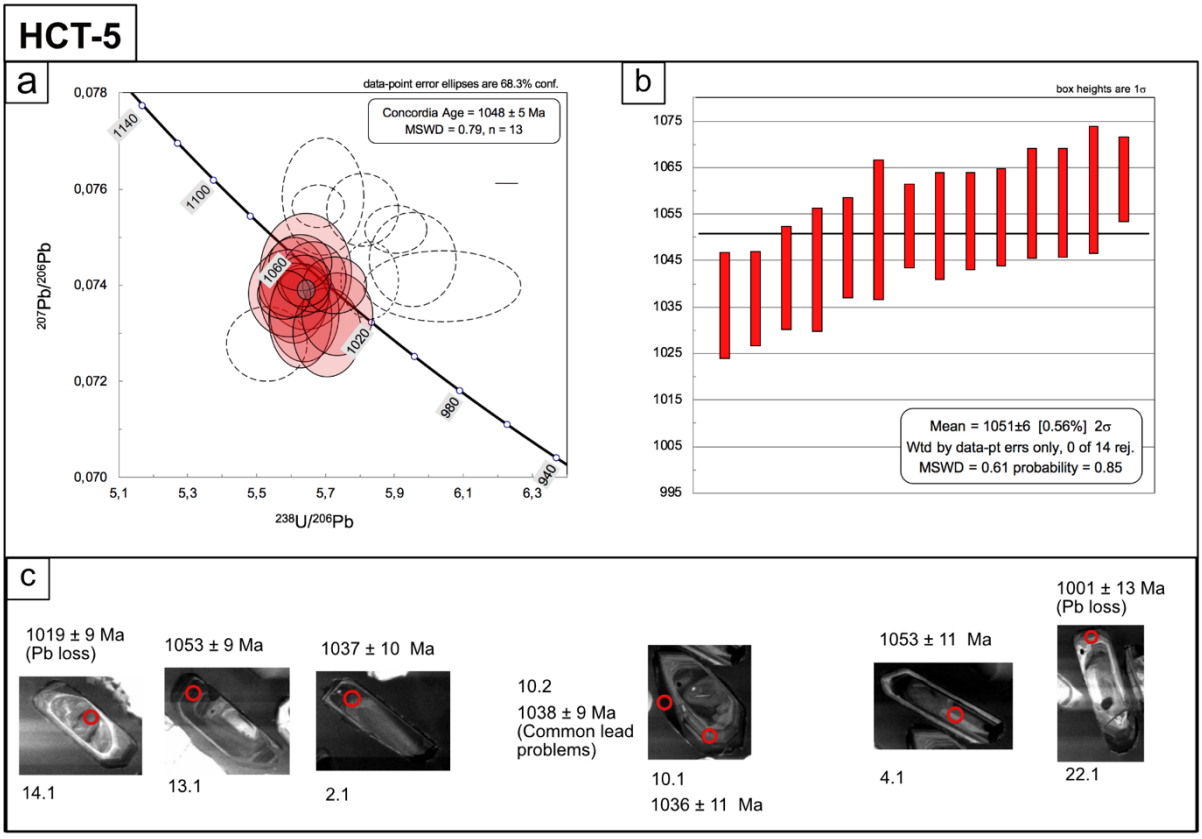

Fig. 28. a) Tera-Wasserburg of all analyses from sample HCT-5, except for one highly discordant age. All analyses are uncorrected data and are plotted at 1σ error. b) Weighted mean age of concordant $^{238}U/^{206}Pb$ ages (n = 13). Box heights are 1σ. c) Representative CL pictures of analysed zircons. Analyses without description are concordant analyses. Red circles are 25 µm in diameter.

Gneissic granite (HCT-12)

Gneissic granite was sampled from a homogeneous and well-exposed roadcut in Valen. The rock appears weakly deformed with small local shear zones (Fig. 29a). The general texture is porphyritic with coarse-grained K-feldspar and a fine-grained matrix of quartz, plagioclase, chlorite, muscovite and biotite (Fig. 29b). Opaque minerals, epidotes, titanite, zircons and apatite are present as accessory minerals. K-feldspars have mostly cross-hatched twinning and some grains show perthitic unmixing. Plagioclase twinning is also shown in the thin section. Recrystallized quartz with undulose extinction and highly saussuritized K-feldspar can be observed in thin section (Fig. 29c).

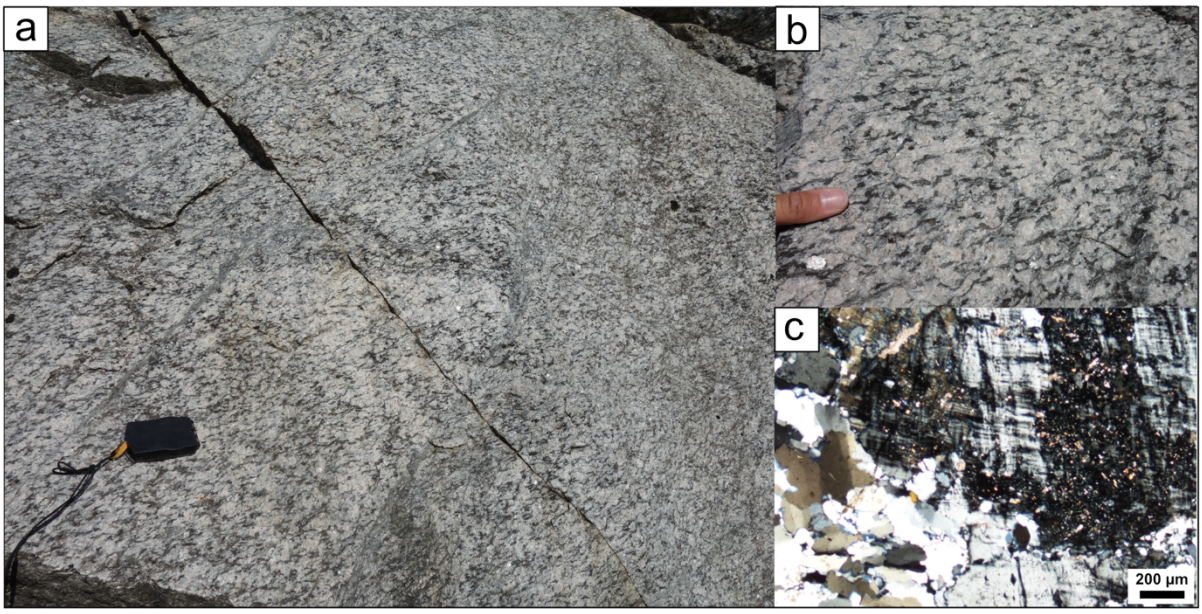

Fig. 29. a) Picture of the sample locality of gneissic granite (HCT-12). Several small local shear zones can be observed. The sample was taken from the most undeformed parts. b) Picture of moderately deformed gneissic granites. c) Thin section showing highly altered microcline and quartz.

The sample yielded euhedral and elongated zircons with lengths along c-axes from 150-200 µm and aspect ratios from 4-5. The zircons are mostly colourless to light-brown, a small number are dark brown. Most have few inclusions and fractures, but some are fragmented. Zircons consist mostly of CL-bright or medium dark oscillatory zoned domains with dark thin rim (Fig. 30c). Some zircons have very dark cores surrounded by brighter oscillatory zoning areas and with dark thin rims (e.g. spot 26.1 and 12.1). A number of zircons show broad zoning parallel to the c-axis (e.g. spot 11.1). The rims were too thin to be analysed.
Thirty spots were analysed on 29 zircons, including 23 oscillatory components and 7 cores. There is no significant age difference between the different domains. U concentrations vary

between 8-340 ppm, most values are below 100 ppm. Cores have generally higher U concentrations. Th/U ratios are spread from 0.25-0.68. The analyses form one population and cluster around Concordia. Seven analyses were excluded from the calculation of a Concordia age because of recent Pb loss, common lead problems, reverse discordance and one analysis had a big error. Twenty-three uncorrected analyses give a Concordia age of 951 ± 4 Ma (MSWD = 0.97, Fig. 30a). The weighted mean of concordant $^{238}U/^{206}Pb$ ages is 947 ± 5 Ma (MSWD = 1.10, Fig. 30b). The Concordia age is interpreted as the crystallization age of the granitic protolith. Zircon texture and Th/U ratios confirm magmatic crystallization.

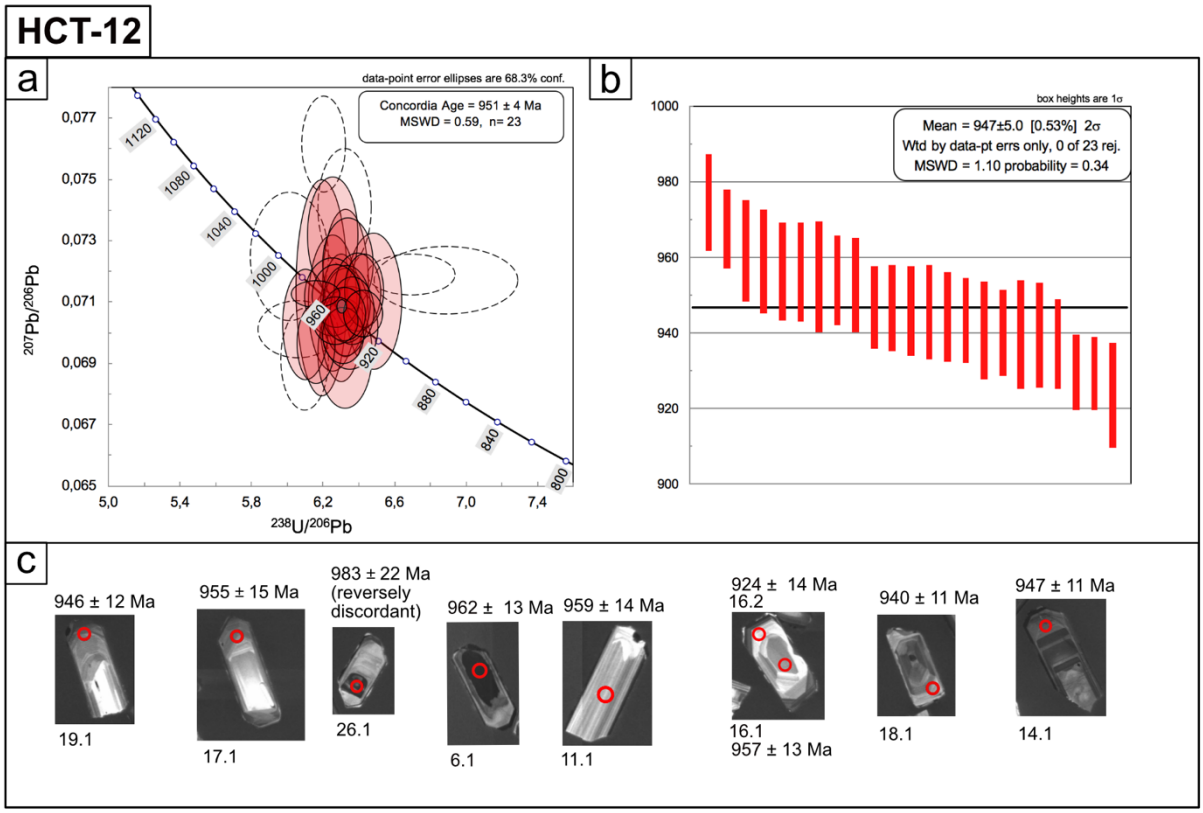

Fig. 30. a) Tera-Wasserburg plot of all analyses from sample HCT-12. Analyses are uncorrected data and plotted with 1σ error. b) Calculated weighted average mean of $^{238}U/^{206}Pb$ concordant ages (n=23). c) CL images of some zircons. Analyses without description are concordant analyses. Red marks are 25 µm in diameter.

Granite (HCT-14)

Granite was collected from a homogenous and limited exposed natural cliff along the trail to Melderskinn, Rosendal (Fig. 31a). The rock is undeformed and shows an inequigranular and medium-grained texture (Fig. 31b). It consists of K-feldspar, quartz, plagioclase and biotite, while opaque minerals, titanite, epidote, zircons and apatite are present as accessory minerals. In thin section, K-feldspars show perthitic exsolution textures and cross-hatched twinning, as well as fine-grained recrystallized quartz and highly saussuritized K-feldspar and plagioclase (Fig. 31c).

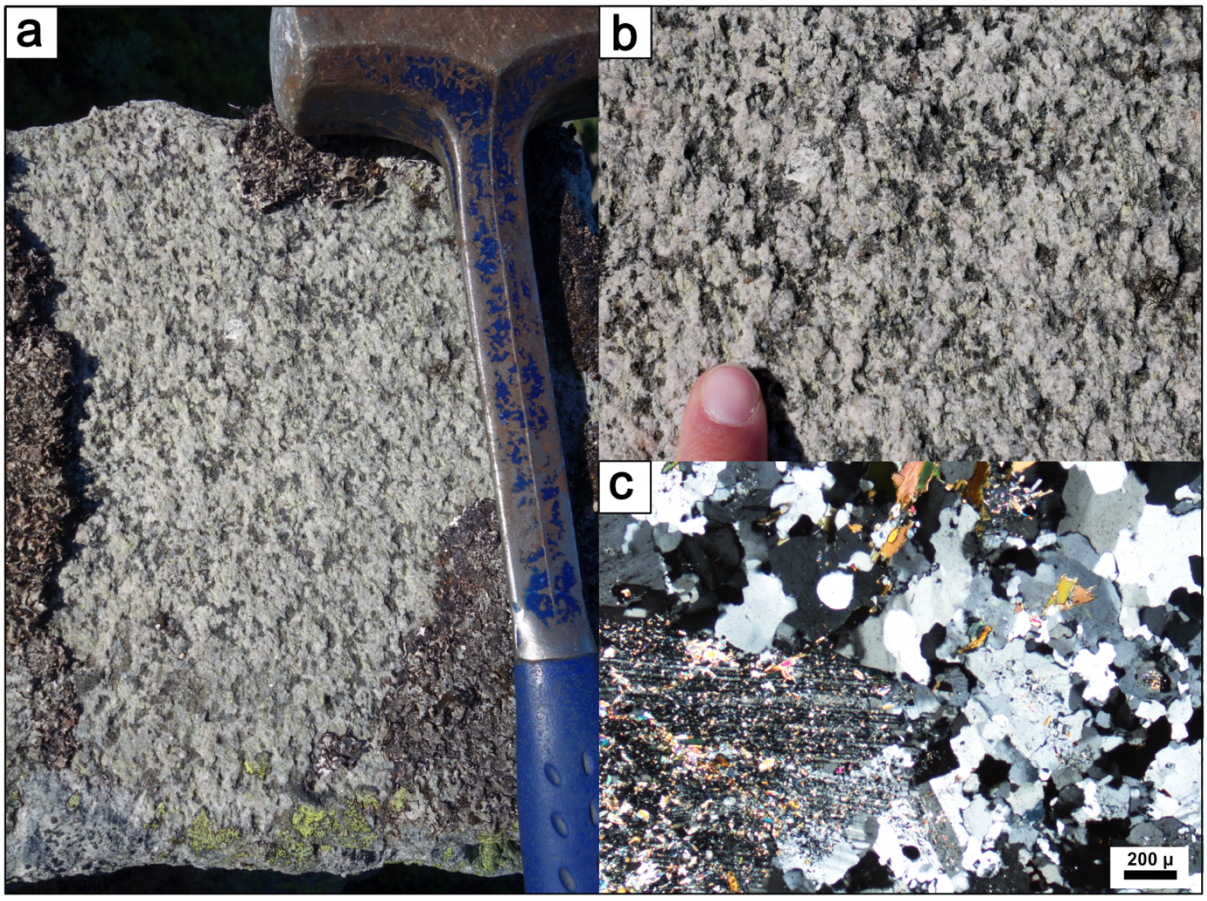

Fig. 31. a) Field photograph of the sampled granite (HCT-14). The outcrop is limited exposed. b) Undeformed granite with K-feldspar, plagioclase, quartz and biotite c) Thin-section with highly altered plagioclase, recrystallized quartz and biotite.

Zircons from this sample are subhedral to euhedral and elongated with length along c-axes from 150-200 µm and length-width ratios around 4. They are either colourless or light brown and with a high content of inclusions and fractures, especially in the brown zircons. In CL images, zircons mostly have dark cores surrounded by bright oscillatory zoned domains and

surrounded by thin textureless rims (Fig. 32c). The rims were too thin to be analysed. A couple of grains are entirely dark (e.g. spot 6.1).

Twenty-seven spots were analysed on 24 zircons, including 21 oscillatory components and 6 cores. One core analysis has an older age (spot 6.1). U concentrations are generally low and vary from 16-44 ppm and Th/U ratios are spread from 0.50-1.18. Spot 6.1 has high U concentration (625 ppm) and Th/U ratio is 0.53. The analyses form a narrow cluster around Concordia, expect from one older analysis and two highly discordant analyses that are not included in the graph. In total, six analyses were excluded from the calculation of the Concordia age because of Pb loss, reverse discordance and high common lead. Twenty-one ages of uncorrected data give a Concordia age of 948 ± 5 Ma (MSWD = 0.57, Fig. 32a). The Weighted mean of concordant $^{238}U/^{206}Pb$ ages is 948 ± 5 Ma (MSWD = 0.45, Fig. 32b).

The Concordia age is interpreted as the crystallization age of the granitic protolith. Texture and Th/U ratios are typical for magmatic zircons. One age is interpreted as inheritance (Spot 6.1). Texture and Th/U ratios of spot 6.1 imply earlier phases of magmatism.

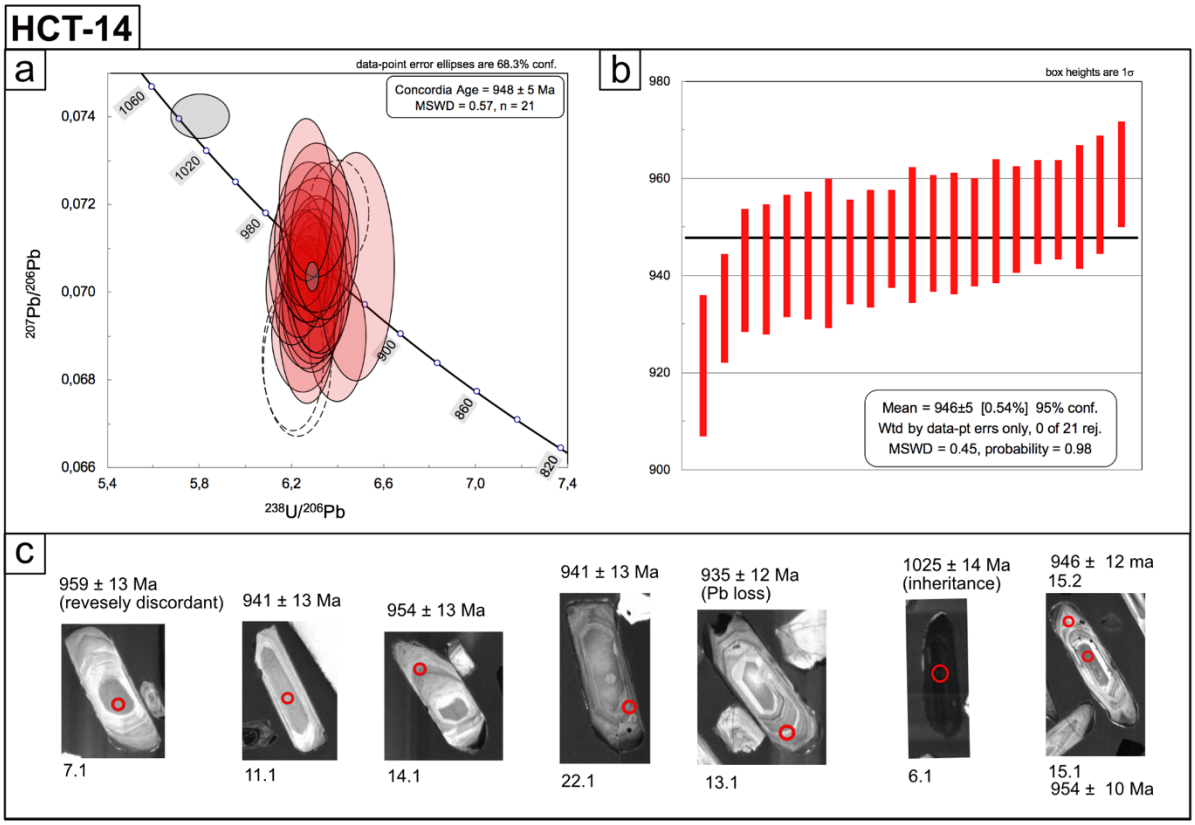

Fig. 32. a) Tera-Wasserburg plot of all analyses from sample HCT-14, except for two highly discordant analyses. All analyses are uncorrected data and plotted at 1σ error. b) Weighted mean age of 21 concordant $^{238}U/^{206}Pb$ ages (n = 21). c) Representative CL pictures of analysed zircon. Analyses without description are concordant. Red circles are 25 µm in diameter.

Biotite granite (HCT-1)

Granite was sampled from a homogenous and well-exposed outcrop in Lussand. The granite contains several (3 to 5 cm-thick) plagioclase rich veins that cross each other (Fig. 33a). The granite appears undeformed with inequigranular and medium-grained texture consisting of K-feldspar, quartz, biotite and minor plagioclase. Titanite, epidote, rutile, zircon, apatite and opaque minerals are present as accessory minerals (Fig. 33b). Under the microscope, K-felspars have cross-hatched twinning or perthitic unmixing. Recrystallized quartz with undulose extinction and highly saussuritized K-feldspar are present (Fig. 33c).

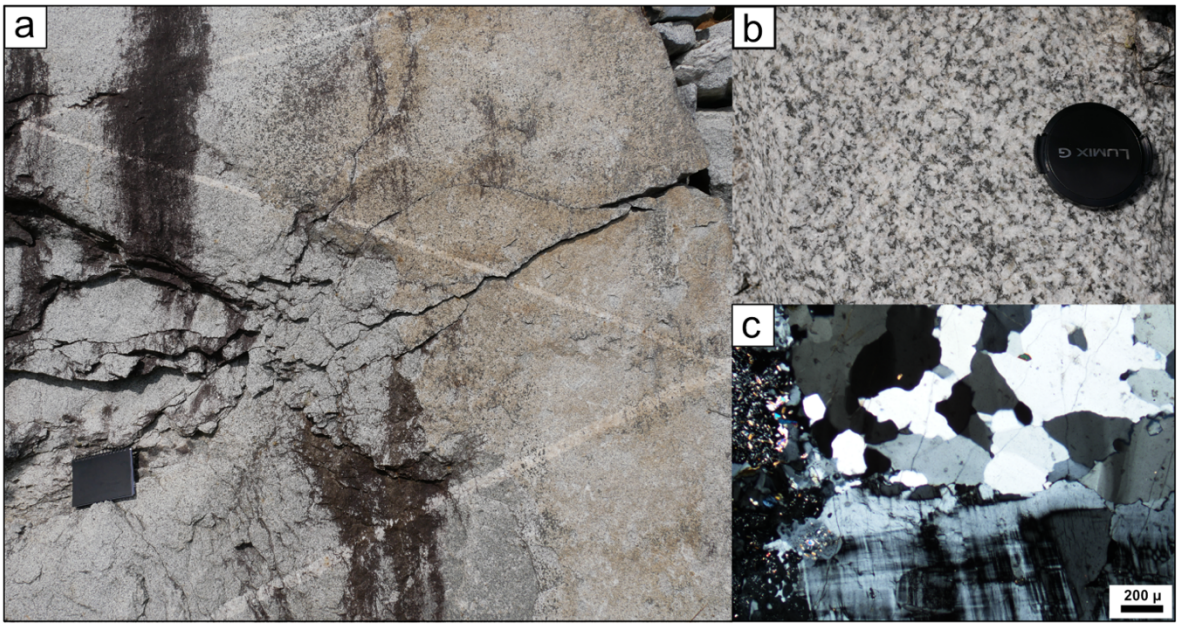

Fig. 33. a) Field photograph of the sampled biotite granite (HCT-1). Outcrop exhibit cross-cutting plagioclase rich veins. Notebook for scale. b) Picture of the undeformed granite.
c) Thin section showing microcline, highly altered K-feldspar and quartz.

Zircons from this sample are typically subhedral to euhedral, and elongated with lengths along c-axes around 200 µm and length-width ratios from 3 - 6. Crystals are in general dark brown with a high content of inclusions and fractures. In CL images, most zircons consist of a bright CL-cores with oscillatory or banded zoning surrounded by dark, structureless rims (Fig. 34c). A few zircons have zoning parallel to c-axes and a thin dark rim (e.g. spot. 10.1). The rims of some zircons, or even the entire grains of some zircons, are metamict and show bright and patchy CL images (e.g. spot 6.1).

Twenty spots were analysed on 20 zircons, placed in 16 cores and 4 rims. Analyses have a wide range in U concentrations, with lower values for cores (23-569 ppm, Th/U: 0.50-1.58) than rims (426-1667 ppm, Th/U: 0.16-0.37). Rim analyses show a range of $^{206}Pb/^{238}U$ ages

from 450 Ma to 882 Ma and are either discordant or have big errors, except from the youngest age which is concordant. Discordant analyses and U concentrations show a strong correlation. This dataset yielded complex results with two different populations, and 12 analyses are excluded from the Concordia age calculation because of ancient Pb loss and reverse discordance. An older population of four uncorrected ages give a Concordant age of 1039 ± 11 Ma (MSWD = 0.63), while a younger population of four corrected ages give a Concordant age of 943 ± 11 Ma (MSWD = 0.37, Fig. 34a). Anchored at 943 ± 11 Ma, a lower intercept can be calculated at 474 ± 11 Ma, (MSWD = 0.30, Fig. 34b). The youngest Concordia age is interpreted as the crystallization age of the granitic protolith, confirmed by zircon texture and Th/U ratio. The oldest Concordia age is interpreted as an inheritance age. The inheritance analyses show Th/U ratio and zircon texture typically for magmatic zircons. The lower intercept at 474 ± 11 Ma may represent a later thermal event.

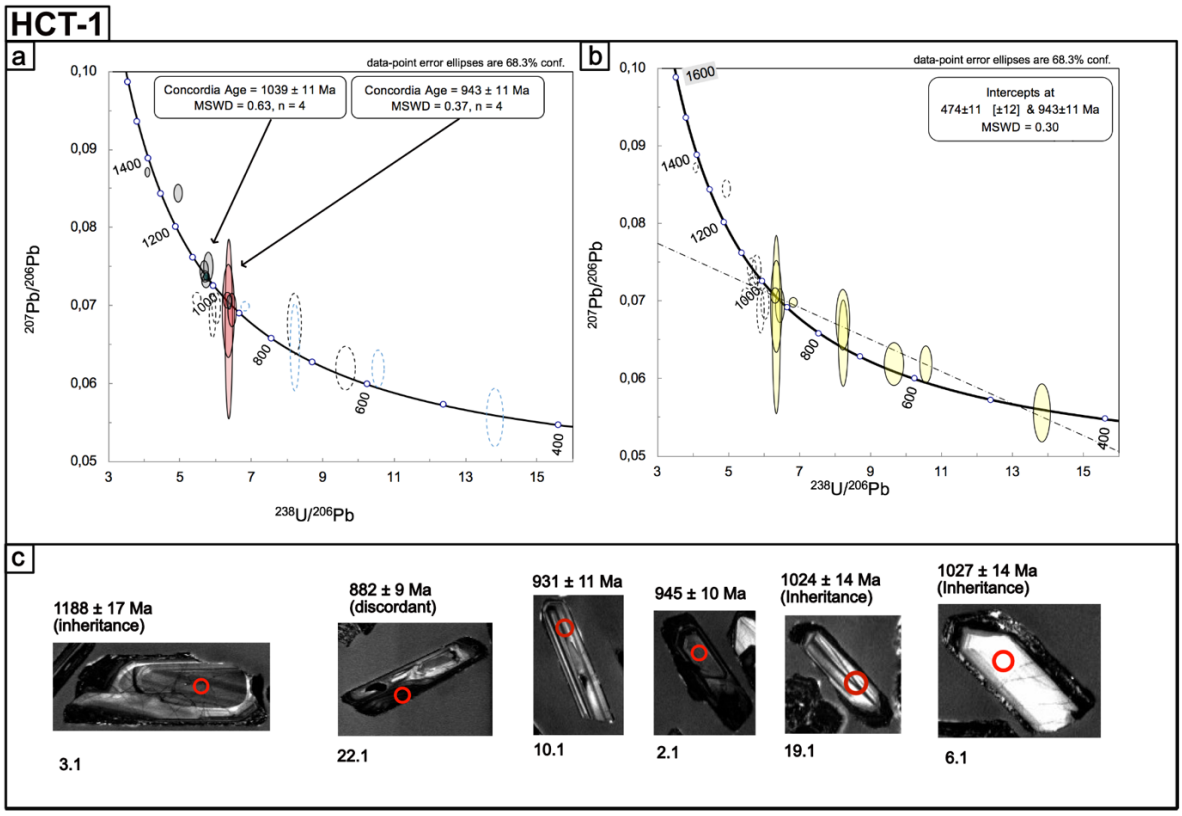

Fig. 34. a) Tera-Wasserburg plot of all analyses from HCT-1, except for one age with a big error. Circles are plotted at 1σ error. Analyses gave two Concordia ages. All analyses are corrected data, except from the four oldest concordant ages which are uncorrected. b) Terra-Wasserburg plot of intercept ages. c) Representative CL analysed zircons. Analyses without description are concordant analyses. Red circles are 25 µm in diameter.

Sotra

The investigated gabbroic and granitic bodies on Sotra were described in detail above (Fig. 14).

Metagabbro (TSS-1)

Metagabbro was sampled from a well-exposed and homogenous outcrop along a road in Telavåg. The general texture is inequigranular and the grain size is fine to medium-grained (Fig. 35a). The rock comprises mostly of amphibole and plagioclase altered to clinozoisite and epidote (mostly zoesite), biotite and some single grains of quartz. In thin section, elongated amphibolite and biotite and very fine-grained clinozoizite with high relief are prominent, as well as fine-grained blueish zoesite together with plagioclase (Fig. 35b and c).

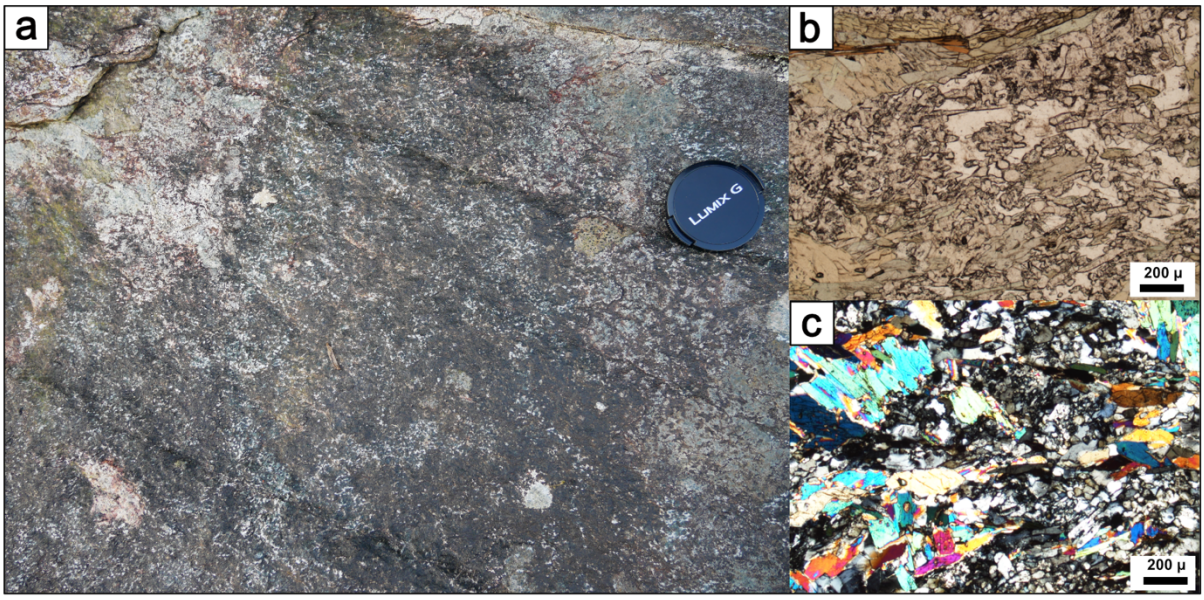

Fig. 35. a) Field photograph of the highly altered sample locality of metagabbro (TSS-1). b) Thin section photo in PPL showing greenish amphibole, biotite and small-grained clinozoisite. c) Thin section photo in XPL. Amphibolite with high interference colours, bluish zoesite and plagioclase.

Sample TSS-1 had a limited number of zircons. The zircons are anhedral, dark brown and extremely metamict (Fig. 36b). In CL images the crystals are entirely black. Only three spots were analysed in the cores of the zircon and yielded highly discordant ages. Measured U is high (417 ppm, 780 ppm and 914 ppm) and Th/U ratios are between 0.3 – 0.4. The three analyses define a Discordia with intercepts at 604 ± 80 and 1475 ± 20 Ma (MSWD = 2.3, Fig. 36a). It is difficult to observe magmatic texture in the zircon, but Th/U ratios indicate magmatic origin. Upper and lower intercept age is highly unreliable.

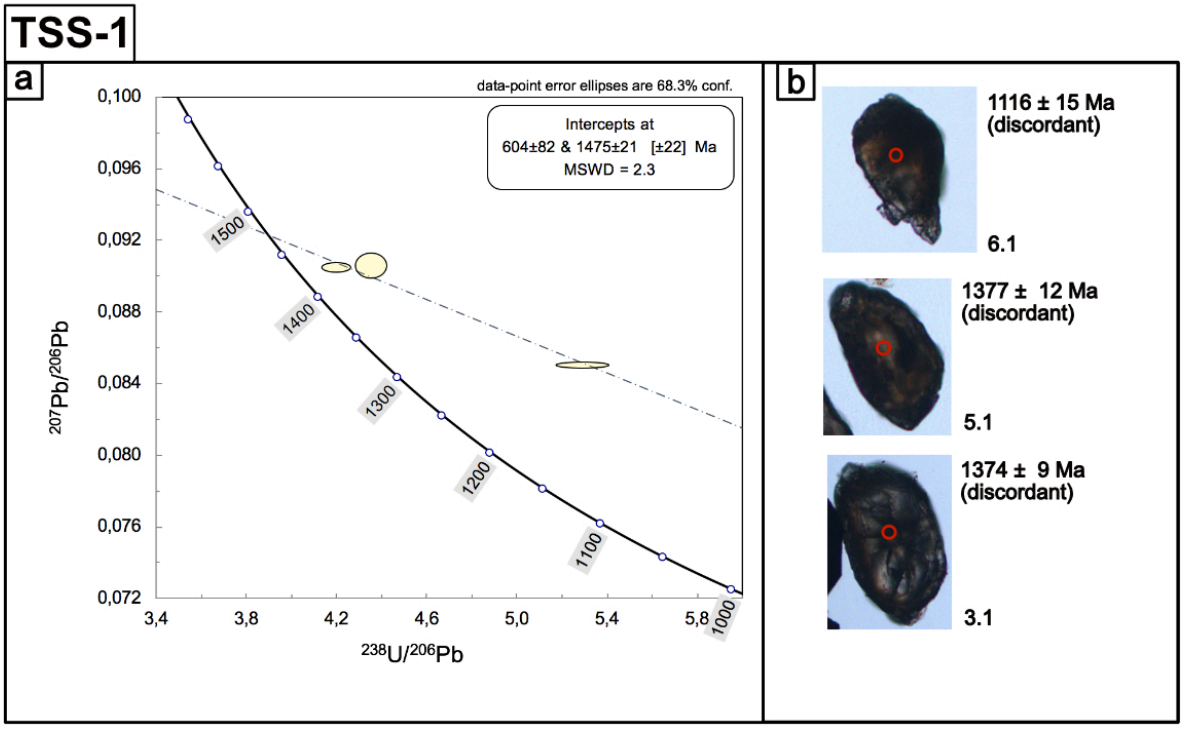

Fig. 36. a) Tera-Wasserburg plot of analyses from sample TSS-1. All analyses are corrected data and plotted at 1σ error. b) Picture of the three analysed zircons. Red circles are 25 µm.

Granitic gneiss (TSS-2)

Granitic gneiss was collected from a homogenous and well-exposed outcrop along a hiking trail in Telavåg (Fig. 37a). The rock is highly deformed with strong lineation fabrics but weak foliation. The general texture is inequigranular and medium-grained (Fig. 37b). The essential minerals are K-feldspar, quartz, and a small content of biotite and plagioclase, while opaque minerals, chlorite, pyrite, zircons and apatite are present as accessory minerals. In thin section, K-feldspars are mostly present as microcline with crosshatched twinning (Fig. 37c). Also, recrystallized quartz shows undulose extinction, whereas biotites are elongated.

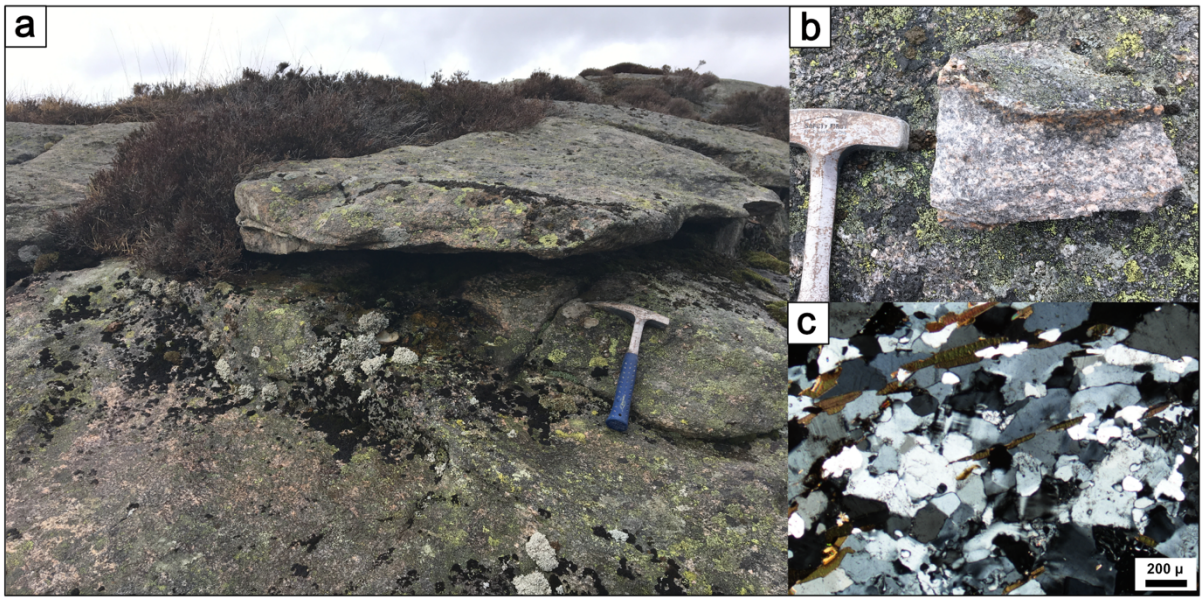

Fig. 37. a) Field photographs of sample locality of the granitic gneiss (TSS-2) with hammer for scale. b) Picture of the sampled granitic gneiss. c) Thin-section in XPL, showing microcline, quartz and biotite.

The sample yielded elongated and subhedral zircons with lengths along c-axes around 100 µm and length-width ratios from 2-4. Crystals are generally brown with a high content of inclusions and fractures. CL images revealed mostly dark zircons with dark cores surrounded by oscillatory zoned domains (Fig. 38c). A number of zircons have bright rims (e.g. spot 4.1). One grain has broad zoning parallel to c-axis and a dark rim (spot 20.1).
Twenty-five spots were analysed on 23 zircons, of which 20 are oscillatory-zoned domains, 3 cores and 2 rims. Measured U concentrations are spread widely from 50 – 877 ppm with Th/U ratios between 0.15 – 0.67 for oscillatory zoned domains. Core analyses have U concentrations between 280 – 780 ppm and Th/U ratios between 0.59 – 0.74, while rim analyses have U concentration between 720 - 630 with Th/U ratios at 0.04 and 0.05. Analyses show a strong correlation between discordance and U concentrations. A high number of discordant ages occurs in this sample, and 18 analyses were excluded from the calculation of the Concordia age because of Pb loss, reverse discordance or big error. Seven analyses of corrected data give a Concordia age of 1029 ± 6 Ma (MSWD = 0.71, Fig. 38a). Anchored at the Concordia age, a lower intercept age was calculated at 551 ± 6 (MSWD = 0.69, Fig. 38b). The Concordia age is interpreted as the crystallization age of the granitic protolith, based on zircon texture and Th/U ratios. The lower intercept is interpreted to have no geological significance.

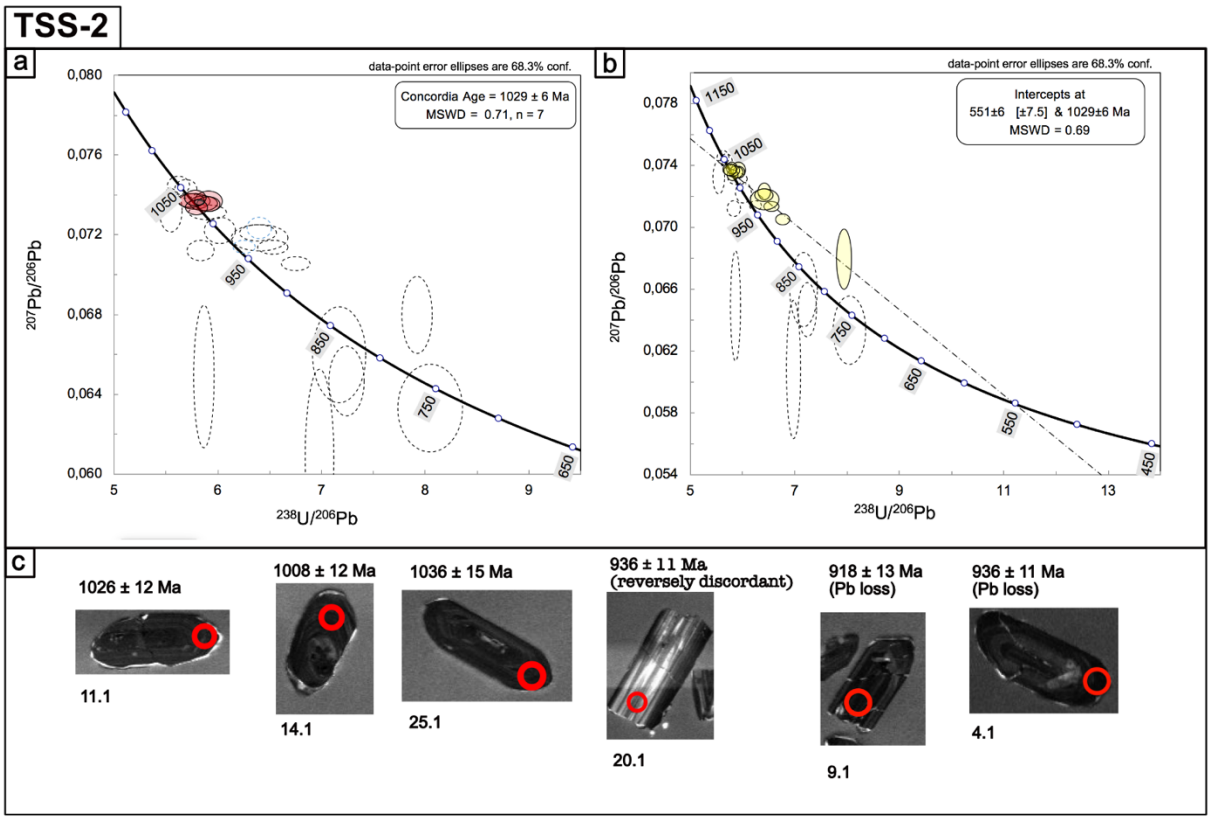

Fig. 38. a) Tera-Wasserburg analyses of sample TSS-2. All analyses are corrected data and plotted with 1σ error b) Upper and lower intercept ages of discordant analyses. c) Pictures of some analysed zircons. Analyses without description are concordant analyses. Red marks are 25 µm.

Gulen

The granitic body in Gulen had earlier been mapped by Kildal (1970) and described as augen gneisses and foliated granites. Field investigations by Wiest et al. (2019) described a weakly deformed granitic body.

Augen gneiss (TSG-3)

Granitic gneiss was collected from a homogenous and well-exposed outcrop close to Eivindvik (Fig. 39a). The rock is weakly deformed, and the general texture is porphyritic with coarse-grained K-feldspar and a fine- to medium-grained matrix of quartz, biotite and plagioclase (Fig. 39b). Opaque minerals, titanite, epidote, zircon and apatite are present as accessory minerals. K-feldspar has mostly cross-hatched twinning, representing microcline (Fig. 39c). Quartz is highly recrystallized and is fine-grained in several places.

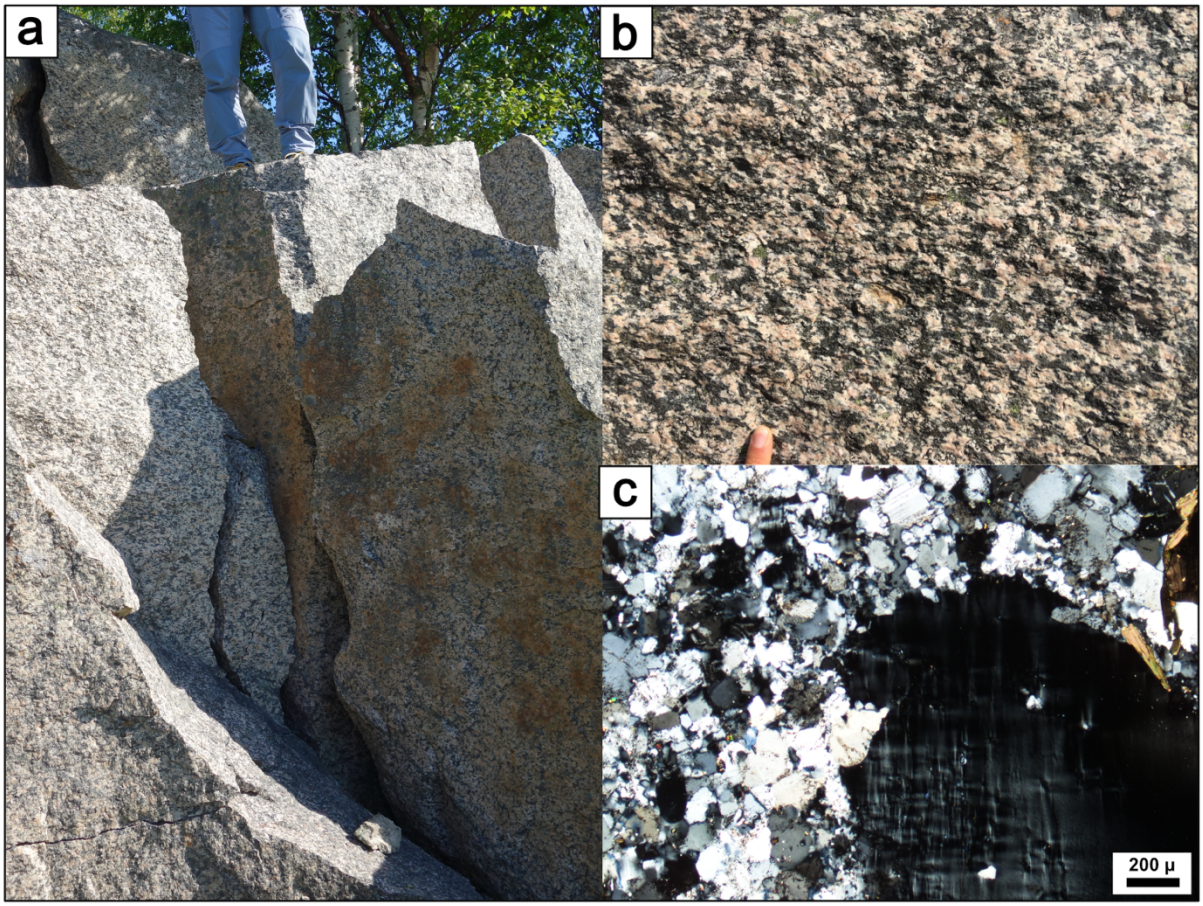

Fig. 39. a) Field photograph of the well-exposed and homogenous outcrop. b) Picture of the sampled augen gneiss (TSG-3). c) Thin section picture in XPL with microcline, recrystallized quartz and biotite.

Zircons from this sample are typically subhedral zircons with length along c-axis ranging from 100-200 µm and with aspect ratios from 2-4. A number of zircons are stubby. Crystals are colourless to light brown with a high content of inclusions and a small number of fractures. CL images shows dark to medium bright cores surrounded by oscillatory zoned domains (Fig. 40c). A few grains have structureless rims (e.g. spot 6.1). One core is CL-bright (spot 17.1).

Twenty-four spots were analysed on 21 zircons, placed in 19 oscillatory-zoned domains, 3 cores and 2 rims. There is no significant age difference between either of the different zircon domains. Measured U range from 25 – 102 ppm, most analyses are below 60. Th/U ratios vary between 0.53 – 1.85. All analyses plot in a narrow cluster around Concordia, except for one highly discordant analysis. Twenty-three analyses of uncorrected data give a Concordia age of 969 ± 5 Ma (MSWD = 0.76, Fig. 40a). Concordant $^{238}U/^{206}Pb$ ages have a weighted mean age of 968 ± 5 Ma (MSWD = 0.98, Fig. 40b). The Concordant age is interpreted as the

crystallization age of the granitic protolith. Zircon texture and Th/U ratios confirm magmatic crystallization.

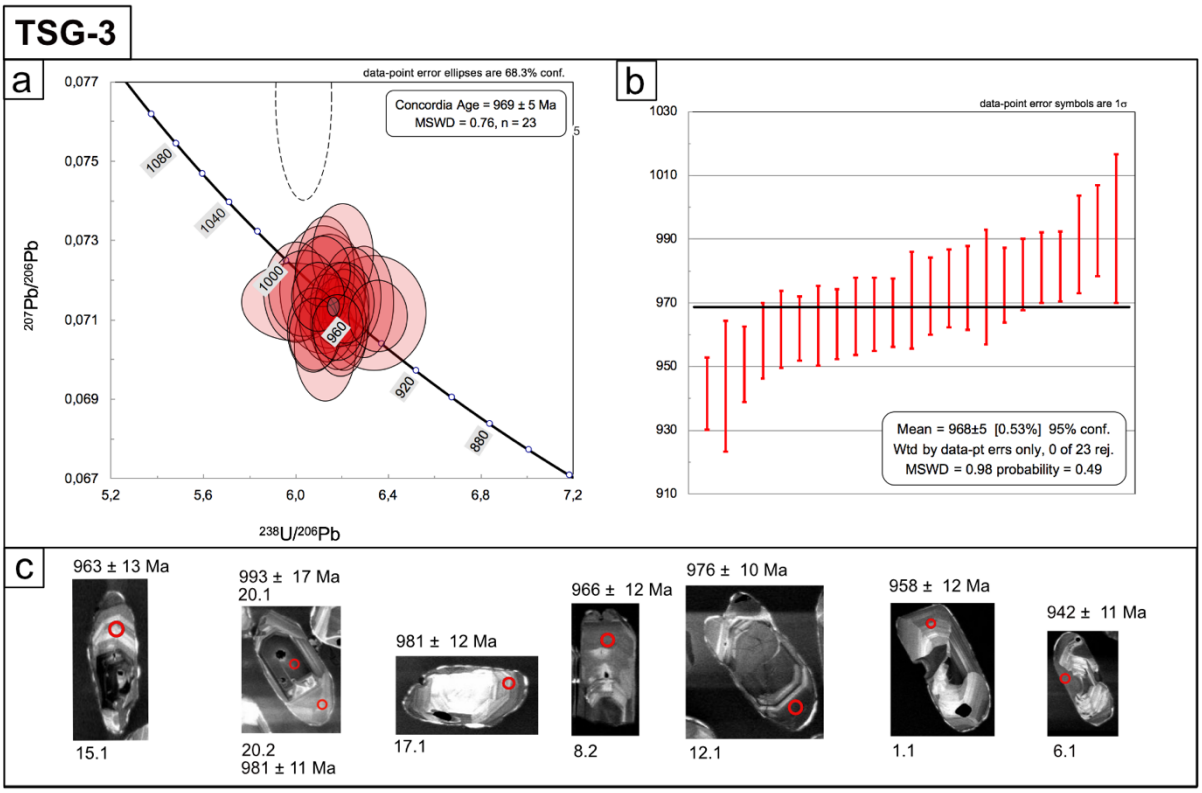

Fig. 40. a) Tera-Wasserburg plot of analyses from sample TSG-3. All analyses are corrected data and plotted at 1σ error. Only one analysis is discordant. b) Weighted mean age of concordant $^{238}U/^{206}Pb$ ages (n = 23). Datapoint error symbols are 1σ. c) Representative CL pictures of analysed zircons. Analyses without description is concordant analyses. Red circles are 25 µm.

Summary

The two oldest Concordia ages were calculated at 1028 ± 6 and 1048 ± 5 Ma, while younger Concordia ages were calculated at 969 ± 5 Ma, 951 ± 4 Ma, 948 ± 5 Ma and 943 ± 11 Ma (Fig. 41). The observed magmatic textures and U/Th ratios are typical for magmatic zircons and the ages are therefore interpreted as the granitic photolith ages. One Concordia age was calculated at 1039 ± 6 Ma, representing inheritance. The youngest age obtained in this study is a lower intercept age at 474 ± 11 Ma that may represent a thermal resetting event. The oldest sample (TSS-1) have an upper intercept age at 1475 Ma, but the age is highly unreliable. Th/U ratios indicates magmatism, but an accurate age is not revealed. For most analyses uncorrected data were used, whereas corrected data were used for HCT-1, TSS-2 and TSS-1 because of high common lead.

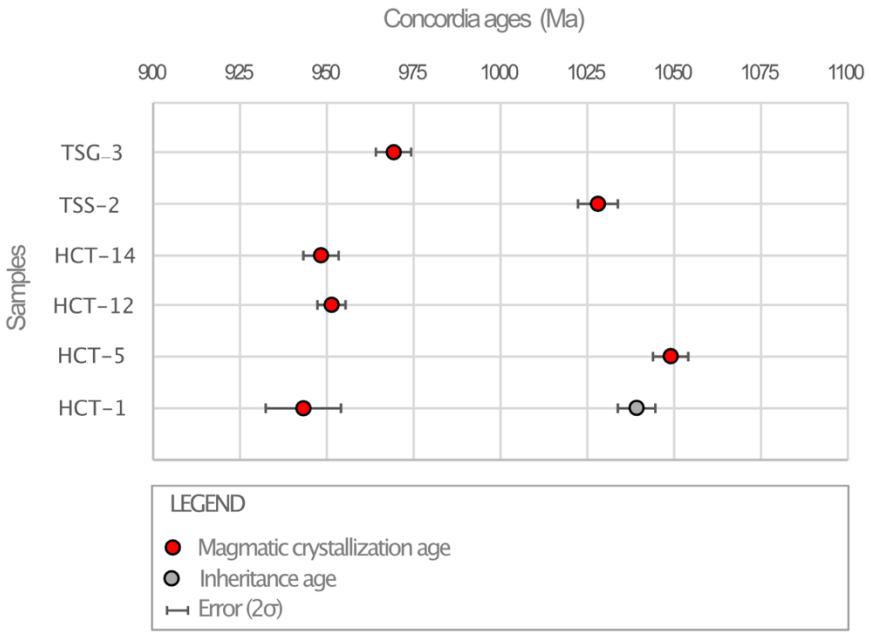

Fig. 41. Summary of Concordia ages obtained in this study of six magmatic ages and one inheritance age.

Chapter 6: Discussion

The U-Pb ages presented in this study can be correlated to the Sveconorwegian and Caledonian orogenies. Magmatic crystallization ages are correlated to the Sveconorwegian orogeny of SW Norway, while the youngest age obtained in this study, is a lower intercept at 474 ± 11 Ma that probably relates to an early Caledonian orogenic event. Additionally, the deformation investigated in this study is interpreted to be Caledonian (as will be discussed below), therefore this chapter is divided into two parts: Sveconorwegian and Caledonian orogenic periods.

6.1 Comparing the U-Pb datasets and samples to each other

The U-Pb ages from this study show magmatism in two age groups at c. 1050 - 1030 Ma and 970 -940 Ma (Fig. 41). Granitic magmatism in the Hardanger area dominates at 1048 ± 5 Ma, 951 ± 4 Ma, 948 ± 5 Ma and 943 ± 11 Ma, while the Gulen area shows magmatism at 969 ± 5 Ma and the Øygarden Complex at 1028 ± 6 Ma. Three of the samples from the Hardanger area have overlapping ages (951 ± 4 Ma, 948 ± 5 Ma and 943 ± 11 Ma) indicating that the granitic bodies were emplaced at the same time.

The Gulen area and the Øygarden Complex are part of the strongly Caledonized Baltic crust, whereas the Hardanger area is only moderately deformed in the footwall of the Hardangerfjord shear zone and is otherwise undeformed. The samples localities in the Hardanger region are close to the Hardangerfjord shear zone, which can explain the only moderately deformed samples augen gneiss (HCT-5) and gneissic granite (HCT-12). The granite from Gulen (TSG-3) is only weakly deformed but is contained in an area of strongly deformed basement.

The most deformed samples from this study from the Øygarden Complex (sample TSS-2 and TSS-1) have zircon with high U concentrations and gave discordant analyses that complicate interpretations. Also, one undeformed sample (HCT-1) from Hardanger has high U concentrations and a high number of discordant analyses. TSS-2, TSS-1 and HCT-1 have high common lead and hence, corrected analyses were used. TSS-2 exhibit a large number of reverse discordance analyses that indicate an overcorrection of the analyses. Therefore, the lower intercept age of TSS-2 are interpreted to have no geological significance. TSS-1 had a poor number of zircons, and the upper intercept is therefore highly unreliable. The lower intercept indicates ancient Pb-loss but is poorly defined. For sample HCT-1, discordance of

U-rich analyses implies that ancient Pb-loss occurred and fell on a discordia line that correspond to the crystallization age. This imply a reliability of the lower intercept age at 474 ± 11 Ma. For all other analyses uncorrected data were used. These analyses have a high number of concordant analyses, low U concentration, low common lead and was straightforward to interpret.

6.2 Sveconorwegian orogenic period

6.2.1 Comparison of new ages to Sveconorwegian magmatic phases

The studied U-Pb datasets coincide with magmatic events in the Sveconorwegian orogeny (Fig. 42, Slagstad et al., 2018). Fig. 42 shows the results from this study together with a compilation of available geochronological data from the Sveconorwegian orogenic period by Slagstad et al. (2018). U-Pb ages revealed from this study match with different peaks magmatic activity in SW Norway and occurred at c. 950 Ma, 970 Ma, 1030 Ma and 1050 Ma. TSS-2 and HCT-5 can be correlated to the SMB magmatism and HCT-1, HCT-12, HCT-14 and TSG-3 to the HBG magmatism.

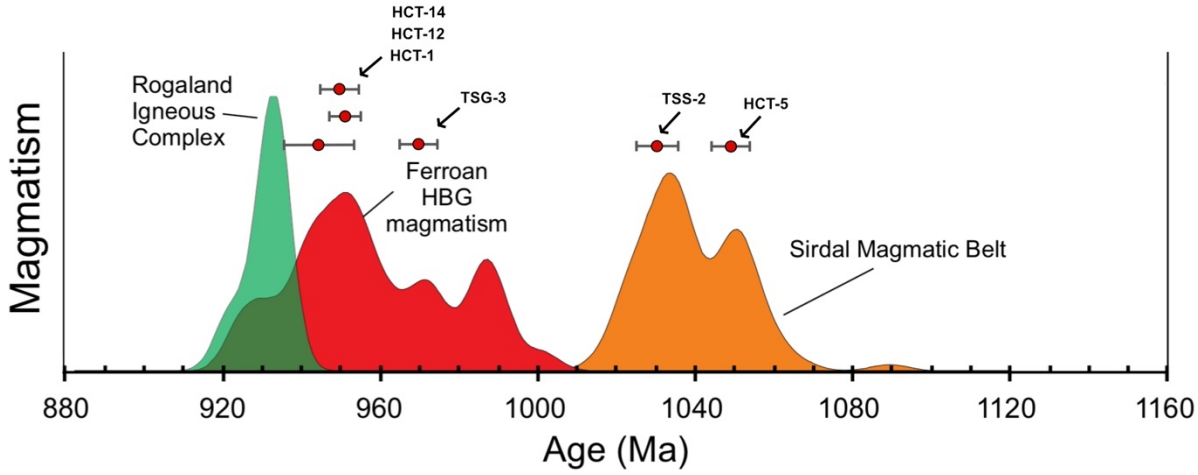

Fig. 42. Main magmatic events in the Sveconorwegian orogeny after Slagstad et al. (2018) and new geochronological data from this study.

Age relationships in the Hardanger area

Earlier dated U-Pb ages of metarhyolites and granites with 1500 Ma ages show that the Hardanger area is part of the Telemarkian Domain, and compares to similar lithological units as the nearby Suldal Arc (Bingen et al., 2005; Roberts et al., 2013). This study shows that the Telemarkian basement was intruded by SMB and HBG granites. Two phases of granitic magmatism dominate in the Hardanger area, around 950 Ma and 1050 Ma. Three of the four granites were emplaced at the same time around 950 Ma, as described above.

The augen gneiss (HCT-5) with crystallization age at 1048 ± 5 Ma corresponds to inheritance ages of sample HCT-1 (calculated Concordia age at 1039 ± 11 Ma). Also, sample HCT-14 shows an inheritance age at 1040. Zircon texture and Th/U ratios indicate magmatic origin. This imply that sample HCT-1 and HCT-14 was affected by an earlier phase of SMB magmatism. An alternative explanation is contamination of a SMB host rock in the intruding HBG granites.

Age relations in the Øygarden Complex

The Øygarden complex has earlier been interpreted as a part of the WGR (Roffeis and Corfu, 2014). Field investigation and geochronological data from Wiest et al. (2018) show that the geological evolution of the Øygarden Complex is different from the main part of the Gothian WGR, and correlates the Øygarden complex to the SMB and the Telemarkian Domain. This study shows that the granitic gneiss (TSS-2) from the western parts of the Øygarden complex confirms the correlation to the SMB. The metagabbro (TSS-1) may imply Telemarkian magmatism, but the age is highly unreliable.

Field observations from Telavåg show intrusion of the granitic gneiss (1028 ± 6 Ma) in the gabbroic rock body (Fig. 13), which is confirmed by the U-Pb ages. In Telavåg, banded gneisses are interpreted to be the oldest lithology, followed by emplacement of gabbroic rock, granitic gneiss and pegmatites. More U-Pb data are necessary to give an exact formation of the gneisses in Telavåg. Regardless, field investigations and U-Pb data confirm earlier studies. Bering (1985) describes intrusion of granitic gneiss in the gabbroic rock body in Telavåg. In addition, Bering (1985) describes that granites and pegmatite intrusions on the southern parts of Sotra intruded older migmatites and gneisses. This coincides with field observations from Telavåg, where banded gneiss is interpreted as the oldest lithology, and was intruded by gabbro, granite and pegmatites. Wiest et al. (2018) dated leucogranites to 1022 ± 11 Ma in the eastern part of the Øygarden Complex. The leucogranites in the eastern

part of the Øygarden Complex has overlapping ages with the granitic gneiss (TSS-2) in Telavåg, which also can be described as a leucogranite. To entirely understand the magmatic and metamorphic evolution of the Øygarden Complex, more geochronological data and field investigations are necessary.

Age relations in the Gulen area

Earlier studies from the southern parts of the WGR show U-Pb ages correlating to the Gothian orogenic period and granitic magmatism with HBG ages (Skår and Pedersen, 2003). A number of granitic bodies in the southern parts of the WGR show magmatism around 970 Ma (Skår and Pedersen, 2003). This study shows HBG ages at 969 ± 5 Ma and correlates well with previous studies. The U-Pb dataset of sample TSG-3 do not show record of Sveconorwegian metamorphic events. Regardless, high-T Sveconorwegian metamorphism is earlier reported from this area by Skår and Pedersen (2003) and Røhr et al. (2004) at 969 ± 8 Ma and at 987 ± 10 Ma with corresponding ages to the calculated Concordia age at 969 ± 5 Ma. Similar age relations are reported by Skår and Pedersen, (2003) which describe that high-T metamorphism in the area was related to heat and mass flux linked to the rise of granitic magma from the lower crust.

Implications to Sirdal Magmatic Belt

The granitic gneiss (TSS-2) from Sotra and augen gneiss (HCT-5) from the Hardanger area can be correlated to the SMB (Fig. 43). The SMB show magmatism in two clusters, around ca. 1050 and 1030 Ma that represents two main periods of magmatic activity (Coint et al., 2015). Concordia ages from Sotra (1028 ± 6) and Hardanger (1048 ± 5 Ma) show a clear relation to the two clusters.

SMB rocks are characterised as undeformed or weakly deformed, in contrast to the strongly deformed granitic gneiss in the Øygarden Complex and the moderately deformed augen gneiss in Hardanger. However, lithological similarities can be recognized. Leucogranite in SMB show resemblance with the detailed studied granitic gneiss in the Øygarden complex with sparse biotite and compositional variation between monzo-and syenogranite (Coint et al., 2015). The augen gneiss in Hardanger has an abundance of hornblende. Hornblende is rare in the SMB but is found in some monzogranites and granodiorites.

Detailed studies by Coint et al. (2015) described the SMB as a voluminous N-S trending belt in the southern parts of Norway. Wiest et al. (2018) correlate the Øygarden Complex to the

SMB and propose the SMB as a continuous NW-SE trending belt. This study confirms Wiest et al. (2018) interpretation. Regardless, only one of the four dated granitic bodies in Hardanger gives a typical SMB age, indicating that the SMB might get less voluminous to the NW.

The eastern limit of the SMB is marked on fig. 43, inferred from this study and the study of Wiest et al. (2018). The sample from Gulen (TSG-3) did not revealed SMB age and coincides with the interpreted NW-SE trending belt. Nevertheless, more U-Pb ages from the Øygarden Complex, the WGR and the Hardanger area will be necessary to entirely understand the extent of the Sirdal Magmatic Belt.

Implications to HBG magmatism

Magmatic crystallization ages from Gulen (TSG-3) and form the Hardanger region (HCT-1, HCT-12, HCT-14) can be correlated to the HBG suite (Fig. 43). The HBG suite represent widespread granitic magmatism from c. 990 – 920 Ma. The investigated granites from this study with HBG ages show magmatism at 950 Ma and 970 Ma. Fig. 42 shows a main peak in magmatic activity around 950 Ma, which coincides with three of the four HBG ages, whereas the sample from Gulen falls within a period with less magmatic activity.

HBG suite have a composition ranging from intermediate (monzodioritic and quartz monzodioritic) to granitic in composition (Auwera et al., 2008; Slagstad et., 2018). The investigated granitic bodies with HBG ages are very homogenous in monzogranitic composition. None of the sample with HBG ages contain hornblende, which is characteristic of the HBG suite, indicating distinct compositional variations within the HBG suite. Also, rare mafic enclaves are common in the HBG suite (Auwera et al., 2008; Auwera et al., 2011), but none of the studied outcrops from this study contains mafic enclaves. Slagstad et al. (2018) report east-to-west compositional variations in the HGB suite with absence of hornblende in the eastern parts of the orogen, signifying that there is more than one group of HBG suite. The result of this study indicates more than one group of HBG suite in the western parts of Norway, and do not correspond to the suggested east-to-west compositional trend within the HBG suite. The compositional variations of HGB suite rocks, indicate that magmatism in this period was more variable than previously known.

Implications to the Sveconorwegian orogeny

This study shows widespread granitic magmatism in western parts of Norway correlated to the SMB and HBG rocks, partly overprinted by Caledonian deformation. The investigated areas and the U-Pb datasets show lack of Sveconorwegian high-T metamorphism. The results correspond to a long-lived accretionary orogenic setting with voluminous magmatism in the Sveconorwegian orogeny and absence of widespread penetrative deformation (Slagstad et al., 2013; Coint et al., 2015; Slagstad et al., 2018). The SMB is interpreted to reflect continental arc magmatism, whereas the HBG granites are commonly described by remelting of SMB lower crustal source during extension of the arc, resulting in mafic underplating (Slagstad et al., 2017; Slagstad et al., 2018). Regardless, the revealed compositional variations within the HBG granites may reflect variations in either tectonic setting or different source (Slagstad et al., 2018). In addition, Slagstad et al. (2018) suggest that mantle-derived heat is the main driver for lower crustal melting and high-grade metamorphic conditions in the Sveconorwegian orogeny. This may be compatible to the earlier dated U-Pb data from Gulen reporting high-T metamorphism and simultaneous granitic magmatism (Skår and Pedersen, 2003; Røhr et al, 2004).

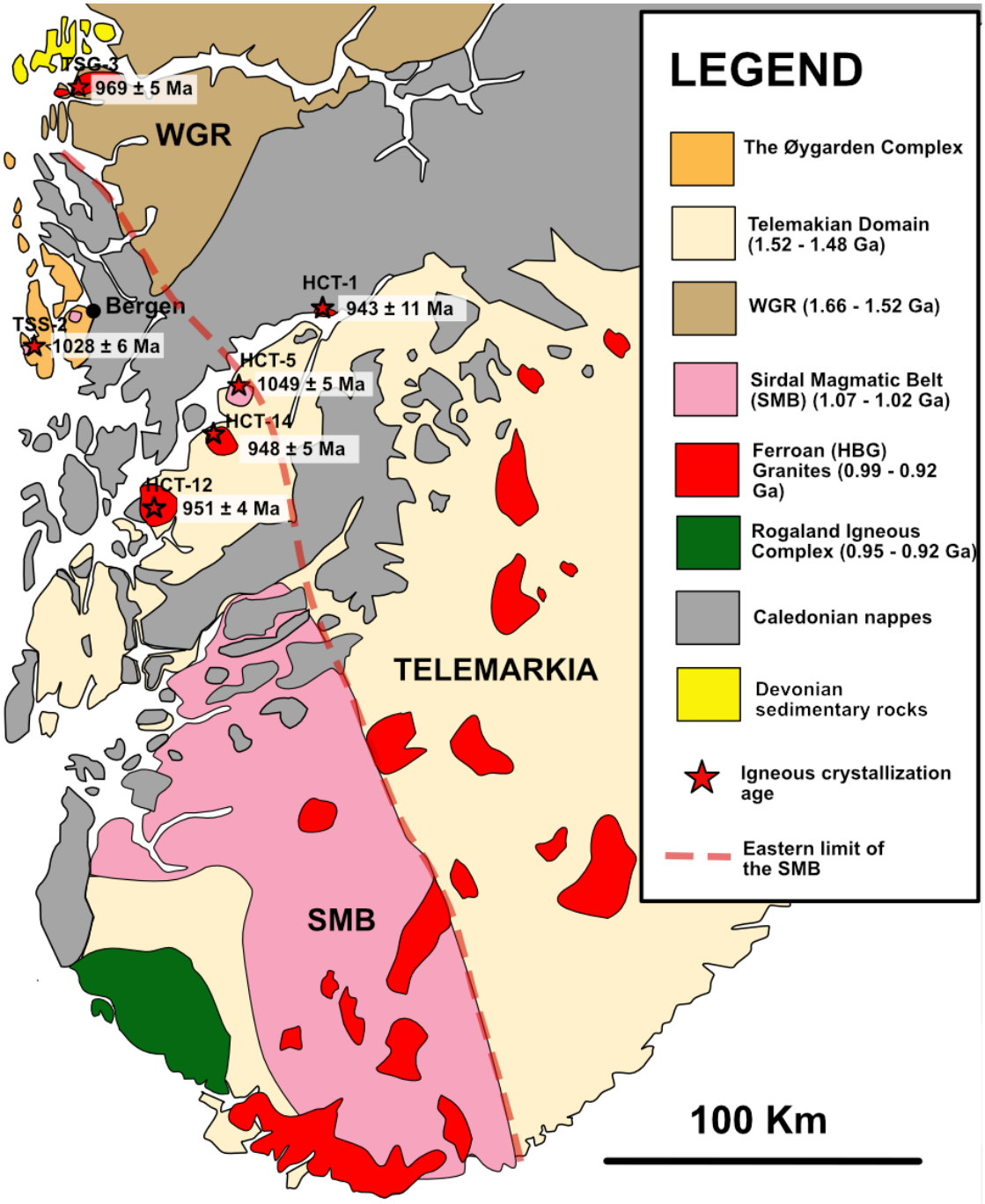

Fig. 43. Simplified geological map of SW Norway comparing results from this study with main features in the Sveconorwegian orogeny. Modified from Fossen and Hurich, (2005), Bingen et al., (2008a), Wiest et al. (2018), Slagstad et al. (2018) and Wiest et al. (2019).

6.3 Caledonian orogenic period

6.3.1 Record of Caledonian metamorphic events in the U-Pb datasets

The studied samples are to varying degrees metamorphosed during the Caledonian orogeny. Whilst the samples from Hardanger and Gulen are undeformed to moderately deformed, the samples from Sotra are strongly deformed. The Caledonian overprint is nevertheless recorded only in one of the datasets. Sample HCT-1, which represents undeformed biotite granite from Hardanger, shows a resetting of metamict zircon at 474 ± 11 Ma, and may represent a low-T thermal event in early Ordovician times. Also, Wiest et al. (2018) presented an early Ordovician age (c. 485 Ma) from the more strongly deformed basement in the eastern Øygarden Complex. This indicates that zircons remained as a closed system during the main continental collision in the Caledonian orogeny, and rather was affected by a thermal event during the poorly understood early Caledonian orogenesis.

The absent of metamorphism related to Caledonian continental collision from this study reflects zircons high resistance of the U-Pb system in high-grade metamorphic events. Pb diffusion is insignificant at temperatures below 900°C (Cherniak and Watson, 2003; Rubatto et al., 2017; Wiest et al., 2018). Besides, Pb-loss is only possible in partially to strongly metamict zircons, and the U-Pb system has to experience a time interval below 600-650°C for radiation damaging to occur (Mezger and Krogstad, 1997).

6.3.2 Structural

Caledonian deformation of the gneisses in the western Øygarden Complex

The main deformation of the gneisses in the Øygarden Complex has been interpreted as Caledonian (Bering, 1984; Fossen and Rykkelid, 1990; Fossen and Dunlap, 1998; Larsen et al., 2003; Wiest et al., 2018). Earlier studies by Bering (1985) and Fossen and Rykkelid (1990), proposed early Caledonian amphibolite facies metamorphism and greenschists facies metamorphism during the Scandian thrusting in the Øygarden Complex. However, evidence from $^{40}Ar/^{39}Ar$ thermochronology by Fossen and Dunlap (1998) shows that the basement in the western parts cooled rapidly through around 500°C at 404 Ma to 350 Ma during top-to-NW movement of the nappes. These ages from the Øygarden Complex correspond with retrograde metamorphism investigated in the Telavåg area, with peak metamorphism at amphibolite facies followed by greenschists facies and brittle fault formation. Measurements from the Telavåg area show an almost constant plunge of linear fabrics towards ESE, indicating that the Precambrian gneisses deformed during one single deformation event.

Cataclastic phyllonites have the same linear fabric orientation as mylonitic gneisses or amphibolites formed in ductile shear zones, with top-to-WNW sense of shear. This implies that both high-grade and low-grade rocks in the western Øygarden Complex are deformed during Devonian extension.

In Telavåg, two different types of folds dominate: largescale upright folds and mesoscale recumbent folds, with fold axes parallel to stretching lineations. These folding patterns show similarities with Christmas three-folding (Fig. 44, Fossen, 2010b) and indicate that the area has been affected by N-S compression, followed by vertical shortening. Also, the strong L-fabrics observed in the granitic gneisses indicate strong NW-SE stretching. The major upright folds in Telavåg, correspond to the upright Sotra and Sund antiforms (Larsen et al., 2003).

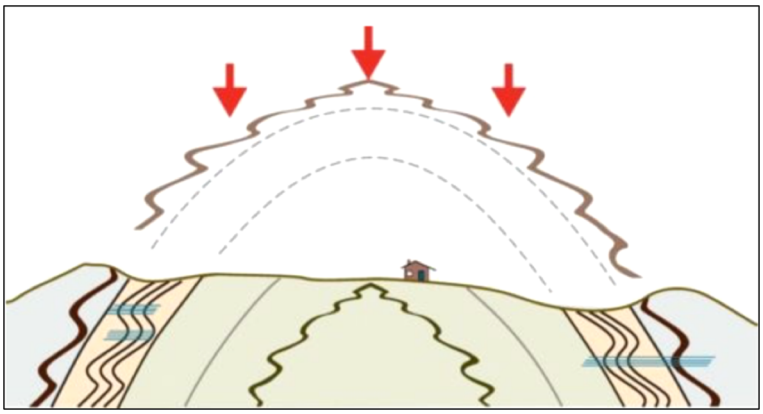

Fig. 44. Figure illustrating Christmas-three folding (Fossen, 2010b).

A lot of the structures observed in Telavåg compare to the ones described by Fossen and Rykkelid (1990), Fossen and Rykkelid (1992), Larsen et al. (2003) and Wiest et al. (2018) in the Øygarden Complex. This includes L-S fabrics, constant stretching lineations towards ESE and top-to-W movement parallel to stretching lineations. There are a lot of similarities between structures revealed in this study and structures investigated from the eastern Øygarden Complex by Wiest et al. (2018), such as upright megafolds, recumbent mesofolds and retrograde metamorphism. Comparing structural data from this study with Wiest et al. (2018) from the eastern part of the Øygarden Complex, show that linear fabrics have constant ENE plunge in the eastern part of the Øygarden and ESE plunge in the western parts (Fig. 45). The ESE plunges in Telavåg are more widespread and might be described by the heterogenous rheology of the different lithologies in Telavåg. An important contrast from the field data from Wiest et al. (2018) involves the absence of top-to-E kinematic indicators.

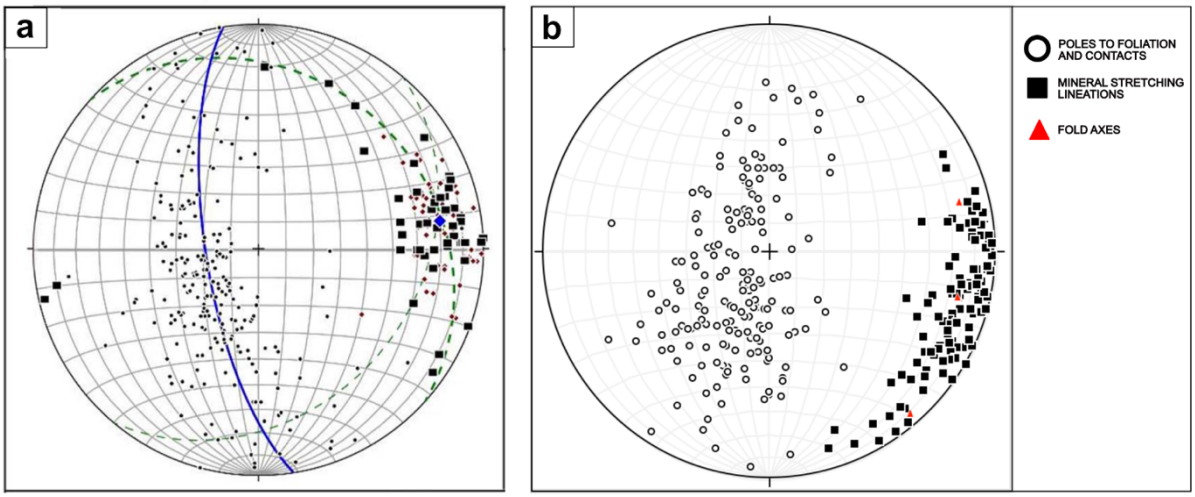

Fig. 45. a) Poles to foliation, lineation and fold axes from eastern part of the Øygarden Complex by Wiest et al. (2018). b) Structural measurements from Telavåg.

Top-to-E and top-to-W fabrics in the Øygarden Complex

The Øygarden Complex exhibits opposite senses of shear (Fig. 46). Top-to-E sense of shear is observed in the eastern parts, while top-to-W sense of shear is seen in the western part of the Øygarden Complex (Fossen and Rykkelid, 1990; Wiest et al., 2018). Earlier models suggested that top-to-E fabrics formed during Scandian thrusting and Top-to-W fabrics formed during early Caledonian events (Fossen and Rykkelid, 1990). Cooling ages are not constrained from eastern Øygarden Complex, but Wiest et al. (2018) field investigations suggest that the top-to-E sense of shear formed during Devonian extension, similar to the dated top-to-NW sense of shear in the western Øygarden Complex. The interpretation is related to the constant fabric orientation indifferent from metamorphic grade indicating one single deformation event, and that Top-to-E deformation in phyllonites do not show any overprinting on top-to-W relationship, which would have been expected if the weak rocks formed during Caledonian thrusting (Wiest et al., 2018). Regardless, western and eastern parts of Øygarden Complex show constant plunge orientation indifferent from metamorphic grade, similarities in metamorphic development and structures, which indicate that the rocks deformed synchronously, and not during two different events.

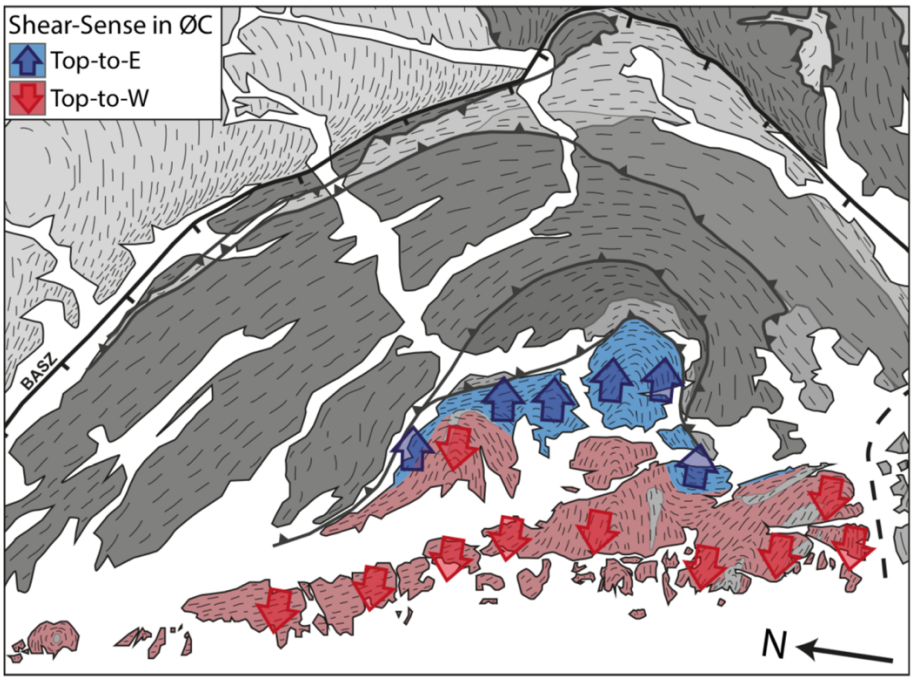

Fig. 46. Opposite sense of shear in the Øygarden Complex (Wiest, 2016).

Wiest et al. (2018) suggest that the opposite sense of shear in the Øygarden Complex formed during Devonian exhumation, signifying that the Øygarden Complex represents a metamorphic core complex. A number of exposed basement windows from the Scandian Caledonides are interpreted as Devonian extensional gneiss domes in the footwall of major extensional faults (Braathen et al., 2000; Osmundsen et al., 2005; Wiest et al., 2019). The Øygarden Complex shows similarities with gneiss domes formation in Mid Norway and the WGR. In Mid Norway and the WGR, gneiss domes are recognized as type 2 culmination (Osmundsen et al., 2005) with extension-parallel shortening in a contrictional field, flanked by extensional detachment zones and faults that cut through mylonites in the footwall and the gneiss dome. Also, Braathen et al. (2000) describes bidirectional and orogen parallel movements in western Norway and linked it to core complex formation. Whitney et al. (2004) describes that upright and recumbent folding are earlier recognized in domes. Also, rapid cooling of the basement at shallower levels, are common in gneiss domes (Whitney et al., 2004). All this implies that folding patterns (upright and recumbent folds), opposite sense of shear and retrograde metamorphism investigated from the Øygarden Complex, can be described by formation of metamorphic core complexes during Devonian extension.

Chapter 7: Conclusion

Based on the results of this study, I propose the following evolution and implication:

- Sveconorwegian orogenic period
  - Granitic magmatism revealed mainly two age groups: 1050-1030 Ma and 960-940 Ma.
  - The protolith ages correlate the Øygarden Complex to the SMB, the Gulen area to the HBG suite and the Hardanger area to both the SMB and HBG granites.
  - The results from this study indicate that the SMB is an NW-SE trending belt that gets less voluminous towards the NW.
  - The HBG-age granites from this study show distinct compositions (lack of hornblende), indicating more than one group of HBG granites in western Norway.
  - Neither the U-Pb datasets nor field investigations show records of Sveconorwegian metamorphism.
  - The lack of Sveconorwegian metamorphism and voluminous magmatism is compatible with a long-lived accretionary orogenic event (Coint et al., 2015, Slagstad et al., 2018).

- Caledonian orogenic period
  - Resetting of strongly metamict zircon at c. 474 Ma in an undeformed granite indicates a low temperature resetting event.
  - All deformation investigated in this study is interpreted to be Caledonian.
  - The deformation in the Øygarden Complex is interpreted to be formed in one single event by amphibolite facies metamorphism followed by greenschists facies metamorphism during Devonian extension.
  - The deformation in the Øygarden Complex shows similarities with metamorphic core complexes investigated in the WGR and the Mid Norway.

Future work

The new insight from this study raised further questions:

- With the lack of U-Pb geochronology for large parts of the western Norway, it would be interesting to sample more granitic rocks to entirely understand the extent of the SMB- and HBG- ages, and to investigate compositional variations within the HBG suite. Also, trace analyses and isotope geochemistry analyses on the sampled lithologies of this study could reveal information about tectonic setting and type of magma source. This could give new insight to the formation of the Sveconorwegian orogeny, and could further prove if it is compatible with a long-lived accretionary setting or a continental collision as previously assumed.
- More U-Pb data and field investigations from the Øygarden Complex are necessary to understand the magmatic and metamorphic evolution, and to further determine if the basement is part of the Telemarkian Domain or the WGR.

-

References

Allegre, C. J. (2008). *Isotope geology*. New York: Cambridge University Press. pp. 512

Bering, D. (1984). *Tektono-metamorf utvikling av det vestlige gneiskompleks i Sund, Sotra.* Cand. real. thesis. University of Bergen.

Bingen, B., Davis, W.J., Hamilton, A.H., Engvik, A.K., Stein, H.J., Øystein, S. And Nordgulen, Ø. (2008a). Geochronology of high-grade metamorphism in the Sveconorwegian belt, S. Norway: U-Pb, Th-Pb and Re-Os data. *Norwegian Journal of Geology* 88, pp. 13-42.

Bingen, B., Nordgulen, O., and Viola, G. (2008b). A four-phase model for the Sveconorwegian orogeny, SW Scandinavia. *Norsk Geologisk Tidsskrift* 88, pp. 43.

Bingen, B., Skår, Ø., Marker, M., Sigmond, E. M., Nordgulen, Ø., Ragnhildstveit, J., Mansfeld, J., Tucker, R. D., and Liégeois, J.-P. (2005). Timing of continental building in the Sveconorwegian orogen, SW Scandinavia. *Norwegian Journal of Geology* 85, pp. 87–116.

Braathen, A., Nordgulen, Ø., Osmundsen, P.-T., Andersen, T.B., Solli, A., Roberts, A. (2000). Devonian, orogen-parallel, opposed extension in the Central Norwegian Caledonides. *Geology* 28, pp. 615-618.

Cherniak, D. J. and Watson, E. B. (2003). Diffusion in zircon. *Reviews in mineralogy and geochemistry* 53, pp. 113–143.

Coint, N., Slagstad, T., Roberts, N., Marker, M., Røhr, T., and Sørensen, B. E. (2015). The Late Mesoproterozoic Sirdal Magmatic Belt, SW Norway: Relationships between magmatism and metamorphism and implications for Sveconorwegian orogenesis. *Precambrian Research* 265, pp. 57-77.

Corfu, F., Andersen, T., and Gasser, D. (2014). The Scandinavian Caledonides: main features, conceptual advances and critical questions. *Geological Society, London, Special Publications* 390, pp. 9–43.

Corfu, F., Hanchar, J. M., Hoskin, P. W., and Kinny, P. (2003). Atlas of zircon textures. *Reviews in mineralogy and geochemistry* 53, pp. 469–500.

Davis, D. W., Krogh, T. E., and Williams, I. S. (2003). Historical development of zircon geochronology. *Reviews in mineralogy and geochemistry* 53, pp. 145–181.

Fossen, H. (1992). The role of extensional tectonics in the Caledonides of south Norway. *Journal of structural geology* 14, pp. 1033–1046.

Fossen, H (1998). Advances in understanding the post-Caledonian structural evolution of the Bergen area, West Norway. *Norsk Geologisk Tidsskrift* 78, pp. 33–46.

Fossen, H. (2000). Extensional tectonics in the Caledonides: Synorogenic or postorogenic. *Tectonics* 19, pp. 213–224.

Fossen, H. (2010a). Extensional tectonics in the North Atlantic Caledonides: a regional view. *Geological Society, London, Special Publications* 335, pp. 767–793.

Fossen, H (2010b). *Structural geology*. New York: Cambridge University Press. pp. 463

Fossen, H. and Dunlap, W. J. (1998). Timing and kinematics of Caledonian thrusting and extensional collapse, southern Norway: evidence from 40 Ar/39 Ar thermochronology. *Journal of structural geology* 20, pp. 765–781.

Fossen, H. and Dunlap, W. J. (1998). Age constraints on the late Caledonian (Scandian) deformation in the Major Bergen Arc, SW Norway. *Norsk Geologisk Tidsskrift* 86, pp. 59.

Fossen, H. and Hurich, C. A. (2005). The Hardangerfjord Shear Zone in SW Norway and the North Sea: a large-scale low-angle shear zone in the Caledonian crust. *Journal of the Geological Society* 162, pp. 675–687.

Fossen, H. and Rykkelid, E. (1990). Shear zone structures in the Øygarden area, West Norway. *Tectonophysics* 174, pp. 385–397.

Gee, D. G., Fossen, H., Henriksen, N., and Higgins, A. K. (2008). From the early Paleozoic platforms of Baltica and Laurentia to the Caledonide Orogen of Scandinavia and Greenland. *Episodes* 31, pp. 44–51.

Hacker, B. R., Andersen, T. B., Johnston, S., Kylander-Clark, A. R., Peterman, E. M., Walsh, E. O., and Young, D. (2010). High-temperature deformation during continental-margin subduc- tion & exhumation: The ultrahigh-pressure Western Gneiss Region of Norway. *Tectonophysics* 480, pp. 149–171.

Harley, S. L. and Kelly, N. M. (2007). Zircon tiny but timely. *Elements* 3, pp. 13–18.

Ireland, T. R. and Williams, I. S. (2003). Considerations in zircon geochronology by SIMS. *Reviews in Mineralogy and Geochemistry* 53, pp. 215–241.

Johannessen, K., Kohlmann, F., Ksienzyk, A., Dunjk,I and Jacobs, J. (2013). Tectonic evolution of the SW Norwegian passive margin based on low-temperature thermochronology from the innermost Hardangerfjord. *Norwegian Journal of Geology* 93, pp. 243-260.

Kildal E.S (1970). Geologisk kart over Norge 1:125000, norsk utgave, Norges geologiske undersøkelse.

Larsen, Ø., Fossen, H., Langeland, K., and Pedersen, R.-B. (2003). Kinematics and timing of polyphase post-Caledonian deformation in the Bergen area, SW Norway. *Norsk Geologisk Tidsskrift* 83, pp. 149–166.

Li, Z.X., Bogdanova, S.V., Collins, A.S, Davidson, A., Waele, B.D., Ernst, R.E., Fritzsimons., I.C.W., Fuck, R.A., Gladkochub, D.P., Jacobs, J., Karlstrom, K.E., Lu, S., Natapov, L.M., Pease, V., Pisarevsky, S.A., Thrane, K., Vernikovsky, V. (2008). Assembly, configuration, and break-up history of Rodinia: A synthesis. *Precambrian Research* 160, pp. 179-210.

Ludwig K.R (2012). *User´s Manual for Isoplot 3.75.* Berkeley: Berkeley Geochronological Center. pp. 75.

Mezger, K. and Krogstad, E. (1997). Interpretation of discordant U-Pb zircon ages: An evaluation. *Journal of metamorphic Geology* 15, pp. 127–140.

Osmundsen, P. T., Braathen, A., Sommaruga, A., Skilbrei, J. R., Nordgulen, Ø., Roberts, D., Andersen, T. B., Olesen, O., and Mosar, J. (2005). Metamorphic core complexes and gneiss-cored culminations along the Mid-Norwegian margin: an overview and some current ideas. *Norwegian Petroleum Society Special Publications* 12, pp. 29–41.

Rino, S., Kon, Y., Sato, W., Maruyama, S., Santosh, M., and Zhao, D. (2008). The Grenvillian and Pan-African orogens: world's largest orogenies through geologic time, and their implications on the origin of superplume. *Gondwana Research* 14, pp. 51–72.

Roberts, D. (2003). The Scandinavian Caledonides: event chronology, palaeogeographic settings and likely modern analogues. *Tectonophysics* 365, pp. 283–299.

Roberts, N. M., Slagstad, T., Parrish, R.R., Norry, M.J., Marker, M., Horstwood, M.S.A. (2013). Sedimentary recycling in arc magmas: geochemical and U-Pb-Hf-O constraints on the Mesoproterozoic Suldal Arc, SW Norway. *Contrib Mineral Petrol* 165, pp. 507-523.

Roberts, N. M. and Slagstad, T. (2015). Continental growth and reworking on the edge of the Columbia and Rodinia supercontinents; 1.86–0.9 Ga accretionary orogeny in southwest Fennoscandia. *International Geology Review* 57, pp. 1–25.

Roffeis, C., Corfu, F. and Gabrielsen, R. (2013). A Sveconorwegian terrane boundary in the Caledonian Hardanger–Ryfylke Nappe Complex: The lost link between Telemarkia and the Western Gneiss Region? *Precambrian Research* 228, pp. 20–35.

Rubatto, D. (2017). The metamorphic Mineral. *Reviews in Mineralogy and Geochemistry* 83, pp: 261-195.

Røhr, T.S., Corfu, F., Austrheim, H. and Andersen, T.B. (2004). Sveconorwegian U-Pb zircon and monazite ages of Granulite-facies rocks, Hisarøya, Gulen, Western Gneiss Region, Norway. *Norwegian journal of Geology* 84, pp. 151-156.

Schoene, B. (2014). *U-Th-Pb Geochronology*. Princeton: Elsevier. pp. 378

Skår, Ø. and Pedersen, R.-B. (2003). Relations between granitoid magmatism and migmatization: U-Pb geochronological evidence from the Western Gneiss Complex, Norway. *Journal of the Geological Society* 160, pp. 935-946.

Solli, A., Naterstad, J., Andresen, A. (1978). Structural succession in a part of the outher Hardangerfjord area, west Norway. *Norges geo. Unders.* 345, 39-51.

Slagstad, T., Henderson, I. H. C., Marker, M., Coint, N., Skår, Ø., Røhr, T. S., Høy, I., Sauer, S., Stormoen, M. A., Roberts, N. M. W., Kirkland, C. L., Sørensen, B. E. and Bybee. G. (2018). Magma-driven, high-grade metamorphism in the Sveconorwegian Province,

southwest Norway, during the termal stages of the Fennoscandian Shield evolution. *Geophere* 14, no. 2.

Slagstad, T., Roberts, N. M., Marker, M., Røhr, T. S., and Schiellerup, H. (2013). A non-collisional, accretionary Sveconorwegian orogen. *Terra Nova* 25, pp. 30–37.

Slama, J. and Pedersen, R. B. (2015). Zircon provenance of SW Caledonian phyllites reveals a distant Timanian sediment source. *Journal of the Geological Society 172*, pp. 2014–143.

Sigmond, E.M (1975) Geologisk kart over Norge 1:125000, norsk utgave, Norges geologiske undersøkelse.

Sigmond, E.M (1998) Geologisk kart over Norge 1:125000, norsk utgave, Norges geologiske undersøkelse.

Sturt, B. A., Skarpenes, O., Pringle, I. R., and Ohanian, A. T. (1975). Reconnaissance Rb/Sr isochron study in the Bergen Arc System and regional implications. *Nature* 253, pp. 595–599.

Tera, F., and Wasserburg, G. J., 1972, U-Th-Pb systematics in three Apollo 14 basalts and the problem of initial Pb in lunar rocks. *Earth and Planetary Science Letters* 14, pp. 281-304.

Torsvik, T. H. and Cocks, L. R. M. (2005). Norway in space and time: a centennial cavalcade. *Norwegian Journal of Geology* 85, pp. 73–86.

Vander Auwera, J., Bogaerts, M., Bolle.,O., Longhi.,J (2008). Genesis of intermediate igneous rocks at the end of the Sveconorwegian (Grenvillian) orogeny (S Norway) and their contribution to intracrustal differentiation. *Contributions to Mineralogy and Petrology* 156, pp. 721-743.

Vander Auwera, J., Bolle, O., Bingen, B., Liégeois, J.-P., Bogaerts, M., Duchesne, J.-C., De Waele, B., and Longhi, J. (2011). Sveconorwegian massif-type anorthosites and related granitoids result from post-collisional melting of a continental arc root. *Earth-Science Reviews* 107, pp. 375–397.

Wetherill, G. W., 1956, Discordant U-Pb ages. *Transactions of the American Geophysical Union* 37, pp. 320-326.

Whitehouse, M. J. and Kamber, B. S. (2005). Assigning dates to thin gneissic veins in high-grade metamorphic terranes: a cautionary tale from Akilia, southwest Greenland. *Journal of Petrology* 46, pp. 291–318.

Whitehouse, M. J., Kamber, B. S., and Moorbath, S. (1999). Age significance of U-Th-Pb zircon data from early Archaean rocks of west Greenland - a reassessment based on combined ion-microprobe and imaging studies. *Chemical geology* 160, pp. 201–224.

Whitney, D. L., Teyssier, C., and Vanderhaeghe, O. (2004). Gneiss domes and crustal flow. *Geological Society of America Special Papers* 380, pp. 15–33.

Wiest, J.D. (2016). *Mesoproterozoic to Early Devonian Evolution of the Lyderhorn Gneiss (Øygarden Complex, SW Norway)*. Master of Science Thesis, University of Bergen.

Wiest, J., Jacobs, J., Ksienzyk, A. and Fossen, H. (2018). Sveconorwegian vs. Caledonian orogenesis in the eastern Øygarden Complex, SW Norway – Geochronology, structural constraints and tectonic implications. *Precambrian Research* 305, pp. 1-18.

Wiest, J.D., Osmundsen, P.T., Jacobs, J and Fossen, H. (2019). Deep crustal Flow within post-orogenic metamorphic core complexes – Insights from the southern Western Gneiss Region of Norway. *American Geophysical Union*.

Yuanbao, W. and Yongfei, Z. (2004). Genesis of zircon and its constraints on interpretation of U-Pb ages. *Chinese Science Bulletin* 49, pp. 1554-1569.

Appendix

- Appendix 1 - SIMS U-Pb Zircon Geochronology results
- Appendix 2 - List of outcrops
- Appendix 3 - Map of outcrop
- Appendix 4 - Structural map of planar fabrics
- Appendix 5 - Structural map of linear fabrics

Appendix 1 - SIMS U-Pb Zircon Geochronology results

			Concentration (ppm)						Total (uncorrected) ratio				Radiogenic (corrected) ratio[4]				Calculated age ± σ (Ma)			
Sample ID	Grain characteristics in CL	Comment	[U]	[Th]	[Pb]	Th/U_{meas}[2]	$^{206}Pb/^{204}Pb$	$f_{206}\%$[3]	$^{206}Pb/^{238}U$	± σ (%)	$^{207}Pb/^{206}Pb$	± σ (%)	$^{207}Pb/^{235}U$	± σ (%)	$^{206}Pb/^{238}U$	± σ (%)	$^{207}Pb/^{206}Pb$	$^{206}Pb/^{238}U$	207-corr age[5]	Conc(%)[6]
HCT-1																				
n6088_24-1	CL-D, UZ, rim	Corcordant age > 95 %	1066,7	170,5	87,4	0,16	624	3,00	0,074638	1,10	0,079058	2,10	0,55577	4,57	0,07240	1,11	439,4	450,6	450,8	97,4
n6088_21-1	CL-D, UZ, rim	Discordant age	799,9	299,6	89,2	0,37	465	4,02	0,098813	1,05	0,093038	0,90	0,80956	2,76	0,09484	1,06	671,0	584,1	582,3	113,0
n6088_13-1	CL-B, Z, core	Discordant age	87,9	44,4	10,5	0,50	155	12,06	0,113340	1,44	0,155656	8,00	0,85711	31,08	0,09967	1,56	686,9	612,5	610,8	110,8
n6088_20-1	CL-D, UZ, rim	Discordant age	568,5	193,1	67,7	0,34	810	2,31	0,106070	1,85	0,079800	1,74	0,88502	3,53	0,10362	1,88	672,2	635,6	634,8	105,4
n6088_18-1	CL-D, Z	Discordant age	458,7	341,4	70,6	0,74	268	6,98	0,130839	1,07	0,118437	2,05	1,08459	5,83	0,12171	1,09	762,4	740,4	739,8	102,9
n6088_9-1	CL-B, Z	Discordant age	371,4	226,9	57,1	0,61	402	4,65	0,127846	1,52	0,103386	1,84	1,13736	4,14	0,12190	1,57	858,4	741,5	738,1	113,6
n6088_22-1	CL-D, UZ, rim	Discordant age	435,5	146,7	74,5	0,34	4515	0,41	0,147274	1,10	0,073057	0,40	1,41322	1,24	0,14666	1,10	925,0	882,2	880,6	104,6
n6088_10-1	CL-M, Z	Concordant age > 95 %	176,1	230,2	40,2	1,31	2074	0,90	0,156774	1,31	0,076406	0,78	1,48867	2,43	0,15536	1,31	913,5	930,9	931,6	98,1
n6088_2-1	CL-D, Z	Concordant age > 95 %	211,2	274,0	49,0	1,30	114	16,34	0,188702	1,06	0,192692	2,50	1,45996	11,38	0,15786	1,10	840,1	944,9	949,0	87,5
n6088_23-1	CL-M, Z	Concordant age > 95 %	89,5	100,6	19,8	1,12	1060	1,76	0,160845	1,70	0,082876	3,36	1,51098	5,92	0,15801	1,72	909,3	945,7	947,2	96,0
n6088_14-1	CL-D, UZ, core	Concordant age > 95 %	336,4	83,6	61,6	0,25	3808	0,49	0,159567	1,25	0,074566	0,37	1,55024	1,56	0,15878	1,25	951,9	950,0	949,9	100,2
n6088_12-1	CL-M, Z	Rev. Discordant age	94,5	72,1	19,8	0,76	1693	1,10	0,167692	1,30	0,078123	0,79	1,59289	2,32	0,16584	1,30	918,4	989,1	992,2	92,3
n6088_4-1	CL-M, Z	Rev. Discordant age	151,0	214,6	37,9	1,42	2339	0,80	0,170633	1,08	0,074915	0,74	1,60530	2,95	0,16927	1,08	892,2	1008,1	1013,2	87,0
n6088_6-1	CL-B, Z	Concordant age > 95 %	22,8	21,8	5,3	0,96	13137	0,14	0,172881	1,46	0,075088	1,62	1,76152	2,27	0,17264	1,46	1041,6	1026,6	1025,9	101,4
n6088_19-1	CL-B, Z	Concordant age > 95 %	63,8	74,1	15,8	1,16	13626	0,14	0,175178	1,38	0,073235	0,77	1,74118	1,63	0,17494	1,38	991,2	1039,3	1041,5	95,2
n6088_7-1	CL-M, PZ	Concordant age > 95 %	87,5	77,9	20,6	0,89	13788	0,14	0,175876	1,50	0,073828	0,66	1,76282	1,68	0,17564	1,50	1008,2	1043,1	1044,8	96,5
n6088_16-1	CL-B, Z	Concordant age > 95 %	39,1	41,7	9,6	1,07	34270	0,05	0,176720	1,43	0,074614	1,12	1,80695	1,83	0,17662	1,43	1046,9	1048,5	1048,6	99,8
n6088_11-1	CL-M, Z	Rev. Discordant age	102,1	161,7	28,6	1,58	10597	0,18	0,182770	1,40	0,072206	0,66	1,78244	1,60	0,18245	1,40	953,3	1080,3	1086,6	86,7
n6088_3-1	CL-M, PZ, core	Discordant age	143,3	56,7	34,8	0,40	2215	0,84	0,204165	1,53	0,090813	0,71	2,35776	1,78	0,20244	1,54	1303,4	1188,4	1181,1	108,8
n6088_8-1	CL-D, Z, core	Rev. Discordant age	216,9	82,5	63,0	0,38	2123	0,88	0,247740	1,03	0,093737	0,32	2,95047	1,13	0,24556	1,03	1363,7	1415,5	>1200	96,2
HCT-5																				
n6082_9-1	CL-M, Z	Pb loss	92,2	40,1	18,5	0,43	32150	0,06	0,165588	2,49	0,073974	0,66	1,67783	2,59	0,16549	2,49	1028,6	987,2	985,4	104,0
n6082_22-1	CL-M, Z,	Pb loss	51,0	20,0	10,2	0,39	96793	{0.02}	0,167979	1,39	0,074532	0,86	1,72623	1,64	0,16798	1,39	1055,9	1001,0	998,4	105,2
n6082_9-2	CL-M, Z,	Pb loss	180,9	57,6	35,9	0,32	68082	0,03	0,169398	1,00	0,075159	0,44	1,75010	1,10	0,16935	1,00	1067,2	1008,5	1005,8	105,5
n6082_14-1	CL-M, PZ, core	Pd loss	76,6	43,8	16,4	0,57	10803	0,17	0,171605	0,95	0,074101	0,71	1,71907	1,25	0,17131	0,95	1007,8	1019,3	1019,8	98,9
n6082_21-1	CL-D, UZ, core	Pb loss	90,2	41,2	18,8	0,46	15970	0,12	0,172197	1,19	0,075559	0,66	1,77074	1,39	0,17200	1,19	1059,6	1023,1	1021,4	103,4
n6082_10-1	CL-D, Z	Corcordant age > 95 %	62,7	25,3	13,1	0,40	20234	0,09	0,174417	1,19	0,073409	0,77	1,74681	1,47	0,17426	1,19	1005,7	1035,5	1036,9	97,0
n6082_2-1	CL-D, Z	Corcordant age > 95 %	135,6	48,4	28,0	0,36	24101	0,08	0,174662	1,06	0,074007	0,52	1,76664	1,20	0,17453	1,06	1025,4	1037,0	1037,6	98,9
n6082_10-2	CL-D, UZ, rim	Pb loss	253,0	53,1	49,7	0,21	2603	0,72	0,176063	0,88	0,075639	0,38	1,69044	1,09	0,17480	0,88	932,4	1038,5	1043,4	88,6
n6082_7-1	CL-M, Z	Corcordant age > 95 %	65,0	27,7	13,7	0,43	46245	{0.04}	0,175356	1,15	0,073030	0,84	1,76572	1,42	0,17536	1,15	1014,8	1041,6	1042,9	97,4
n6082_12-1	CL-D, Z	Pb loss	33,0	10,6	6,8	0,32	27277	{0.07}	0,175677	1,37	0,075840	1,06	1,83703	1,74	0,17568	1,37	1090,9	1043,3	1040,9	104,4
n6082_5-1	CL-D, Z	Disc. age	95,8	35,9	20,0	0,37	1788	1,05	0,178011	1,27	0,081302	1,62	1,78090	3,27	0,17615	1,27	1023,0	1045,9	1047,0	97,8
n6082_16-1	CL-D, weackly Z	Corcordant age > 95 %	143,5	48,4	29,9	0,34	117073	{0.02}	0,176537	1,11	0,074185	0,64	1,80572	1,28	0,17654	1,11	1046,5	1048,0	1048,1	99,9
n6082_11-1	CL-M, Z	Corcordant age > 95 %	31,4	16,4	6,9	0,52	27241	{0.07}	0,177241	1,54	0,074299	1,08	1,81572	1,88	0,17724	1,54	1049,6	1051,9	1052,0	99,8
n6082_13-1	CL-D, Z	Corcordant age > 95 %	209,8	73,9	44,0	0,35	65782	0,03	0,177424	0,92	0,074100	0,48	1,80691	1,04	0,17737	0,92	1038,3	1052,6	1053,3	98,6
n6082_4-1	CL-D, Z	Corcordant age > 95 %	44,0	13,7	9,1	0,31	47712	{0.04}	0,177376	1,18	0,073436	0,92	1,79600	1,49	0,17738	1,18	1026,0	1052,6	1053,9	97,4
n6082_3-1	CL-D, Z	Corcordant age > 95 %	74,6	28,4	15,7	0,38	22096	0,08	0,177716	1,07	0,073333	0,93	1,77958	1,44	0,17757	1,07	1005,2	1053,7	1056,0	95,2
n6082_6-1	CL-D, Z	Corcordant age > 95 %	136,7	48,2	28,8	0,35	116550	{0.02}	0,177718	1,07	0,074486	0,51	1,82519	1,19	0,17772	1,07	1054,7	1054,5	1054,5	100,0
n6082_15-2	CL-D, UZ, rim	Corcordant age > 95 %	143,2	36,4	29,4	0,25	65292	0,03	0,178313	1,21	0,073909	0,98	1,81124	1,56	0,17826	1,21	1033,0	1057,5	1058,7	97,6
n6082_5-2	CL-D, UZ, rim	Corcordant age > 95 %	317,3	33,6	62,6	0,11	120079	0,02	0,178316	1,20	0,073908	0,50	1,81391	1,30	0,17829	1,20	1035,7	1057,6	1058,7	97,9
n6082_15-1	CL-B, Z	Corcordant age > 95 %	56,6	25,1	12,2	0,44	39167	{0.05}	0,178802	1,39	0,073844	0,81	1,82050	1,61	0,17880	1,39	1037,2	1060,4	1061,6	97,8
n6082_18-1	Missing CL picture	Corcordant age > 95 %	211,2	62,8	44,1	0,30	86516	0,02	0,179247	0,92	0,073810	0,46	1,81972	1,03	0,17921	0,92	1031,8	1062,6	1064,2	97,0
n6082_8-1	CL-D, Z	Rev. Discordant age	73,7	37,6	16,3	0,51	31339	0,06	0,180832	1,40	0,072770	0,70	1,80195	1,58	0,18072	1,40	994,8	1070,9	1074,7	92,3

			Concentration (ppm)						Total (uncorrected) ratio				Radiogenic (corrected) ratio[4]				Calculated age ± σ (Ma)			
Sample ID	Grain characteristics in CL	Comment	[U]	[Th]	[Pb]	Th/U_{meas}[2]	$^{206}Pb/^{204}Pb$	f_{206}%[3]	$^{206}Pb/^{238}U$	± σ (%)	$^{207}Pb/^{206}Pb$	± σ (%)	$^{207}Pb/^{235}U$	± σ (%)	$^{206}Pb/^{238}U$	± σ (%)	$^{207}Pb/^{206}Pb$	$^{206}Pb/^{238}U$	207-corr age[5]	Conc(%)[6]
HCT-12																				
n6086_21-1	CL-M, Z	Concordant age > 95%	18,4	10,8	3,7	0,59	2627	0,71	0,166318	2,41	0,072476	1,91	1,52560	3,67	0,16513	2,43	837,9	985,2	991,5	82,4
n6086_26-1	CL-D, PZ, core	Rev. Concordant age	130,3	60,5	25,8	0,46	8912	0,21	0,165030	2,43	0,070121	0,87	1,55565	2,62	0,16468	2,44	884,0	982,8	987,0	88,8
n6086_13-1	CL-B, Z	Rev. Concordant age	17,8	8,8	3,5	0,49	4676	0,40	0,164001	1,43	0,069145	1,58	1,48796	2,63	0,16335	1,43	808,5	975,3	982,2	79,4
n6086_3-1	CL-M, Z	Concordant age > 95%	14,7	7,0	2,9	0,48	4724	0,40	0,163910	1,40	0,070299	1,70	1,51399	2,71	0,16326	1,40	845,7	974,9	980,3	84,7
n6086_7-1	CL-M, Z	Concordant age	39,7	10,9	7,4	0,27	8777	0,21	0,162324	1,14	0,069670	1,24	1,51944	1,81	0,16198	1,14	869,6	967,8	971,8	88,7
n6086_6-1	CL-D, UZ core	Concordant age	339,7	174,9	66,0	0,51	2079	0,90	0,162412	1,46	0,071281	0,41	1,42785	3,24	0,16095	1,47	752,9	962,1	970,4	72,2
n608_11-1	CL-B, Z	Concordant age > 95%	8,1	5,3	1,6	0,65	2683	0,70	0,161576	1,53	0,071488	3,26	1,46286	4,58	0,16045	1,53	810,3	959,3	965,3	81,6
n6086_16-1	CL-D, UZ core	Concordant age > 95%	12,0	6,6	2,4	0,55	6875	{0.27}	0,159973	1,44	0,070979	2,07	1,56558	2,52	0,15997	1,44	956,8	956,6	956,6	100,0
n6086_15-1	CL-B, Z	Concordant age > 95%	15,0	5,8	2,9	0,39	13879	{0.13}	0,159952	1,47	0,073203	1,71	1,61444	2,25	0,15995	1,47	1019,6	956,5	953,8	106,2
n6086_17-1	CL-M, Z	Concordant age > 95%	32,3	9,5	6,0	0,29	9433	0,20	0,160038	1,64	0,071193	1,19	1,53437	2,14	0,15972	1,64	918,8	955,2	956,7	96,0
n6086_28-1	CL-M, UZ	Pb loss	75,4	21,3	13,8	0,28	1869	1,00	0,161201	1,30	0,076153	1,34	1,50672	2,51	0,15959	1,31	883,0	954,5	957,4	91,9
n6086_23-1	CL-D, Z	Concordant age > 95%	89,0	24,6	16,4	0,28	76870	{0.02}	0,159561	1,31	0,070409	0,72	1,54900	1,50	0,15956	1,31	940,3	954,3	954,9	98,5
n6086_10-1	CL-M, Z	Concordant age > 95%	50,8	14,8	9,4	0,29	25945	0,07	0,159460	1,39	0,071229	0,94	1,55282	1,72	0,15935	1,39	948,1	953,1	953,3	99,5
n6086_14-1	CL-M, Z,	Concordant age > 95%	61,8	16,9	11,2	0,27	18295	0,10	0,158422	1,20	0,069931	0,86	1,50886	1,52	0,15826	1,20	903,1	947,1	948,9	95,1
n6086_8-1	CL-M, Z	Concordant age > 95%	69,0	20,8	12,7	0,30	24216	0,08	0,158349	1,27	0,070623	0,81	1,52784	1,53	0,15823	1,27	929,3	946,9	947,6	98,1
n6086_29-1	CL-B, Z	Concordant age > 95%	12,9	3,6	2,4	0,28	9034	{0.21}	0,158098	1,32	0,071656	2,22	1,56199	2,58	0,15810	1,32	976,2	946,2	944,9	103,1
n6086_19-1	CL-M, Z	Concordant age > 95%	33,4	10,8	6,2	0,32	33916	{0.06}	0,158023	1,40	0,070950	1,17	1,54588	1,82	0,15802	1,40	956,0	945,8	945,4	101,1
n6086_20-1	CL-M, Z	Concordant age > 95%	26,0	12,9	5,0	0,50	8159	0,23	0,158155	1,32	0,070702	1,33	1,49999	2,06	0,15779	1,33	897,1	944,5	946,4	94,7
n6086_5-1	CL-M, UZ	Concordant age > 95%	15,0	7,2	2,8	0,48	2867	0,65	0,158702	1,26	0,070514	1,94	1,42371	3,73	0,15767	1,26	790,1	943,8	949,8	80,6
n6086_2-1	CL-B, Z	Concordant age > 95%	25,4	6,0	4,6	0,24	5247	0,36	0,157731	1,47	0,072288	1,36	1,50733	2,22	0,15717	1,47	915,3	941,0	942,1	97,2
n6086_18-1	CL-M, Z	Concordant age > 95%	43,1	15,4	7,9	0,36	16945	0,11	0,157231	1,28	0,070729	1,03	1,51333	1,70	0,15706	1,28	924,9	940,4	941,0	98,3
n6086_25-1	CL-M, Z	Pb loss	16,3	9,0	3,2	0,55	2498	0,75	0,158222	1,55	0,074091	1,71	1,47986	3,29	0,15704	1,56	879,1	940,3	942,7	93,0
n6086_4-1	CL-M, Z	Concordant age > 95%	28,3	13,0	5,3	0,46	4759	0,39	0,157591	1,63	0,070176	1,27	1,45347	2,46	0,15697	1,64	842,6	939,9	943,8	88,5
n6086_22-1	CL-M, Z	Concordant age	15,9	9,5	3,1	0,60	2419	0,77	0,158169	1,57	0,069338	1,71	1,37124	3,16	0,15695	1,58	720,6	939,8	948,1	69,6
n6086_9-1	CL-B, Z	Concordant age > 95%	32,7	11,8	6,0	0,36	98620	{0.02}	0,156520	1,35	0,071344	1,18	1,53967	1,79	0,15652	1,35	967,3	937,4	936,2	103,1
n6086_30-1	CL-M, Z	Concordant age > 95%	36,3	11,5	6,6	0,32	7051	0,27	0,155602	1,13	0,071390	1,11	1,48408	1,76	0,15519	1,14	909,4	930,0	930,8	97,7
n6086_24-1	CL-D, PZ, core	Concordant age	141,8	95,9	28,0	0,68	5083	0,37	0,155706	1,10	0,070640	0,71	1,45054	1,43	0,15513	1,10	862,9	929,7	932,3	92,3
n6086_16-2	CL-M, Z	Concordant age > 95%	15,1	6,9	2,8	0,45	16370	0,11	0,154256	1,59	0,071055	2,06	1,49095	2,77	0,15408	1,59	933,6	923,8	923,4	101,1
n6086_12-1	CL-D, Z core	Pb loss	129,2	58,5	23,1	0,45	3408	0,55	0,149401	2,42	0,071903	0,61	1,38669	2,74	0,14858	2,43	859,0	893,0	894,3	96,0
n6086_27-1	CL-B, Z	Pb loss	36,7	18,2	6,5	0,50	4305	0,43	0,145191	3,86	0,071723	1,01	1,36313	4,30	0,14456	3,87	880,4	870,4	870,0	101,1
HCT-14																				
n6085_26-1	CL-M, Z	Rev. Discordant age	18,5	13,6	3,9	0,73	11001	{0.17}	0,160609	1,57	0,068383	1,60	1,51433	2,24	0,16061	1,57	880,2	960,2	963,5	90,9
n6085_7-1	CL-M, UZ, core	Rev. Discordant age	18,5	21,5	4,2	1,16	4126	0,45	0,161117	1,43	0,068491	1,58	1,43737	2,58	0,16039	1,43	774,3	958,9	966,3	76,1
n6085_3-1	CL-M, Z	Concordant > 95 %	22,6	12,2	4,3	0,54	11194	0,17	0,156062	1,28	0,069032	1,43	1,45537	2,07	0,15580	1,28	860,9	933,4	936,3	91,6
n6085_14-1	CL-M, Z	Concordant > 95 %	29,0	17,3	5,8	0,60	12818	0,15	0,159778	1,43	0,069069	1,26	1,49475	2,01	0,15955	1,43	867,0	954,2	957,8	89,9
n6085_19-1	CL-B, Z	Concordant age	16,1	12,0	3,3	0,74	4405	0,42	0,159282	1,25	0,069273	1,71	1,44345	2,59	0,15861	1,25	806,5	949,0	954,7	82,3
n6085_12-1	CL-B, Z	Concordant > 95 %	23,7	16,2	4,8	0,68	12164	0,15	0,158807	1,35	0,069663	1,38	1,49722	2,10	0,15856	1,35	883,2	948,8	951,4	92,6
n6085_25-1	CL-M, Z	Concordant > 95 %	23,2	14,8	4,7	0,64	10249	0,18	0,159319	1,43	0,069789	1,42	1,49956	2,13	0,15903	1,43	880,4	951,4	954,3	91,9
n6085_17-1	CL-B, Z	Concordant > 95 %	26,0	16,7	5,2	0,64	82221	{0.02}	0,158572	1,41	0,069813	1,34	1,52639	1,95	0,15857	1,41	922,9	948,8	949,9	97,2
n6085_4-1	CL-M, Z	Concordant > 95 %	21,9	10,9	4,2	0,50	8657	0,22	0,158089	1,42	0,070048	1,45	1,48750	2,21	0,15775	1,42	880,4	944,2	946,8	92,7
n6085_21-1	CL-M, Z	Concordant > 95 %	32,9	21,7	6,7	0,66	14421	0,13	0,160979	1,20	0,070081	1,18	1,53146	1,79	0,16077	1,20	901,3	961,1	963,5	93,4
n6085_20-1	CL-M, Z	Concordant > 95 %	35,9	23,7	7,3	0,66	43119	{0.04}	0,158367	1,13	0,070190	1,46	1,53265	1,85	0,15837	1,13	933,9	947,7	948,3	98,5
n6085_11-1	CL_B, Z	Concordant > 95 %	16,4	18,4	3,6	1,13	4356	0,43	0,157878	1,44	0,070383	1,66	1,45402	2,67	0,15720	1,44	840,4	941,2	945,2	88,0
n6085_5-2	CL-M, Z	Concordant > 95 %	32,3	22,2	6,6	0,69	19256	{0.10}	0,159353	1,20	0,070600	1,18	1,55120	1,69	0,15935	1,20	945,9	953,2	953,5	99,2
n6085_1-1	CL-M, Z	Concordant > 95 %	21,5	16,2	4,3	0,75	8532	0,22	0,154031	1,68	0,070609	2,43	1,46067	3,10	0,15369	1,68	896,6	921,6	922,6	97,2
n6085_23-1	CL-M, Z	Concordant > 95 %	32,6	20,7	6,6	0,64	12731	0,15	0,160242	1,36	0,070684	1,58	1,53458	2,17	0,16001	1,36	915,4	956,8	958,5	95,5
n6085_15-2	CL-M, Z	Concordant > 95 %	23,4	15,0	4,7	0,64	12046	0,16	0,158248	1,36	0,070723	1,39	1,51481	2,07	0,15800	1,36	914,6	945,7	946,9	96,6
n6085_2-1	CL-M, Z	Concordant > 95 %	37,6	25,6	7,5	0,68	5185	0,36	0,158461	1,22	0,070739	1,11	1,47969	1,87	0,15789	1,22	867,6	945,0	948,2	91,1
n6085_15-1	CL-M, UZ, core	Concordant > 95 %	43,9	51,7	10,0	1,18	10885	0,17	0,159731	1,14	0,070796	1,03	1,52757	1,64	0,15946	1,15	913,0	953,8	955,4	95,5
n6085_27-1	CL-B, Z	Concordant > 95 %	36,4	23,8	7,3	0,66	9692	0,19	0,158142	1,73	0,071105	1,42	1,51526	2,34	0,15784	1,74	917,4	944,7	945,9	97,0
n6085_18-1	CL-B, Z	Concordant > 95 %	16,0	10,9	3,2	0,68	5547	0,34	0,159046	1,57	0,071166	1,69	1,49882	2,65	0,15851	1,57	886,1	948,5	951,0	93,0
n6085_22-1	CL-M, Z	Concordant > 95 %	35,1	27,6	7,2	0,79	18064	0,10	0,157405	1,52	0,071178	1,66	1,52599	2,29	0,15724	1,52	939,6	941,4	941,5	99,8
n6085_13-1	CL-M, Z	Pb loss	37,6	25,1	7,5	0,67	34516	{0.05}	0,156123	1,35	0,071810	1,12	1,54580	1,75	0,15612	1,35	980,6	935,2	933,3	104,6
n6085_16-1	CL-B, Z	Concordant > 95 %	22,7	21,8	4,9	0,96	5669	0,33	0,158271	1,48	0,071889	1,41	1,50863	2,30	0,15775	1,49	909,5	944,3	945,7	96,2
n6085_10-1	CL-D, Z	Concordant > 95 %	17,1	12,6	3,5	0,74	8780	0,21	0,159421	1,24	0,072131	1,69	1,54639	2,30	0,15908	1,24	943,0	951,7	952,0	99,1
n6085_6-1	CL-D, UZ, core.	Discordant age	625,4	332,0	133,3	0,53	108972	0,02	0,172417	1,45	0,074039	0,45	1,75670	1,52	0,17239	1,45	1039,0	1025,3	1024,6	101,3
n6085_24-1	CL-B, Z	Discordant age	19,2	17,2	4,0	0,90	1861	1,00	0,156023	1,46	0,077348	1,50	1,48333	2,98	0,15446	1,47	918,1	925,9	926,2	99,2
n6085_5-1	CL-M, PZ, core	Discordant age	27,0	28,9	5,9	1,07	1021	1,83	0,159114	2,11	0,088670	10,62	1,60938	14,01	0,15620	2,14	1061,2	935,6	930,3	111,8

			Concentration (ppm)						Total (uncorrected) ratio				Radiogenic (corrected) ratio[4]				Calculated age ± σ (Ma)			
Sample ID	**Grain characteristics in CL**	**Comment**	**[U]**	**[Th]**	**[Pb]**	**Th/U_{meas}[2]**	**$^{206}Pb/^{204}Pb$**	**f_{206}%[3]**	**$^{206}Pb/^{238}U$**	**± σ (%)**	**$^{207}Pb/^{206}Pb$**	**± σ (%)**	**$^{207}Pb/^{235}U$**	**± σ (%)**	**$^{206}Pb/^{238}U$**	**± σ (%)**	**$^{207}Pb/^{206}Pb$**	**$^{206}Pb/^{238}U$**	**207-corr age[5]**	**Conc(%)[6]**
TSG-3																				
n6087_6-1	CL-M, UZ, rim	Concordant age > 95 %	63,0	33,2	12,2	0,53	23535	0,08	0,157384	1,30	0,071127	0,84	1,52905	1,59	0,15726	1,30	943,5	941,5	941,4	100,2
n6087_2-1	CL- D, UZ, core	Concordant age > 95 %	36,0	54,1	8,7	1,50	17460	0,11	0,157832	2,33	0,071194	1,34	1,52984	2,73	0,15766	2,34	939,3	943,8	944,0	99,5
n6087_5-1	CL-B, Z	Concordant age > 95 %	25,4	35,3	6,0	1,39	18639	{0.10}	0,158910	1,34	0,071472	1,30	1,56599	1,87	0,15891	1,34	971,0	950,7	949,9	102,1
n6087_1-1	CL-M, Z	Concordant age > 95 %	32,6	43,2	7,6	1,32	23804	{0.08}	0,160248	1,33	0,071617	1,15	1,58238	1,76	0,16025	1,33	975,1	958,2	957,4	101,7
n6087_7-1	CL-M, Z	Concordant age > 95 %	48,0	63,8	11,3	1,33	22592	0,08	0,161011	1,34	0,071449	0,95	1,57082	1,68	0,16088	1,34	952,1	961,7	962,1	99,0
n6087_14-1	CL-M, Z	Concordant age > 95 %	30,7	39,5	7,2	1,29	16225	0,12	0,161109	1,13	0,071016	1,18	1,55614	1,72	0,16092	1,13	932,3	961,9	963,1	96,8
n6087_15-1	CL-M, Z	Concordant age > 95 %	36,0	44,3	8,4	1,23	16325	0,11	0,161272	1,40	0,072680	1,15	1,59484	1,87	0,16109	1,40	980,4	962,8	962,1	101,8
n6087_19-1	CL-B, UZ	Concordant age > 95 %	38,4	71,0	10,0	1,85	10816	0,17	0,161462	1,23	0,070738	1,06	1,54262	1,72	0,16118	1,23	911,0	963,3	965,5	94,3
n6087_8-1	CL-M, Z	Concordant age > 95 %	44,2	49,6	10,0	1,12	40762	{0.05}	0,161623	1,35	0,071404	0,98	1,59121	1,67	0,16162	1,35	969,0	965,8	965,6	100,3
n6087_11-1	CL-M, Z	Concordant age > 95 %	48,7	55,2	11,1	1,13	81434	{0.02}	0,161747	1,28	0,070922	1,07	1,58169	1,67	0,16175	1,28	955,2	966,5	967,0	98,8
n6087_4-2	CL-M, UZ	Concordant age > 95 %	73,5	37,3	14,6	0,51	>1e6	{0.00}	0,161819	1,18	0,070829	0,77	1,58031	1,41	0,16182	1,18	952,5	966,9	967,5	98,5
n6087_16-1	CL-M, UZ	Concordant age > 95 %	24,4	35,7	6,0	1,46	12921	0,14	0,162754	1,68	0,071737	1,32	1,58267	2,28	0,16252	1,69	946,7	970,8	971,8	97,5
n6087_13-1	CL-M, Z	Concordant age > 95 %	41,1	34,1	8,9	0,83	16873	0,11	0,162957	1,34	0,071069	1,03	1,57600	1,74	0,16278	1,34	934,8	972,2	973,8	96,0
n6087_17-1	CL-M, Z	Concordant age > 95 %	28,2	32,8	6,6	1,16	92426	{0.02}	0,163204	1,35	0,072286	1,23	1,62662	1,82	0,16320	1,35	994,0	974,6	973,7	102,0
n6087_4-1	CL-M, Z	Concordant age > 95 %	28,2	35,6	6,7	1,26	18038	{0.10}	0,163231	1,46	0,070394	1,32	1,58431	1,97	0,16323	1,46	939,9	974,7	976,2	96,3
n6087_18-1	CL-M, Z	Concordant age > 95 %	19,6	29,8	4,9	1,52	10479	0,18	0,163560	1,98	0,071775	1,48	1,58502	2,60	0,16327	1,98	940,3	974,9	976,4	96,3
n6087_12-1	CL-D, Z	Concordant age > 95 %	64,1	61,0	14,3	0,95	23732	0,08	0,163503	1,29	0,072240	0,82	1,61372	1,56	0,16337	1,29	975,7	975,5	975,5	100,0
n6087_9-2	CL-M, Z	Concordant age > 95 %	65,8	59,4	14,5	0,90	35676	0,05	0,164072	1,23	0,071602	0,80	1,60990	1,49	0,16399	1,23	963,2	978,9	979,6	98,4
n6087_22-2	CL-M, Z	Discordant age	41,0	52,2	9,7	1,27	2073	0,90	0,165750	1,34	0,076600	2,22	1,57833	4,23	0,16426	1,34	919,3	980,4	983,0	93,4
n6087_20-2	CL-M, Z	Concordant age > 95 %	44,2	53,2	10,4	1,20	11503	0,16	0,164628	1,21	0,070752	0,99	1,57516	1,67	0,16436	1,22	913,8	981,0	983,8	92,7
n6087_3-1	CL-D, Z	Concordant age > 95 %	102,5	69,7	21,5	0,68	48641	0,04	0,164505	1,19	0,070651	0,85	1,59523	1,48	0,16444	1,19	938,8	981,4	983,3	95,5
n6087_9-1	CL-M, UZ	Concordant age > 95 %	42,1	65,7	10,7	1,56	41525	{0.05}	0,165704	1,67	0,071687	1,00	1,63785	1,94	0,16570	1,67	977,1	988,4	988,9	98,8
n6087_10-1	CL-M, Z	Concordant age > 95 %	51,2	79,5	13,0	1,55	19824	0,09	0,166613	1,55	0,071726	1,16	1,62962	1,98	0,16646	1,55	957,5	992,6	994,1	96,3
n6087_20-1	CL- D, UZ	Concordant age > 95 %	52,0	80,1	13,3	1,54	15870	0,12	0,166780	2,53	0,071471	0,91	1,62087	2,74	0,16658	2,54	945,0	993,3	995,4	94,9
TSS-1																				
n6089_3-1	UZ	Discordian age	417,5	150,9	113,8	0,36	2269	0,82	0,231602	1,07	0,096791	0,25	2,87095	1,18	0,22969	1,08	1439,3	1332,9	>1200	107,4
n6089_4-1	UZ	Discordian age	1514,1	249,6	238,6	0,16	14888	0,13	0,139520	2,54	0,080388	0,83	1,52622	2,68	0,13934	2,54	1183,1	841,0	827,9	128,9
n6089_5-1	UZ	Discordian age	780,1	241,5	219,4	0,31	102086	0,02	0,238106	1,00	0,090708	0,19	2,97291	1,02	0,23806	1,00	1437,6	1376,6	>1200	104,2
TSS-2																				
n6089_6-1		Discordian age	2280,6	914,3	522,4	0,40	17018	0,11	0,189158	1,49	0,085921	0,13	2,21696	1,50	0,18895	1,49	1317,7	1115,7	1103,9	115,3
n6084_23-1	CL-D, Z	Rev. Discordant age	730,1	423,6	125,1	0,58	1013	1,85	0,145961	1,30	0,075092	0,76	1,20088	5,01	0,14327	1,31	631,9	863,1	870,8	63,4
n6084_8-1	CL-D, Z	Concordant age >95 %	571,5	318,7	84,2	0,56	1906	0,98	0,125500	2,54	0,070892	0,40	1,08482	3,45	0,12427	2,57	718,8	755,1	756,1	94,9
n6084_18-1	CL-D, Z	Rev. Discordant age	496,5	197,1	82,3	0,40	979	1,91	0,140795	1,55	0,079389	1,14	1,23111	2,37	0,13810	1,57	763,1	833,9	836,3	90,7
n6084_12-1	CL-D, Z,	Rev. Discordant age	436,5	179,7	86,9	0,41	1255	1,49	0,173012	1,13	0,076377	0,76	1,52477	3,80	0,17043	1,13	770,6	1014,5	1025,0	68,4
n6084_7-1	CL-D, Z	Concordant age >95 %	779,4	457,8	136,6	0,59	1267	1,48	0,141565	2,35	0,077341	0,78	1,26878	3,39	0,13947	2,38	805,6	841,7	842,9	95,5
n6084_15-1	CL-D, Z	Pb loss	537,0	279,2	85,5	0,52	2267	0,82	0,127252	1,21	0,074305	1,38	1,18277	2,24	0,12620	1,22	867,7	766,2	763,1	111,7
n6084_17-1	CL-D, Z	Pb loss	877,5	128,3	143,1	0,15	7736	0,24	0,148486	1,33	0,072402	0,30	1,44093	1,37	0,14813	1,33	944,5	890,5	888,4	105,7
n6084_5-1	CL-D, Z	Rev. Discordant age	430,7	189,5	88,4	0,44	4804	0,39	0,172045	1,49	0,074180	0,30	1,68250	1,56	0,17137	1,49	963,3	1019,7	1022,3	94,1
n6084_9-1	CL-D, PZ, core	Pb loss	600,1	431,1	119,5	0,72	21121	0,09	0,153254	1,46	0,072059	0,27	1,50700	1,50	0,15312	1,46	968,4	918,4	916,4	105,2
n6084_15-2	CL-D, UZ, rim	Concordant age >95 %	630,0	27,7	109,1	0,04	35211	0,05	0,160004	1,15	0,071808	0,27	1,57439	1,19	0,15992	1,15	968,9	956,3	955,8	101,3
n6084_26-1	CL-D, Z	Pb loss	609,7	317,5	117,5	0,52	5307	0,35	0,156740	2,81	0,074536	0,56	1,54717	2,88	0,15619	2,82	981,5	935,6	933,7	104,7
n6084_16-1	CL-D, Z	Pb loss	465,4	204,5	87,8	0,44	39710	0,05	0,156559	1,83	0,072463	0,36	1,55572	1,87	0,15649	1,83	988,9	937,2	935,1	105,2
n6084_3-1	CL-D,PZ, core	Concordant age >95 %	279,1	205,5	59,1	0,74	9388	0,20	0,166533	1,65	0,073749	0,46	1,65517	1,76	0,16620	1,65	992,4	991,1	991,1	100,1
n6084_4-1	CL-D, UZ, rim	Pb loss	719,7	35,4	122,3	0,05	32041	0,06	0,156388	1,23	0,072783	0,48	1,55889	1,33	0,15630	1,23	995,5	936,2	933,7	106,0
n6084_21-1	CL-D, Z	Concordant age >95 %	434,0	59,3	82,5	0,14	34268	0,05	0,169478	2,05	0,073541	0,32	1,70783	2,07	0,16939	2,05	1017,4	1008,7	1008,3	100,9
n6084_20-1	CL-D, Z	Rev. Discordant age	49,6	33,0	11,4	0,67	22441	0,08	0,180424	1,33	0,073864	0,89	1,82019	1,66	0,18027	1,33	1020,3	1068,5	1070,9	95,3
n6084_11-1	CL-D, Z	Concordant age >95 %	409,4	161,9	84,2	0,40	34376	0,05	0,172654	1,23	0,073828	0,32	1,74669	1,28	0,17256	1,23	1025,4	1026,2	1026,2	99,9
n6084_14-1	CL-D, Z	Concordant age >95 %	641,1	188,7	126,3	0,29	174554	0,01	0,169279	1,27	0,073666	0,33	1,71729	1,31	0,16926	1,27	1030,1	1008,0	1007,0	102,1
n6084_2	CL-D, Z	Concordant age >95 %	476,1	164,8	95,7	0,35	24437	0,08	0,170778	1,49	0,074199	0,30	1,73209	1,53	0,17065	1,49	1031,0	1015,7	1015,0	101,5
n6084_10-1	CL-D, Z	Concordant age >95 %	351,4	154,3	73,4	0,44	37101	0,05	0,173270	1,71	0,074100	0,34	1,76021	1,74	0,17318	1,71	1033,7	1029,6	1029,4	100,4
n6084_6-1	CL-D, Z	Concordant age >95 %	517,0	196,7	103,8	0,38	72110	0,03	0,169237	1,50	0,073920	0,46	1,71982	1,57	0,16919	1,50	1033,9	1007,7	1006,5	102,5
n6084_25-1	CL-D, Z	Concordant age >95 %	546,0	209,1	113,1	0,38	98561	0,02	0,174299	1,52	0,073912	0,32	1,77247	1,56	0,17427	1,52	1035,1	1035,6	1035,6	100,0
n6084_13-1	CL-D, PZ	Concordant age >95 %	475,3	194,7	98,6	0,41	149147	0,01	0,173009	1,18	0,073971	0,34	1,76205	1,23	0,17299	1,18	1038,1	1028,6	1028,1	100,9
n6084_2-1	CL-D, Z	Concordant age >95 %	349,2	138,2	73,3	0,40	140951	0,01	0,175767	1,21	0,074394	0,42	1,80023	1,28	0,17574	1,21	1049,4	1043,7	1043,4	100,5
n6084_22-1	CL-D, Z	Concordant age >95 %	399,0	152,3	84,7	0,38	192378	0,01	0,177924	1,29	0,074561	0,40	1,82715	1,35	0,17791	1,29	1054,7	1055,5	1055,6	99,9

Notes:

(1) CL-B/M/D = bright/medium/dark; Z = zoned, UZ = unzoned, PZ = patchily zoned.

(2) Based on measured Th and U signals.

(3) f_{206} is the percentage of common Pb estimated from 204Pb counts; in parentheses where these are insignificant;

(4) Ratios after subtraction of common Pb (if detected)

(5) Age based on projecting a line in inverse concordia space from assumed common Pb through the total (uncorrected) ratios onto concordia (Ludwig, 2001)

(6) Concordance in %. Values in parentheses indicate concordant within 2 σ uncertainty; for discordant data, the second number reports the closest approach to concordia at 2 σ limit.

Appendix 2 – List of outcrops

Loc	Coordinates	Unit	Structural	Foliation	Lineation	Limb1	Limb2	Fold Axis
1	60°12`56`N 005°08`45`E	Mixed lithologies (amphibolite, pegmatite and granitic gneiss)	Shear zone S and L tectonite Top to NW	327/28 328/26 305/30 334/25	22-> 136 15 -> 120 32 -> 125 17 ->112			
2	60°11`04`N 005°09`07`E	Granitic gneiss Ultramylonite	Shear zone S and L tectonite	051/25 050/27 049/25	25 -> 118 20 -> 113 04->106			
3	60°13`21`N 005°04`12`E	Metagabbro Homogenous outcrop						
4	60°12`40`N 005°03`02`E	Mixed lithologies (Amphibolite, granitic gneiss and pegmatite)	Shear zone S and L tectonite	056/30 093/26 119/32 178/88 183/83 206/74	17 -> 112 19 -> 114			
5	60°15`28`N 004°58`47`E	Granitic pegmatite		288/30 291/45 293/31 298/29	10 -> 087 04 -> 094			
6	60°15`38`N 004°58`51`E	Amphibolite						
7	60°15`45`N 004°59`07`E	Amphibolite and metagabbro with pegmatite intrusion and overlying granitic gneiss.	S and L tectonite	313/38 235/11 287/25 311/24	26 ->105 08 -> 099 04 -> 094 15 ->100			
8	60°15`41`N 004°59`31`E	Amphibolite with pegmatite intrusion.	Shear zone S and L tectonite	073/24 070/46 066/35 042/33	10 -> 095 19 -> 092			
9	60°14`27`N 005°02`40`E	Banded gneiss, Pegmatite intrusion	S and L tectonite Top to NW	310/35 317/19 310/24 315/31 316/18	06 -> 113 05 -> 116 04 -> 116			
10	60°15`40`N 004°04`23`E	Banded gneiss	S and L tectonite Ultramylonite	027/29 027/29	29 -> 114 27 -> 108			
11	60°13`53`N 005°08`31`E	Banded gneiss	S and L tectonite Ultramylonite	315/51 353/34 333/42 336/35 330/55	18 -> 114 14 -> 121 21 -> 119			
12	60°15`47`N 005°05`26`W	Banded gneiss	Mesomylonite S and L tectonite Top to NW	353/32 356/27	21->109			
13	60°12`22`N 005°02`26`E	Amphibolite with tonalitic veins.						
14	60°14`33`N 005°03`01`E	Banded gneiss	Augen mylonite S and L tectonite Top to NW	291/54 290/25 311/35 294/38	05->101			
15	60°11`10`N 005°07`35`E	Banded gneiss	Ultramylonite S and L tectonite	059/17 076/31 085/34	17 -> 110 20 -> 114			
16	16°12`42`N 005°08`42`E	Dioritic to granitic gneiss.	Mesomylonite S and L tectonite	319/32 326/29 328/40	20 -> 112 15 -> 111			

17	60°12`57`N 005°09`09`E	Amphibolite	S and L tectonite	310/45 303/42	12 -> 111			
18	60°13`24`N 005°09`28`E	Augen Gneiss	S and L tectonite	341/35 340/46	15 -> 103			
19	60°10`02`N 005°03`54`E	Granitic gneiss	Ultramylonite S and L tectonite	074/34 071/27 073/21	10 -> 102 15 -> 112			
20	60°11`07`N 005°03`10`E	Amphibolite	Recumbent and tight folding	083/26 097/30	16 -> 114			
21	60°12`25`N 005°04`25`W	Mixed lithologies (amphibolite, granitic gneiss and pegmatite)	S and L tectonite Top to NW Boudinage	305/33 319/42 315/40 314/35	08 -> 127 16 -> 123 14 -> 112			
22	60°15`17``N 004°58`37`E	Granitic gneiss and amphibolite.	Sharp boundary, parallel to foliation. Granitic gneiss is mesomylonitic. S and L tectonite	335/17 G 290/45 G 289/38 contact	12 -> 093 G 09 -> 095 15 -> 104 contact			
23	60°15`04`N 005°00`03`E	Dioritic to tonalitic gneiss.	Ultramylonite S and L tectonite	280/48 284/41 292/45	04 -> 116 00 -> 115 45 -> 292			
24	60°16`04`N 004°57`48`E	Amphibolite	Similar folds, tight and recumbent. S and L tectonite	064/16 038/18	11 ->076			
25	60°16`05`N 004°57`40`E	Amphibolite	Similar fold, tight and reclined. S and L tectonite	078/19	17->160			
26	60°15`57``N 004°57`35``E	Granitic pegmatite						
27	60°15`48``N 004°57`34``E	Bodie of granitic gneiss in the amphibolite	L>S	309/10	11->085			
28	60°15`45`N 004°57`48`E	Bodie of granitic gneiss in the amphibolite.	Similar fold, tight, recumbent. S and L tectonite	023/29	19->080			
29	60°15`37``N 004°58`47``E	Metagabbro Homogenous outcrop (sample TSS-1)	S and L tectonite	308/15 225/25 282/21	03->089			
30	60°16`15`N 004°57`14`E	Tonalitic pegmatite						
31	60°15`59`N 004°58`08`E	Granitic gneiss	S and L tectonite Mesomylonitic	227/30 314/38	14 -> 112 00 -> 120			
32	60°15`48`N 004°58`38`E	Metagabbro and amphibolite		087/30	15 -> 122			
33	60°15`33`N 004°58`51`E	Metagabbro and amphibolite.	Similar folding, tight and recumbent. S and L tectonite	331/70	21 -> 133	289/35	115/38	05 ->139
34	60°15`33`N 004°58`37`E	Amphibolite	S and L tectonite	357/14 322/32	09 -> 132 14 -> 112			
35	60°15`27`N 004°58`31`E	Tonalitic pegmatite						
36	60°15`42`N 004°59`39`E	Granodioritic gneiss	L tectonite		03 -> 145			
37	60°15`07`N 004°59`16`E	Banded gneiss with pegmatite layer.	Augen mylonite Top to west	271/40 289/48 289/47	04 -> 095 03 -> 087			
38	60°15`22`N 004°59`37`E	Metagabbro. Content of hornblende and biotite.	Anastomosing	297/16 301/30 305/24	11 -> 099			

39	60°15`22`N 004°59`25`E	Metagabbro	Local shear zone with amphibolite. S and L tectonite	254/22 266/18 290/32	12 -> 082			
40	60°15`08`N 004`58`43`E	Dioritic to granitic gneiss with granitic gneiss on top.	Boundary parallel to foliation. Shear zone Sheath folding Boudinage Top to NW	316/41 332/46	06 -> 107			
41	60°15`12`N 004°58`37`E	2 m wide layer of Amphibolite in the granitic gneiss.	S and L tectonite	278/32 Contact	107->13 Contact			
42	60°15`16`N 004°59`30`	Metagabbro and amphibolite. Granite on top High content of chlorite and plagioclase.	Anastomosing	294/45	16 -> 098			
43	60°15`15`N 004°57`57`E	Granitic pegmatite with amphibolite xenolith and quartz veins.						
44	60°15`15`N 004°57`57`E	Granitic pegmatite						
45	60°15`15`N 004°58`04`E	Amphibolite	S and L tectonite	290/68 301/55	15 -> 103			
46	60°15`18`N 004°59`45`E	Metagabbro with some zones of amphibolite. High content of chlorite	S and L tectonite	317/32 297/35	11 -> 116			
47	60°15`06`N 004°59`50`E	Dioritic to granitic gneiss	Augen mylonite S and L tectonite	295/45 270/53	01 -> 088			
48	60°16`25`N 004°57`05`E	Boundary between the granite and the amphibolite	Vertical brittle fault between the units. S and L tectonite Pegmatite in the granitic gneiss.	294/69	07 -> 111 19 -> 123 16 -> 109			
49	60°16`21`N 004°57`10`E	Amphibolite with tonalite veins	S and L tectonite	287/60 300/49	14 -> 115 08 -> 117			
50	60°15`59`N 004°58`38`E	Boundary between granitic gneiss and amphibolite	L>S in Granite S and L in amphibolite	063/39 G 083/30 A	18->103 G 09->139			
51	60°15`48`N 004°59`34`E	Amphibolite layer in the granitic gneiss. .	Boundary follows the foliation.	055/13 030/15 Contact	12 -> 117 Contact			
52	60°15`59`N 004°59`43`E	Granite gneiss	Local shear zone in the outcrop L>S tectonite	075/11 079/15	07 -> 125			
53	60°18`53`N 005°21`53`E	Banded gneiss	Shear zone Sheath folding Boudinage	271/37 282/44 275/85	02 -> 091			
54	60°15`12`N 004°59`43`E	Granitic gneiss with ultracataclasite	Ultramylonite S and L tectonite	264/47 261/43 264/48	05 -> 083			
55	60°15`14`N 004°59`45`E	Boundary between the granitic gneiss and amphibolite. Granitic gneiss on top of the amphibolite.	Sharp boundary, parallel to foliation. S and L tectonite	274/21 288/11 Contact	03 -> 102 Contact			
56	60°15`29`N 004°59`33`E	Boundary between the granitic gneiss and amphibolite.	Sharp boundary, parallel to foliation. S and L tectonite	285/20 303/17	10 -> 079 15 ->065			

57	60°15`13`N 004°59`53`E	Amphibolite layer in the granitic gneiss.		272/55 270/39 265/54	18 ->092 06->84			
58	60°15`15`N 004°59`27`E	Granitic gneiss	S and L tectonite	284/12 276/33	06 -> 083			
59	60°15`09`N 004°58`39`E	Metagabbro						
60	60°15`16`N 004°58`19`E	Granitic to granodioritic gneiss	Mesomylonite S and L tectonite	276/37	05 -> 089			
61	60°15`24`N 004°58`46`E	Amphibolite and metagabbro	S and L tectonite	319/45	25 -> 282			
62	60	Tonalitic pegmatite						
63	60°15`29`N 004°58`49`E	Granitic to tonalitic pegmatite. Grainsize is medium grained and pegmatitic.						
64	60°15`36`N 004°58`51`E	Granitic gneiss with amphibolite layer	Mesomylonite S and L tectonite	277/27	07->296 08->301			
65	60°15`39`N 004°59`10`E	Amphibolite	Mesomylonite S and L tectonite	128/36 097/19 163/15 177/08	08 -> 156			
66	60°15`56`N 004°57`19`E	Metagabbro with Pegmatite intrusions.	Local shear zone consisting of amphibolite. Tight folding, recumbent. Anastomosing foliation.	332/50	11 -> 144			
67	60°16`00`N 004°59`44`E	Granitic gneiss Sample TSS-2	L>S tectonite	050/18 045/21	11 -> 140			
68	60°16`02`N 004°59`53`E	Granitic gneiss and phyllonites	Shear zone S-C fabric Top to NW S and L tectonite	060/12 071/07	04 -> 150			
69	60°15`42`N 004°58`26`E	Granitic pegmatite						
70	60°15`42``N 004°58`06`E	Granite with pegmatite intrusion. Granite overlying amphibolite.	Folding in the amphibolite. Tight, recumbent and refolded. Anastomosing foliation.	252/31	16->111	327/12	349/21	15->104
71	60°15`41`N 004°57`50`E	Granitic gneiss.	L>S tectonite	074/25 059/15	06 -> 107 18 -> 112			
72	60°15`46`N 004°57`50`E	Granitic gneiss	Shear Zone Mesomylonite S and L tectonite	10/060 05/004				
73	60°15`56`N 004°57`38`N	Granitic pegmatite with amphibolite xenolith.		294/24 (fault)				
74	60°15`55`N 004°58`14`E	Amphibolite with medium grained plagioclase rich vein.	S and L tectonite	53/310 54/317	23->119			
75	60°15`42´N 004°58`40`E	Small body of granite in amphibolite.						
76	60°15`11`N 004°57`59`E	Granitic gneiss	L>S tectonite	297/32 280/38	07 -> 101 08 -> 100			
77	60°15`16`N 004°58`17`E	Amphibolite.	Folding Recumbent and tight. S and L tectonite.	270/52	05 -> 080	268/76	308/10	14->076
78	60°15`59`N	Amphibolite	S and L tectonite	078/55	14->127			

	004°58`01`E			043/30				
79	60°16`18`N 004°57`47`E	Boundary between Granitic gneiss and amphibolite. Pegmatite intrusion in the granitic gneiss	Vertical fault between the units. S and L tectonite	303/84 158/80 (Fault)	09->119 06->120			
80	60°16`31`N 004°57`57`E	Boundary between the granitic gneiss and amphibolite. Granitic gneiss intruding the amphibolite.	S and L tectonite in both units. Boudinage structures	093/30 097/40 098/19	02->102			
81	60°16`34`N 004°58`00`E	Phyllonite shear zone in the granitic gneiss. Folded pegmatite intrusions in the granitic gneiss.		092/57(c) 106/61(c)	06->098			
82	60°15`46`N 004°57`47`E	Granitic gneiss	L>S tectonite	352/12 333/20	15->112			
83	60°15`29`N 004°59`41`E	Granitic gneiss	L>S tectonite	274/28 285/21	07->078			
84	60°15`28`N 004°59`50`E	Granitic gneiss with Pegmatite intrusion	S and L tectonite	305/13 257/31 250/23	13->061			
85	60°15`24`N 005°00`05`E	Granitic gneiss with pegmatite intrusion.	Boudinage Top to west S and L tectonite	285/18 322/12	09 -> 082			
86	60°15`23`N 004°00`00`E	Boundary between granitic gneiss and gabbro. Granite intruding the amphibolite. Pegmatite in the amphibolite.		302/24 Contact	21 -> 081 Contact			
87	60°15`13`N 005°00`23`E	Amphibolite with granitic gneiss on top.	Boundary follows the foliation. Top to NW.	291/14 282/32	08 ->106			
88	60°15`13`N 005°00`19`E	Mixed lithologies (Amphibolite, pegmatites and granitic gneiss) Bonded gneiss	Folding in amphibolite. Vertical and tight.	245/31	07 -> 086	267/75	269/60	32->357
89	60°16`42.5`N 004°58`01`E	Granitic gneiss with folded pegmatite intrusions.	Tight, recumbent, refolded. S and L tectonite	101/57	06 -> 098			
90	60°16`09.7`N 004°57`46`E	Amphibolite	Shear zone S and L tectonite	348/27 003/22	10->163			
91	60°15`41`N 004°57`47`E	Granitic gneiss with pegmatite intrusions.	Shear zone Top to NW anastomosing	270/27	03 -> 106			
92	60°15`44`N 004°57`35`E	Tonalitic pegmatite						
93	60°15`55`N 004°57`35`E	Granitic pegmatite						
94	60°15`15`N 004°57`48`E	Amphibolite and Metagrabbro (various composition and grain size) with pegmatite and granitic gneiss intrusions		285/79 290/73	109->36			
95	60°15`17.9`N 004°57`49`E	Granitic to tonalitic pegmatite and small body of granitic gneiss						
96	60°15`24.5`N 004°57`41`E	Metagabbro		294/58	12->111			

		(various composition/ grain size)						
97	60°15`34.7`N 004°57`47`E	Granitic pegmatite		264/79 237/51	03->086			
98	60°15`26.4`N 004°57`45`E	Granitic pegmatite and metagabbro with varied composition/grain size. Some layers are amphibolite's		301/68	16->103			
99	60°15`30.2`N 004°58`25`E	Granitic pegmatite		271/36 296/38	12 -> 101			
101	60°16`08`N 004°58`41`E	Granitic gneiss	Shear zone Mesomylonite S and L tectonite and some places anastomosing.	004/20 007/18 082/45	19->102			
102	60°16`15`N 004°58`26`E	Granitic gneiss	L>S tectonite	099/19	08->121			
103	60°16`27`N 004°58`04`E	Granitic gneiss with pegmatite intrusions	S and L tectonite	112/48	01->115			
104	60°16`39`N 004°57`51`E	Granitic gneiss with pegmatite intrusions	L>S tectonite	089/63 098/61	10->100 08->097			
105	60°16`22´N 004°57`50`E	Granitic gneiss	L tectonite		10->122			
106	60°15`45´N 004°58`52`E	Amphibolite	S and L tectonite	326/60	21 -> 111			
107	60°15`47´N 004°59`12`E	Amphibolite	S and L tectonite	355/20	03 -> 141			
108	60°15`51´N 004°59`17`E	Amphibolite	S and L tectonite	015/26 044/14	15 -> 114			
109	60°15`43´N 004°58`23`E	Amphibolite	Shear zone S and L tectonite	339/25 328/27	21 -> 095			
110	60°15`42´N 004°58`02`E	Amphibolite	S and L tectonite	082/35	02 -> 256			
111	60°15`45`N 004°57`45`E	Amphibolite	S and L tectonite	262/43	06 -> 074			
112	60°15`47`N 004°57`35`E	Amphibolite	S and L tectonite	271/21	02 -> 095			
113	60°15`47`N 004°57`35`E	Amphibolite Pegmatite with xenolith	S and L tectonite	285/30	02 -> 088			
114	60°15`50`N 004°57`35`E	Metagabbro	Bodies of granites S and L tectonite	291/20	09 -> 095			
115	60°15`56`N 004°57`35`E	Metagabbro						
116	60°15`05`N 004°57`36`E	Amphibolite	S and L tectonite	073/29	13 -> 129			
117	60°16`08`N 004°57`30`E	Metagabbro	S and L tectonite	008/21	12 -> 149			
118	60°16`11`N 004°57`20`E	Amphibolite	S and L tectonite	328/46 322/31	15 -> 119			
119	60°16`16`N 004°57`09`E	Amphibolite	S and L tectonite	020/17	16 -> 083			
120	60°16`20`N 004°57`15`E	Metagabbro	S and L tectonite	347/14	15 -> 120			
121	60°16`13`N 004°57`36`E	Metagabbro	S and L tectonite	359/25	19 -> 127			
122	60°16`25`N 004°57`47`E	Granitic gneiss	L – tectonite		01 -> 105			
123	60°16`26`N 004°57`45`E	Granitic gneiss	S and L tectonite	087/29	06 -> 103			
124	60°16`25`N 004°57`37`E	Granitic gneiss	L>S tectonite	095/45	04 -> 114			

125	60°16`05`N 004°57`55`E	Amphibolite	S and L tectonite	342/45	22 -> 137			
126	60°15`51`N 004°58`31`E	Amphibolite	S and L tectonite	322/40	32 -> 079			
127	60°14`56`N 004°59`30`E	Granitic gneiss	Ultramylonite	283/43	04 -> 101			
128	60°15`36`N 004°59`08`E	Metagabbro	S and L tectonite	345/26	17 -> 132			
129	60°15`32`N 004°58`53`E	Metagabbro						
130	60°15`36`N 004°58`31`E	Metagabbro and amphibolite with pegmatite intrusion	Top to NW	317/47 292/35	17 -> 122			
131	60°15`24`N 004°58`46`E	Metagabbro and amphibolite	S and L tectonite	263/61	11 -> 086			
132	60°15`25`N 004°59`26`E	Metagabbro	S and L tectonite	292/35	06 -> 111			

Appendix 3 - Map of outcrops

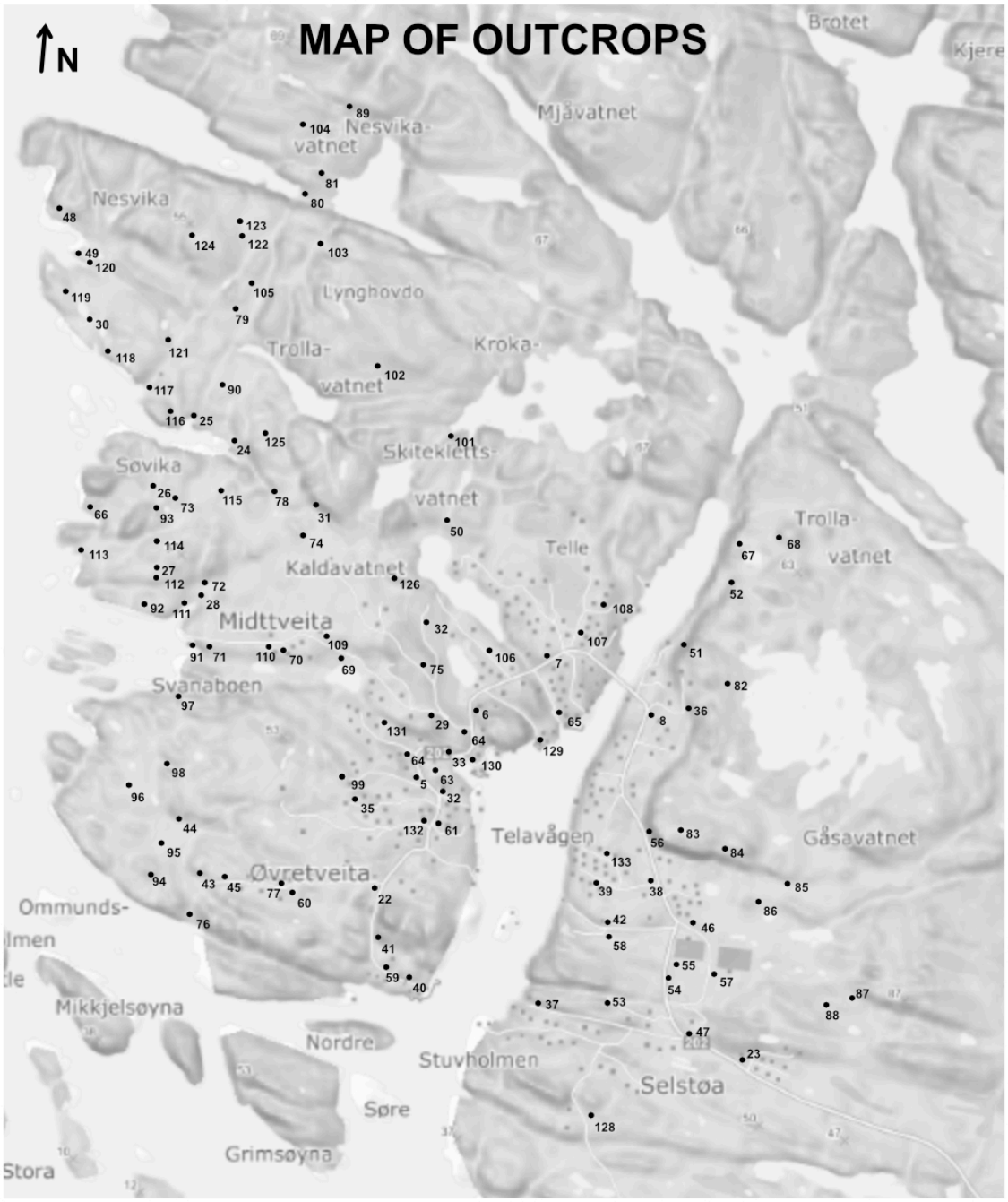

Appendix 4 - Structural map of planar fabrics

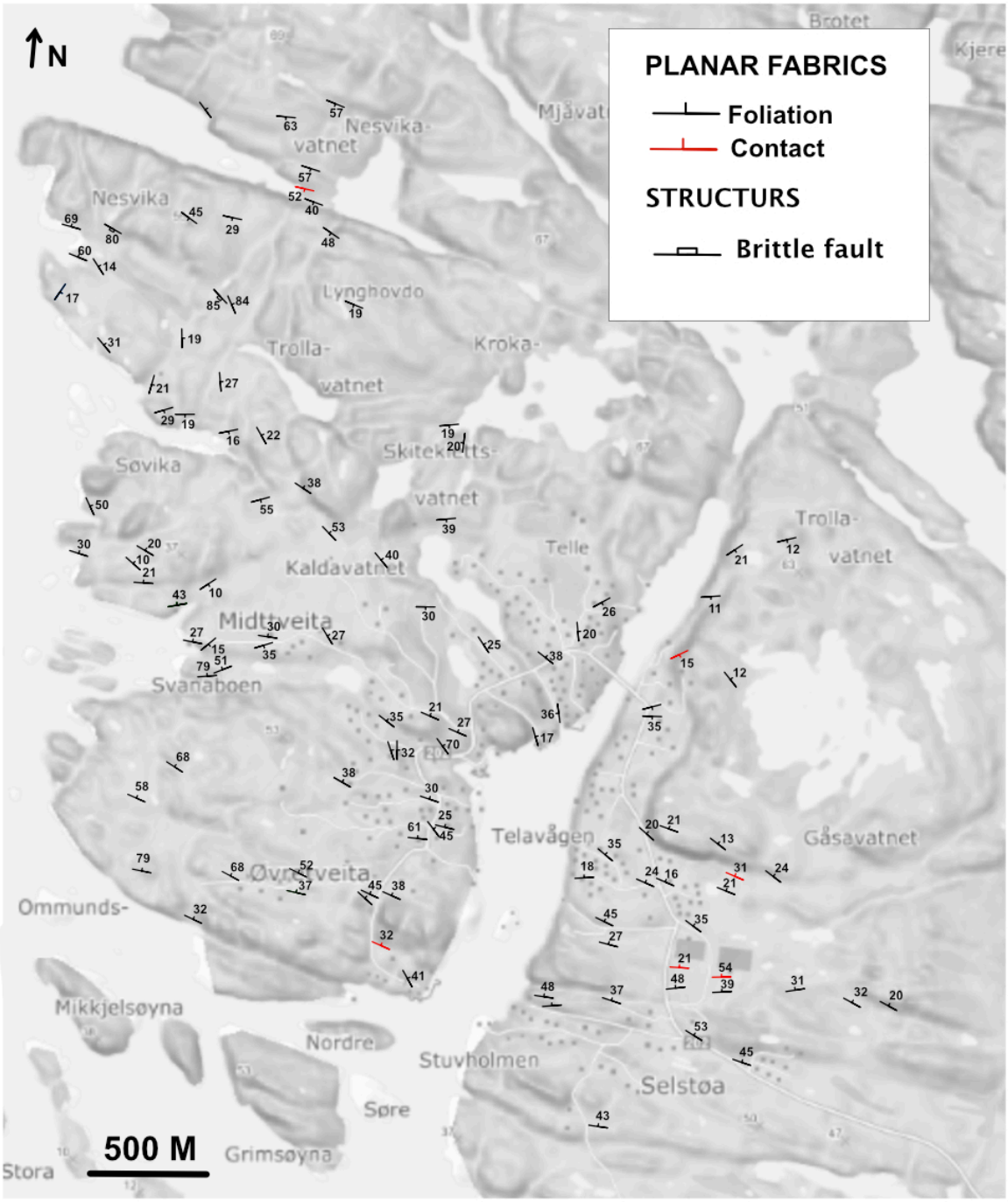

Appendix 5 - Structural map of linear fabrics